Aalto University
School of Chemical
Engineering

Petri Puikkonen

PHOTORESPONSIVE HYBRID THIN FILMS CONTAINING AZOBENZENE BY ALD/MLD

Master's Programme in Chemical, Biochemical and Materials Engineering
Major in Chemistry

Master's thesis for the degree of Master of Science in Technology
submitted for inspection, Espoo, 07 August 2017.

Supervisor	Professor Maarit Karppinen
Instructor	M.Sc. Aida Khayyami

Aalto University
School of Chemical
Engineering

Aalto University, P.O. BOX 11000, 00076 AALTO
www.aalto.fi

Abstract of master's thesis

Author Petri Puikkonen

Title of thesis Photoresponsive hybrid thin films containing azobenzene by ALD/MLD

Degree Programme Master's programme in Chemical, Biochemical and Materials Engineering

Major Chemistry

Thesis supervisor Professor Maarit Karppinen

Thesis advisor(s) / Thesis examiner(s) M.Sc. Aida Khayyami

Date 07.08.2017 **Number of pages** 87 **Language** English

Abstract

Photochromic molecules show a change in their absorption spectrum when they are irradiated at a suitable wavelength. The difference is caused by a change in the structure of the molecule and is usually reversible. Such molecules can be used in applications utilizing their optical properties, such as lenses and filters, as well as applications utilizing the changes in their chemical or physical properties, such as optical switches. In this thesis, different photochromic molecules and thin film techniques are compared.

In hybrid materials, the efficiency of the photoisomerization reaction depends on the ability of the photochromic molecule to change from one form to another. Free volume around the molecule has a great effect on its photoisomerization. A rigid matrix with a layered structure helps immobilize the molecules and thus improves the photochromic response. As atomic and molecular layer deposition (ALD/MLD) is based on self-limiting reactions by surface saturation, it should provide uniform, conformal thin films with a suitable layered matrix and accurate control of thickness.

In the experimental part, the goal was to deposit photoresponsive thin films containing azobenzene using the ALD/MLD method. The organic precursor was azobenzene-4,4'-dicarboxylic acid and the inorganic precursor was trimethylaluminium. Both hybrid and superlattice thin films were deposited on silicon and quartz. The resulting films were amorphous and nearly homogenous, with a slight gradient seen on hybrid films. The growth rate of the hybrid thin films was lower than expected, and the decreased growth rate upon increasing the number of cycles suggested the presence of double surface reactions in the process. The hybrid thin film showed minor irreversible photoresponsivity after UV irradiation. Superlattice films with very thin oxide layers showed absorption bands related to azobenzene, but with increasing oxide thickness the bands disappeared. None of the superlattice films showed any response to UV irradiation. Poor photoresponsivity was attributed to steric hindrance, likely to be partially caused by the double surface reactions. The results were compared to similar hybrid systems found in literature.

Keywords ALD/MLD, atomic and molecular layer deposition, azobenzene, hybrid thin film, photochromism, photoisomerization

Aalto-yliopisto
Kemian tekniikan
korkeakoulu

Aalto-yliopisto, PL 11000, 00076 AALTO
www.aalto.fi

Diplomityön tiivistelmä

Tekijä Petri Puikkonen

Työn nimi Valoon reagoivat atsobentseeniä sisältävät hybridiohutkalvot ALD/MLD-menetelmällä

Koulutusohjelma Master's programme in Chemical, Biochemical and Materials Engineering

Pääaine Chemistry

Työn valvoja Professori Maarit Karppinen

Työn ohjaaja(t)/Työn tarkastaja(t) DI Aida Khayyami

Päivämäärä 07.08.2017 **Sivumäärä** 87 **Kieli** englanti

Tiivistelmä

Fotokromaattisten yhdisteiden absorptiospektri muuttuu, kun niitä säteilytetään sopivalla aallonpituudella. Niiden eroavuus johtuu muutoksessa molekyylin rakenteessa, joka on usein reversiibeli. Kyseisiä yhdisteitä voidaan käyttää sovelluksissa jotka hyödyntävät niiden optisia ominaisuuksia, esimerkiksi linsseissä ja suodattimissa, sekä sovelluksissa jotka hyödyntävät niiden kemiallisia tai fysikaalisia ominaisuuksia, esimerkiksi optisissa kytkimissä. Tässä työssä vertaillaan eri fotokromaattisia yhdisteitä ja ohutkalvotekniikoita.

Hybridimateriaaleissa fotoisomerisaation tehokkuus riippuu fotokromaattisen yhdisteen kyvystä muuttua muodosta toiseen. Vapaa tilavuus molekyylin ympärillä vaikuttaa suuressa määrin sen fotoisomerisaatioon. Jäykkä kerrosrakenteinen matriisi auttaa pitämään molekyylit paikallaan ja siten parantaa fotokromaattista vastetta. Atomi- ja molekyylikerroskasvatus (ALD/MLD) perustuu itserajoittuviin reaktioihin, joissa pinnat saturoituvat, joten sillä pitäisi saada kasvatettua tasalaatuisia, pinnan muotoihin mukautuvia ohutkalvoja, joissa on sopiva kerrosrakenteinen matriisi, ja joiden paksuutta voidaan kontrolloida tarkasti.

Kokeellisessa osuudessa päämääränä oli kasvattaa atsobentseeniä sisältäviä valoon reagoivia ohutkalvoja käyttäen ALD/MLD-menetelmää. Orgaaninen prekursori oli atsobentseeni-4,4'-dikarboksyylihappo ja epäorgaaninen prekursori oli trimetyylialumiini. Hybridi- ja superhilaohutkalvoja kasvatettiin sekä pii- että kvartsisubstraateille. Kasvatetut kalvot olivat amorfisia ja lähes homogeenisiä. Hybridiohutkalvojen pinnalla nähtiin pieni gradientti. Hybridiohutkalvojen kasvunopeus oli odotettua matalampi, ja pienenevä kasvunopeus syklien määrän kasvaessa viittasi kaksoispintareaktioiden olevan osa kasvuprosessia. Hybridiohutkalvo reagoi UV-säteilytykseen vain hieman ja irreversiibelisti. Superhilaohutkalvoissa, joissa oksidikerrokset olivat hyvin ohuita, nähtiin atsobentseenille ominaiset absorptiovyöt, mutta paksummilla oksidikerroksilla vöitä ei enää nähty. Superhilaohutkalvot eivät reagoineet UV-säteilytykseen lainkaan. Huonon säteilyyn reagoivuuden syyksi epäiltiin steerisiä esteitä, todennäköisesti johtuen osaksi kaksoispintareaktioista. Tuloksia vertailtiin vastaaviin hybridirakenteisiin kirjallisuudessa.

Avainsanat ALD/MLD, atomi- ja molekyylikerroskasvatus, atsobentseeni, fotokromaattisuus, fotoisomerisaatio, hybridiohutkalvo

Preface

This work was done at Aalto University School of Chemical Engineering in the Laboratory of Inorganic Chemistry between January and July of 2017.

I would like to thank my supervisor Professor Maarit Karppinen for guidance and help throughout the work, and my advisor M.Sc. Aida Khayyami for teaching me how to use the reactor and all the instruments and helping me solve any problems I had during this work. Thank you to the staff of the Laboratory of Inorganic Chemistry for helping me with the instruments and answering an endless amount of questions.

Last but not least, I am very grateful for all the support from my family and friends throughout my studies. Special thanks to my husband Mitchel for always being encouraging, patient and supportive.

Espoo 07.08.2017

Petri Puikkonen

Table of contents

Abbreviations and symbols

ADA	azobenzene-4,4’-dicarboxylic acid
AFM	atomic force microscopy
ALD/MLD	atomic and molecular layer deposition
BIPS	1’,3’,3’-trimethylspiro-[2H-1-benzopyran-2,2’-indoline]
CVD	chemical vapor deposition
FTIR	Fourier transform infrared spectroscopy
GIXRD	grazing incidence x-ray diffraction
GPC	growth per cycle
HOMO	highest occupied molecular orbital
IRRAS	infrared reflection absorption spectroscopy
LDH	layered double hydroxide
MOF	metal-organic framework
PSS	photostationary state
RGB	red-green-blue
TBA	tetra-tert-butyl-azobenzene
TGA	thermogravimetric analysis
TMA	trimethylaluminium
UV	ultraviolet
UV-Vis	ultraviolet-visible light
XRR	x-ray reflectivity

A	[g/mol]	average molecular weight
K		number of organic layers
m		number of oxide layers
N		number of repetition cycles
N_A	[mol^{-1}]	Avogadro’s constant
r_e	[m]	classical electron radius
R_q	[m]	root mean squared roughness
t_{ADA}	[s]	pulse time of azobenzene-4,4’-dicarboxylic acid
t_{TMA}	[s]	pulse time of trimethylaluminium

T_{dep}	[°C]	deposition temperature
T_{sub}	[°C]	sublimation temperature
Z		average atomic number
λ	[m]	wavelength
ρ_e	[m^{-3}]	average electron density
ρ_m	[g/m^3]	density of the thin film
θ_c	[°]	critical angle

1. Introduction

Photoresponsive thin films are based on the use of photochromic molecules. When these molecules are irradiated at a suitable wavelength, they undergo reactions such as cis-trans isomerization or ring-closing reaction. This has an effect on their absorption spectrum, which can often be seen as a color change. The change between the two forms is reversible and can be repeatedly cycled [1].

In hybrid materials, a reaction between the organic and inorganic components forms a covalently bound framework. The interaction between the components results in a combination of properties for the hybrid material [2]. Using photochromic molecules as the organic component opens a way to affect the properties of the inorganic component remotely. During irradiation, photochromic molecules such as azobenzene change their geometry [3] and dipole moment [4], in addition to the change in absorption. All of these changes can be used in photoswitching applications, enabling control of many different chemical and physical properties of the inorganic component. In thin film applications of hybrid materials, superlattice thin films are of particular interest, as oxides have diverse interesting properties. Photoswitching of these properties would be useful in many applications.

Several classes of organic photochromic molecules exist, but only a few have been previously used in hybrid thin films. Examples of these are azobenzenes, stilbenes, spiropyrans [5] and dithienylethenes [6,7]. Different photochromic molecules have varying useful properties, which further increase the amount of suitable applications. Azobenzenes are chemically stable and certain derivatives show rapid thermal back-isomerization, which can be useful in applications where a fast response is needed [3]. Spiropyrans have potential uses in display and high-density optical memory applications due to the adjustability of the absorption spectra [8]. The advantages of dithienylethenes, especially dithienylperfluorocyclopentenes, are their thermal bistability [9] and fatigue resistance [10], which are important factors when

considering the cyclability of the material. Photoresponsive hybrid thin films based on organic photochromic molecules have been previously prepared by Langmuir-Blodgett method [5], layer-by-layer self-assembly [11], spin-coating [12] and intercalation [13].

Atomic and molecular layer deposition (ALD/MLD) has not been previously used for preparing photoresponsive thin films. The layered, rigid structure of the films deposited using ALD/MLD immobilizes the photochromic molecules, which should improve the photochromic response. Films deposited with ALD/MLD are uniform and show great conformity. The technique also allows easy and accurate control of the thickness and composition of the thin films. These factors make it a viable alternative to techniques currently in use for preparing photoresponsive thin films, perhaps even improving the performance compared to films prepared with other methods.

The aim of the literature part is to review the suitability of different organic photochromic molecules for use in ALD/MLD technique. The literature part gives an overview on photochromism and the use of ultraviolet (UV) irradiation to study the photoresponsivity of materials. The most commonly used organic photochromic molecules are presented, as are the methods previously used to prepare photoresponsive hybrid thin films. In the experimental part, the goal was to develop a process for preparing photoresponsive hybrid and superlattice thin films with ALD/MLD technique. The inorganic precursor used in the depositions was trimethylaluminium and the organic precursor was azobenzene-4,4'-dicarboxylic acid. Photoresponsivity of the hybrid thin films was examined by preparing hybrid and superlattice thin films on quartz and comparing their ultraviolet-visible light (UV-Vis) absorption spectra before and after irradiation with UV light. As a common goal for the literature part and experimental part, comparisons were made to previously prepared hybrid thin films and the suitability of ALD/MLD for the preparation of photoresponsive hybrid thin films was assessed to make suggestions for further research in the field.

LITERATURE PART

2. Photochromism

Photochromism can be defined as the reversible change in the absorption spectrum of a chemical species, when it is exposed to electromagnetic irradiation and changes from one form to another [14]. This chapter presents a general overview of photochromism, as well as the use of UV irradiation to induce photoisomerization and therefore, a photochromic response.

2.1 General overview of photochromism

Photochromism as a phenomenon was already known in the late 19th century as certain compounds were observed to change color upon irradiation, but the name itself was suggested by Hirshberg in 1950. The research of photochromic molecules increased greatly from 1940 onward as more advanced analysis methods became available. The development and manufacturing of photochromic sunglasses in the 1960s further increased interest in the phenomenon [14]. Recently, more commercial applications, such as photochromic ophthalmic lenses, have been developed. New photochromic molecules have also been found and researched extensively [1].

When the thermodynamically stable form of the chromophore absorbs irradiation at a suitable wavelength, it is converted to another form. The chromophore can return to its original form thermally or by irradiation [1]. The change between the two forms is accompanied by a change in the absorption spectrum of the chromophore. The irradiation used for the photochromic reaction, or photoisomerization, is often in the near-UV range, or sometimes in the visible light range [15]. The thermodynamically stable form absorbs in the UV range and is often colorless, whereas after photoisomerization the chromophore becomes colored. This is caused by the appearance of an absorption maximum in the visible light range for the photoisomerized form [1].

Photochromic systems mostly involve unimolecular reactions, where one molecule is transformed to another form. Bimolecular photochromic systems exist as well, and they often involve cycloadditions or electron transfer processes. Back-isomerizations can also be unimolecular or bimolecular depending on the system [14].

Most photochromic processes are based on a one-photon mechanism. The chemical species absorbs a photon and forms a singlet or triplet excited state. The excited state reacts to form the photochromic product. Other photochromic processes are based on a two-photon mechanism, where the reactive excited state is formed after absorption of two photons [1]. Two-photon processes can be two-, three- or four-level systems. In a three-level system, the first photon absorption forms a singlet excited state. The second photon absorption forms a higher singlet excited state, which reacts to form the product [14]. The two-level system for two-photon processes is based on the simultaneous absorption of two photons, where the reactive excited state is reached through a virtual level, unlike the real intermediate level in the three-level system [1]. In the four-level system, the first photon absorption forms a singlet excited state, which relaxes to the triplet ground state. The second photon absorption then forms the reactive triplet excited state [14].

The photochromic systems are by definition reversible. The back reaction from the photochemically induced form to the original form can occur thermally or by irradiation. Some systems are predominated by a fast thermal mechanism, although they can still be transformed photochemically. Other systems are thermally bistable because the thermal back-reaction is very slow. These systems are predominated by the photochemical back-reaction [15]. In some cases, the thermal and photochemical back reactions occur at comparable rates and contribute to conversion to the original state [14]. The half-life of the molecule is determined as the time it takes for the thermal back reaction to decrease the absorbance maximum of the photochromic product to 50% of its original intensity [1].

When a photochromic system is cycled repeatedly, its performance is affected by fatigue. Fatigue is a result of side reactions occurring during the process, oxidation

being the most common side reaction in photochromic systems. The side reaction converts the photochromic molecule to a species that is not photoresponsive. This is seen as a decrease in the intensity of the absorption maximum. The cyclability of a system is determined as the number of cycles the system can undergo until the absorption maximum of the original form of the photochromic molecule has decreased to 50% of its original intensity [1].

Known chemical processes for organic photochromic molecules are limited to a few classes. Pericyclic reactions, such as electrocyclizations and cycloadditions are common for photochromic molecules. For example, diarylethenes undergo electrocyclization during the photochemical process. Cis-trans isomerization is another common process seen in molecules like stilbenes and azobenzenes. Other possible processes are intramolecular hydrogen transfer, intramolecular group transfer, dissociation process and electron transfer [1].

Applications for photochromic molecules can be divided to two groups based on the phenomenon they utilize. Applications can use the change in the absorption spectra of the photochromic molecule. Examples of this are photoresponsive optical materials such as ophthalmic lenses and camera filters, optical memory applications, color changing inks and novelty items as well as cosmetics. Other applications utilize the changes in physical or chemical properties of the photochromic molecule, usually caused by a change in the geometry or the dipole moment of the molecule. The properties used in such applications are for example conductivity, refractive index, electrical moment, and viscosity. Examples of applications are optoelectronic systems, such as semi-conductors with photochromic modulators, optical switches, optical memory applications and photoresponsive enzymatic systems [15]. Photochromic sunglasses remain the most well-known commercial application thus far [1].

2.2 Use of irradiation in photochromism

As photoisomerization is based on the absorption of light, the characterization requires knowledge of the amount of light the material absorbs. Absorption properties of the material are described with absorption coefficient, which is wavelength dependent. The coefficient can be given as natural absorptivity, which is based on the natural logarithm, or decadic absorptivity based on the 10-based, decadic logarithm [16].

Depth of penetration describes how far into the material the radiation is able to penetrate. It is the inverse of the absorption coefficient of the material at the observed wavelength. At the depth determined from decadic absorptivity, the radiant power is one tenth of the value on the surface, and at the depth from natural absorptivity, the radiant power is 1/e of the value on the surface [17].

Quantum yield describes the ratio of the molecules in which the observed reaction, in this case photoisomerization, takes place compared to the amount of quanta the molecules absorb. It describes the efficiency of the reaction and the system. True quantum yield describes only the absorption for the observed molecule, whereas apparent quantum yield includes other absorbers in the system. Quantum yield can also be defined differentially at a particular moment or integrally as a mean value over time [3].

The concentrations of the isomers change during irradiation as the photoisomerization reaction progresses in both directions. Their values depend on the quantum yields of the reactions, the incoming flux of photons and the fraction of the photons that are absorbed by the observed species. It is assumed that both isomers absorb at the irradiation wavelength and that the quantum yield for neither reaction is zero. This is true for chromophores such as azobenzene. The thermal back reaction progresses as a first order process [18]. When considering all processes happening simultaneously, the system reaches a photoequilibrium, a stationary state, as the irradiation continues. In photoequilibrium, the trans-cis composition of

the sample does not change over time. The concentrations of the species in photoequilibrium depend on the absorption coefficients of the two isomers at the chosen wavelength, quantum yields of the trans-cis and cis-trans photoisomerization reactions and the rate constant for the thermal back-isomerization. The intensity of the irradiation affects the photoequilibrium only if the thermal reaction is present [3]. The three relevant processes are presented in Figure 1.

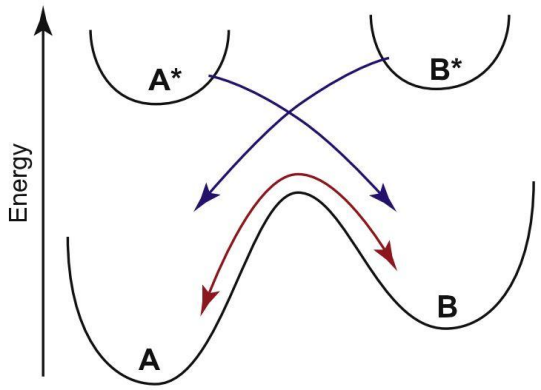

Figure 1. The photoisomerization processes for two isomers and the thermal back-isomerization [18].

The determination of quantum yield depends on the information available. In the case of photoisomerization reaction, if one of the isomers cannot be isolated or only a very small amount is available, this may mean that the required spectrum and absorption coefficient information cannot be obtained [3]. Fischer [19] developed a method for these situations, where the determination is done by measuring the absorption spectra after irradiation at two wavelengths until the system reaches photoequilibrium. The quantum yield of the reaction and absorption spectra of the other isomer can be estimated by comparing the changes in absorbance. Both isomers must absorb at both wavelengths used in the measurement and the ratio of quantum yields should not differ between the two measuring wavelengths [19]. Because the measurements are performed in photoequilibrium, the molecules must not exhibit thermal back-isomerization. If the thermal reaction is very slow, like with azobenzene, it has less of an effect on the results [3].

In homogeneous solutions, photoisomerization can be regarded as a first order reaction as the reaction sites are equal. In solid matrices, nonequivalent reaction sites may influence the quantum yield of the reaction. The number of kinetically independent reactions can be determined with Mauser diagrams [3].

Photoisomerization is usually characterized by using absorption spectrometry, comparing the absorption spectra before and after UV irradiation. For azobenzene, the absorption spectra of the trans- and cis-isomers are different, and this can be used to follow the photoisomerization reaction and to determine when photoequilibrium has been reached [3].

The observable species can in certain cases have a lifetime too short to be studied with absorption spectroscopy. In these cases, the technique needs to be able to generate the species fast and with good yield, and the spectrum must be measured in less time than it takes for the species to return to its original state. Flash photolysis and spectroscopy can be used to solve these problems. The technique uses two sources with flash discharge capabilities perpendicular to one another, a photochemical source with an emission spectrum suitable for photolysis and a spectroscopic source with a spectrum covering the entire observed region [20]. Flash photolysis has been used to investigate the photoisomerization reaction in some azobenzene derivatives. The lifetime of the short-lived species can be determined with this technique [21]. The weak and short-lived fluorescence of azobenzenes has been used to study the kinetics and mechanism of the photoisomerization reaction with time-resolved fluorescence spectroscopy using a similar setup [22].

2.3 UV sources

UV radiation sources are commonly identified by their input energy. The values can be given as watts or watts per inch or centimeter of bulb. Generally, increasing the input power will increase the output power as well. However, the actual value of output energy cannot be determined from the input energy, nor can the type of UV radiation emitted from the lamp [23].

The output energy of the UV radiation source is often given as irradiance. Irradiance describes the amount of radiation reaching the observable surface. It contains radiation arriving from all angles. Irradiance is given as watts per square centimeter [23]. Irradiance depends on the power input of the lamp, as well as the lamp geometry [24]. As irradiance corresponds to the distance from the lamp, the value is often reported as peak irradiance measured at a specific distance when considering the output of the lamp [23].

Energy density accounts for the time factor of the UV irradiation on the surface. The unit of energy density is Joule per square centimeter, meaning watt times second per square centimeter. Energy density is measured by monitoring both irradiance and time of irradiation. Possible changes in irradiance have to be taken into account as well, especially in continuous processes where the product moves in relation to the lamp [23].

In addition to UV radiation, the lamps output other forms of energy as well. Only 28 % of the output of the most common source type, mercury vapor lamp, is UV radiation. Visible radiation accounts for 21 % of output, infrared radiation 33 % of the output, and heat losses the remaining 18 % of the total output of the lamp [24]. The heat produced in the process may affect the measurement of irradiance [23], as well as damage the object being irradiated if it is sensitive to heat [24].

The type of UV lamp chosen for the characterization depends on the sample and the application. Most commonly used UV lamp type is a mercury vapor lamp. They are based on the excitation of the mercury inside the lamp. By applying a voltage between the electrodes, the mercury atoms transition to the first excited state. When they return to the ground state, they emit at wavelengths that are characteristic to mercury [25].

Mercury vapor lamps are categorized by the pressure of the bulb, and they are commonly grouped into low-, medium- and high-pressure mercury vapor lamps. The

pressure of the mercury vapor also determines other properties of the lamp, such as its operating temperature and its output [24]. Emission spectra of the bulb changes with the mercury vapor pressure as well [25].

Low-pressure mercury vapor lamps have pressures between 10^{-2} and 10^{-3} Torr [24] and operation temperatures between 40 and 80 °C. The emission spectrum shows a maximum at 253.7 nm with 85 % of the UV radiation emitted at this wavelength, a local maximum at 185 nm and weaker bands above 300 nm [25]. The output of the lamp is usually between 0.2 and 0.5 watts per cm of the bulb. Low-pressure lamps can also contain small amounts of argon to help with the excitation process of mercury [24].

Low-pressure high output mercury vapor lamps operate with a higher voltage, which in turn makes the intensity of the lamp higher. The lamps contain solid mercury amalgams with gallium or indium on the surface of the quartz tube, which help control the vapor pressure, allowing the use of higher input voltage up to 1000 watts [25].

Medium-pressure mercury vapor lamps operate at pressures from 20 to 100 Torr [24]. The operating temperatures range between 600 and 900 °C and the electrical input is also higher than that of low-pressure lamps. The emission spectrum shows many peaks compared to the one maximum in low-pressure lamp spectra, making it polychromatic in the UV range [25]. Their output is between 40 and 120 watts per cm of bulb [24]. The spectra of low-pressure and medium-pressure mercury vapor lamps are presented in Figure 2.

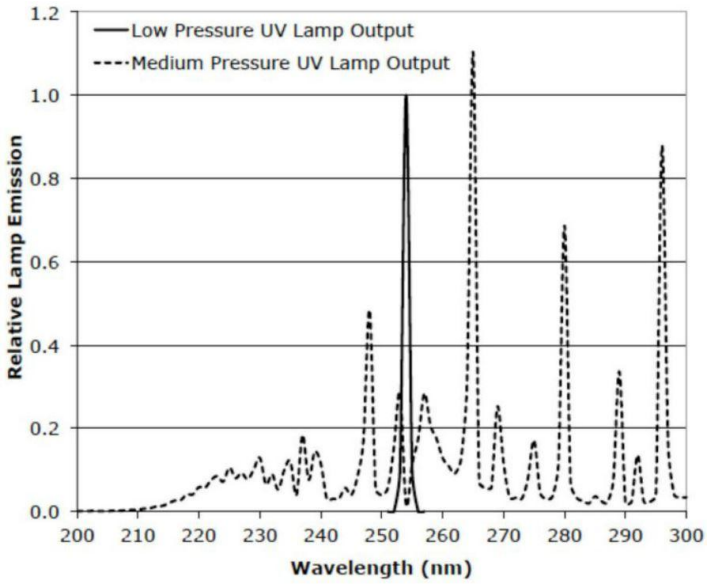

Figure 2. Emission spectra of low pressure and medium pressure mercury vapor lamps [25].

High-pressure mercury vapor lamps operate at pressures between 7600 and 76000 Torr. Their operating temperature is similar to medium-pressure lamps. However, their output power is higher than that of low- and medium-pressure lamps [24].

Mercury vapor lamps can be electrodeless. In electrodeless lamps, excitation happens with microwave energy. This can increase the lifetime of the lamp, since electrodes can deteriorate over time. They generate less infrared radiation than mercury vapor lamps with electrodes [24] and their warm-up time can also be significantly shortened. The microwaves are usually generated with a magnetron and fed inside the lamp through waveguides [25].

UV light-emitting diodes (LED) are made of layers of p- and n-doped AlGaN and AlInGaN with a layer of AlInGaN with multi-quantum wells in between, which is the active region of the diode. The diodes have their emission maximum ranging from 247 to 365 nm [26]. Light-emitting diodes do not have a warm-up time, making them better than mercury lamps for intermittent use. They are highly energy efficient [25] and have low system noise. Their small size makes the systems scalable and they are

low in cost when manufactured in bulk [26]. Their low output can limit their use to smaller systems [25].

The spectral output of both mercury vapor lamps and UV LEDs can be tuned for specific needs. Mercury vapor lamps can be doped with certain metal halides to add spectral lines or to adjust intensities of lines [24]. For light-emitting diodes, chips with the emission maxima at different wavelengths can be combined to fabricate a lamp with desired spectral output [26].

Xenon lamps are similar to mercury vapor lamps, but they are filled with xenon instead. Xenon does not react with the electrode materials, which causes less deterioration. They also have no warm-up time. Because xenon's excited states are higher in energy than in mercury, the lamps operate at a higher temperature [24]. Xenon lamps can be operated in pulsed or continuous manner. Pulsed xenon lamps are fed with high-power electrical pulses, which discharge as high intensity light pulses [25]. Hybrid xenon/mercury lamps also exist, where mercury is added to xenon to increase the intensity of spectral lines characteristic to mercury [24].

Excimer lamps contain rare gases and/or halogens, which form dimers with each other upon excitation [25]. The excited state, and therefore the dimer, has a short lifetime, after which it dissociates and emits at a highly selective wavelength, making the emission almost monochromatic. The wavelength of the emission is determined by the dimer pairing. No infrared radiation is generated in the discharge process, which keeps the operating temperatures of the excimer lamps low [24].

3. Organic photochromic molecules

Some organic molecules can undergo a reversible photoreaction. The reactions are usually cis-trans isomerizations, like in the case of azobenzene and stilbene, or ring-opening and ring-closing reactions seen for spiropyrans and dithienylethenes. These can be utilized in many applications related to the change in absorption spectra or

properties of the molecule after the photoreaction [17]. This chapter highlights some examples of photoisomerizable molecules that have been previously used in thin film applications.

3.1 Azobenzene

In azobenzene, two phenyl rings are connected by nitrogen atoms with a double bond between them. This functional group of two double bonded nitrogen atoms is known as the azo group. Azobenzene has two configurations, the thermally stable trans-isomer and the metastable cis-isomer. The trans-isomer can be converted to the cis-isomer with UV light [27], which gives rise to many interesting properties and possible applications. The trans-cis isomerization reaction of azobenzene is presented in Figure 3.

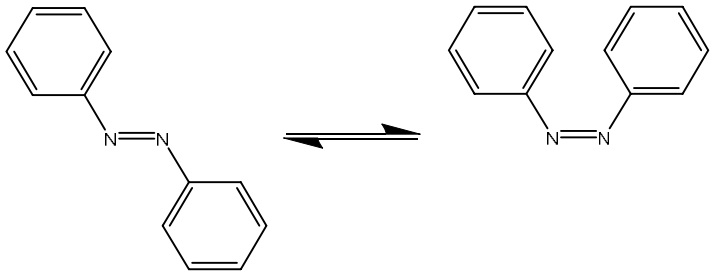

Figure 3. Trans-cis isomerization of azobenzene.

In 1937, Hartley [28] first identified the cis-form of azobenzene through exposing azobenzene solutions to sunlight and performing fractional crystallizations to isolate it. He discovered that the trans-cis isomerization reaction is reversible, occurring in both directions by irradiation with light, and that the cis-trans back-isomerization happens through a thermal reaction. Hartley [4] later reported that cis-azobenzene is, however, stable in the crystalline form.

The absorption spectrum of azobenzene shows an intense absorption maximum at 316 nm [29], which corresponds to the (π, π^*) transition [30]. Another, much weaker, local absorption maximum is seen at 449 nm [29], which in turn corresponds to the (n, π^*) transition [30]. In addition, there's a third local maximum at 229 nm [29],

which is the second band for the (π, π*) transition [3]. When irradiating azobenzene at the wavelength of the stronger (π, π*) band, the absorption maximum at this wavelength decreases in intensity and the maximum corresponding to the (n, π*) band increases in intensity as the isomerization reaction progresses. The trans-isomer absorbs preferentially at the wavelength of the (π, π*) transition, whereas the cis-isomer absorbs mainly at the wavelength of the (n, π*) transition, allowing the use of different wavelengths for photoswitching between the two isomers [31]. The change in the absorption spectrum during irradiation is presented in Figure 4.

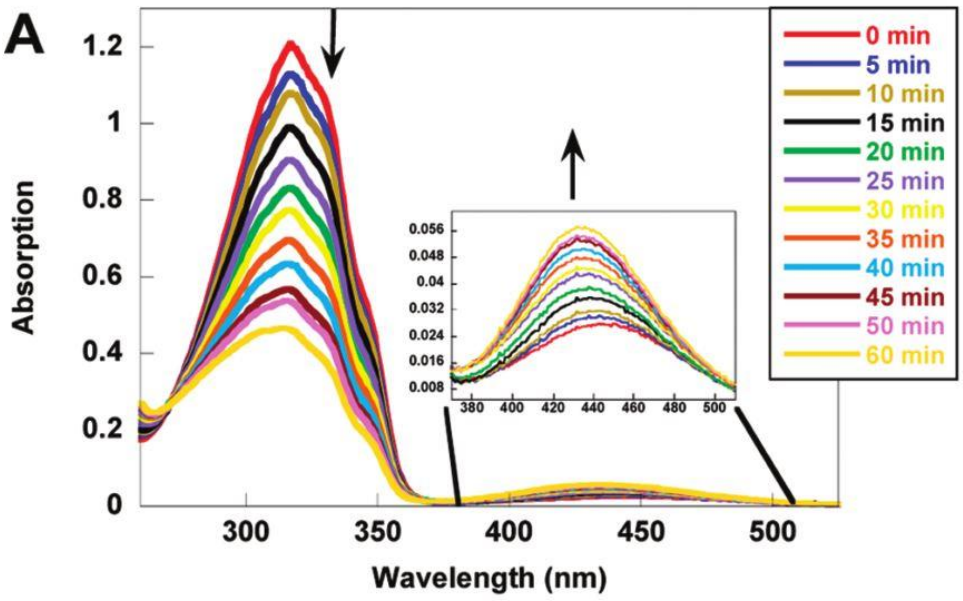

Figure 4. Irradiation induced change in the absorption spectrum of azobenzene [32].

The absorption spectrum shows that azobenzenes absorb light in the visible range. The (n, π*) absorption occurs at about 450 nm depending on the solvent [30] which gives them their colors, ranging from yellow to red [27]. Azobenzenes are also used as dyes, most commercial azo dyes being the pseudo-stilbene type [31].

The mechanism of the trans-cis isomerization has been debated for a long time. The early consensus was that the isomerization happens through a rotation around the double bond [3]. Curtin *et al.* [33] suggested an inversion mechanism, where the one of the phenyl rings attached to a nitrogen moves to the other side of the molecule through a planar transition stage.

In 1982, Rau and Lüddecke [34] suggested two separate pathways for the isomerization depending on the excitation that takes place. According to their theory, the mechanism for isomerization caused by excitation from n to π* state would be inversion, but excitation from π to π* would cause isomerization through rotation. Fujino *et al.* [22] later claimed using femtosecond fluorescence measurements that no rotational isomerization happens through the (π, π*) excitation, but instead the molecule relaxes from the (π, π*) state to the excited (n, π*) state with a near-unity quantum yield and isomerizes through inversion. However, the exclusivity of inversion mechanism conflicts with other studies made on the subject.

More recent work by Diau [35] brings forward another possible isomerization pathway through concerted inversion, where both phenyl rings in the azobenzene system move to the same direction at the same time. This pathway opens after relaxation from the (π, π*) state, forming a vibrationally excited (n, π*) state and it yields only the trans-isomer, but possibly also some side products. This may explain the lower quantum yield for excitation to the (π, π*) state. Cis-isomer is generated via the rotation pathway by direct excitation to the (n, π*) state or after relaxation from the (π, π*) state to the vibrationally relaxed (n, π*) state. Work done by Crecca and Roitberg [36] with ab initio calculations seems to support this theory. Azobenzenes in which the rotation around the double bond between nitrogen atoms is blocked can still isomerize. In this case the trans-cis isomerization must occur through the energetically unfavorable inversion mechanism or the concerted inversion mechanism [37].

The thermal back-isomerization reaction is believed to occur through the inversion mechanism. Asano *et al.* [38] synthesized an azobenzene-bridged crown ether that cannot isomerize through rotation due to the covalent bonds between both benzene rings and the crown ether. The crown ether showed thermal cis-trans isomerization with a rate constant comparable to an analogous azobenzene where rotation would be possible. Pressure effect experiments also suggested the inversion pathway, since the increase in pressure did not affect the rate of the reaction. The rate should

increase with pressure in reactions where the polarity of the reactant changes during activation, as it would in the case of the dipolar transition state in the rotational mechanism. The inversion pathway has a smaller barrier than the rotation pathway when the molecule is in ground state [36].

The quantum yield for the trans-cis isomerization reaction is about twice as large when the (n, π*) state is excited compared to the higher (π, π*) state, which contradicts Kasha's rule. This could partially be explained by the concerted inversion pathway yielding the trans-isomer upon excitation to the (π, π*) state. The quantum yield for the reverse cis-to-trans isomerization reaction is higher than the yield for the trans-to-cis reaction, and higher for the (n, π*) excitation compared to the (π, π*) excitation. However, when rotation around the double bond is prevented for example with substituents on the phenyl ring, the quantum yields for both (n, π*) and (π, π*) excitations are equal. The quantum yields are also solvent dependent [31].

None of the azobenzene types show phosphorescence, but the triplet states of azobenzene have been found by the quenching effect azobenzene has on other molecules' triplet states [3]. For aminoazobenzenes, energy transfer experiments have been used to locate the lowest triplet state, and for pseudo-stilbenes, transient absorption spectroscopy can be used in some cases to locate triplet states [31].

Isomerization of azobenzenes can be initiated by triplet sensitization. For sensitizers with triplet energy above the triplet states of trans- and cis-isomers of azobenzene the transfer of energy is efficient, but the yield is very small for the trans-cis isomerization reaction. The yield for the sensitized cis-trans isomerization reaction is unity [31].

Azoaromatics are commonly divided into three separate types based on the relative energies of the (n, π*) and (π, π*) states. In azobenzene-type molecules, the (n, π*) state is lower in energy and the gap between the two states is large [3] and the molecules are similar to unsubstituted azobenzene [27]. In aminoazobenzene-type molecules, the (n, π*) and (π, π*) states are close in energy and their relative

positions may depend on the environment [3]. Aminoazobenzene-type molecules are substituted with an electron-donating group in the ortho- or para-position [27]. In pseudo-stilbene-type molecules, the (π, π^*) state is lower in energy than the (n, π^*) state [3]. Pseudo-stilbenes are 4,4'-substituted with an electron-donating group in one position and an electron-withdrawing group at the other position [27].

The different types of azobenzenes have different lifetimes of the cis-isomer. For pseudo-stilbenes with the electron-donating and electron-withdrawing groups providing a push-pull effect, the thermal back-isomerization is very fast and the lifetime of the cis-isomer can be mere seconds. Therefore, the cis-isomer of a pseudo-stilbene-type molecule cannot be isolated. Azobenzene-type molecules have longer lifetimes and stay stable for hours, even days if kept in the dark. Aminoazobenzenes have intermediate lifetimes of minutes [3]. The inclusion of a hydroxyl-group to an azobenzene seems to be an exception, as it shortens the lifetime of the cis-isomer to the millisecond range, even without the push-pull effect from an additional electron-withdrawing group. The hydroxyl group makes it possible for the molecule to form an azo-hydrazone tautomeric equilibrium, where the hydrazone-like form with a simple bond between the nitrogen atoms shows fast thermal back-isomerization [21].

Substituents on the phenyl rings of the azobenzene molecule affect the absorption spectra. They can shift the (n, π^*) energy band to a higher wavelength. The size of the shift depends on the substituents [3]. Gegiou *et al.* [39] also noted a slight shift in wavelength and a decrease in absorption for the (π, π^*) energy band and an increase in absorption for the (n, π^*) energy band with methylation in the ortho position.

The effect of substituents is also seen in the thermal cis-to-trans isomerization. Dokić *et al.* [40] performed expansive theoretical calculations on different substituents on the phenyl rings and found that electron-accepting groups in ortho and para positions stabilize the linear transition state associated with the inversion mechanism. This lowers the inversion barrier height at ground state, whereas electron-donating

substituents on the benzene ring raise the inversion barrier, making isomerization harder [36]. García-Amorós and Velasco [21] determined that the shorter lifetime of cis-isomers of hydroxy-substituted azobenzenes is related to the change in the isomerization mechanism from inversion to rotation, when the double bond between the nitrogen atoms is broken in the hydrazone-like transition state, allowing rotation. Alkoxy-substituted azobenzenes isomerize through the inversion mechanism, making their lifetimes longer.

It is possible to hinder isomerization of azobenzenes by preventing movement of the double-bonded nitrogen atoms and adjacent carbon atoms. This can be done for example with a boron-substituent on the phenyl ring coordinating to one of the nitrogen atoms [41], with hydrogen bonds between the substituents and the nitrogen atoms [32] or with strong electron-donating substituents on the phenyl rings [42]. Bunce *et al.* [43] noted that if an alkyl substituent in the ortho position is large enough, isomerization does not occur. However, they found no linear correlation between the size of the substituent and isomerization. Thermal cis-to-trans isomerization can also be hindered sterically with bulky substituents, specifically in the ortho position [44].

The chemical environment of azobenzene molecules has a major effect on the isomerization. For solvents, a slight shift for the (n, π*) band can be seen in the absorption spectra [3]. The polarity of the solvent affects both the isomerization and the thermal back-isomerization reaction constants. The viscosity of the solvent has a much smaller effect [45]. Because of these effects, small variations are seen in the quantum yields of the isomerization for both (π, π*) and (n, π*) excitations in different solvents.

The solvent chosen for azobenzenes in solutions can increase the lifetimes of pseudo-stilbene type and hydroxy-substituted azobenzene molecules from a few hundred milliseconds in ethanol to half an hour in toluene. This is due to the hydrogen bonding between the protons in the solvent molecules and the nitrogen atoms in the azobenzenes. Ethanol is a polar protic solvent, and the hydrogen bonding results in

an electronic distribution that is closer to a simple nitrogen-nitrogen bond. This makes the fast back-isomerization process possible. In non-polar toluene, a similar effect is not seen due to a lack of hydrogen bonding [21]. Dokić *et al.* [40] suggested based on quantum chemical calculations that for pseudo-stilbene type azobenzenes, the thermal reaction mechanism changes from inversion to rotation for polar solvents, which explains the change in lifetimes of the cis-isomer in different solvents.

Because the environment has a great impact on photoisomerization, incorporation of azobenzenes into inorganic matrices has been used to improve the photoisomerization reaction. Han *et al.* [11] prepared thin films of layered double hydroxides (LDH) with a polymer containing azobenzene groups between the monolayers with layer-by-layer technique. This provides enough free volume for the isomerization to occur, since the rigid matrix prevents interpenetration of adjacent polymer layers. Free volume around the molecule can also be increased for example by introducing azobenzenes in a LDH structure with a co-intercalator. Using a rigid matrix immobilizes the dye molecules and ensures fixed orientation [13].

Azobenzenes have also been incorporated into metal-organic frameworks (MOF) as a means to control storage and release of guest molecules in pores. Yu *et al.* [46] investigated the thermal cis-trans isomerization by using azobenzene as a side group in the organic linkers of a MOF material. The samples were irradiated with UV light and the thermal reaction was monitored with infrared reflection absorption spectroscopy (IRRAS). The activation energy of the back-isomerization determined through this method was in agreement with theoretical calculations done for the free azobenzene molecule without solvent interaction, suggesting that no inhibiting interactions take place in such matrices. This would provide an efficient release of guest molecules from pores. Azobenzenes such as azobenzene-4,4’-dicarboxylic acid have also been used as linker molecules in MOFs, where the azo moiety is located in the framework itself [47]. Photoisomerization has not been observed for such frameworks, possibly because the rigidity of the three-dimensional structure prevents it. The stress caused to the structure by photoisomerization would require the crystal structure to break down or change.

The inorganic matrix may affect the trans-cis and cis-trans photoisomerization reactions in the opposite way. Ramakrishnan *et al.* [48] found that a hybrid film prepared from a polyfluoroalkyl azobenzene derivative intercalated into a clay mineral showed a quantum yield well over unity for the cis-trans photoisomerization upon irradiation with visible light. They noted that the activation energy for the cis-trans isomerization is lower in a rigid matrix, suggesting a destabilization of the cis-isomer in such environments. The trans-cis reaction was retarded in the same environment, showing lower yields in dry films than in other environments. The local heating caused by energy from relaxation unable to dissipate in the rigid matrix seemed to favor the trans-isomer.

Azobenzenes in contact with metal surface generally do not photoisomerize. This is due to the quenching by steric hindrance, changes in the potential energy surface of the molecule from interactions between the metal surface and the molecule, or new decay channels for excited states. Azobenzene on Au(111) surface can still isomerize, but in this case the reaction is initiated by tunneling electrons in a scanning tunneling microscope junction and requires 10^{18} electrons to isomerize just one azobenzene molecule, compared to 10^{7} photons to isomerize one azobenzene molecule with UV irradiation [49]. Tseng *et al.* [50] studied gold nanoparticles coated with self-assembled monolayers of azobenzenes between a silicon oxide and a pentacene thin film as a transistor-like environment and noted that although photoisomerization does not occur, the UV irradiation influences the memory window and the source-drain current of the transistors. This was attributed to additional charge trapping by the azobenzene derivatives, as well as their ability to mediate and facilitate trapping in the gold nanoparticles.

Tetra-tert-butyl-azobenzene (TBA) on Au(111) surface, on the other hand, can reversibly photoisomerize. The irradiation creates a hole in the d-bands of gold, which tunnels into the highest occupied molecular orbital (HOMO) of the TBA molecule. This results in positive ion resonance, which is the driving force of the isomerization. The HOMO of TBA is close to the d-band edge, which facilitates the charge transfer between the two. The HOMO of azobenzene is higher in energy and

further from the gold d-band edge, explaining why no photoisomerization is seen [49].

Photoisomerization of azobenzenes is an angle-selective process. The preferred polarization direction is along the long axis of the molecule, which is the transition dipole axis of azobenzenes [51]. Molecules oriented parallel to the polarization are more likely to be excited, whereas molecules oriented perpendicular to the polarization cannot be excited [52].

During isomerization, the dipole moment of the molecule changes. For the trans-isomer, the dipole moment is 0 [53]. For the cis-isomer, the dipole moment is 3.0 Debye [4]. The change in dipole moment along with the change in conformation of the molecule during isomerization are the main features of azobenzene utilized in photoswitching applications [13].

When irradiating azobenzenes with polarized light, photo-orientation of the molecules may take place. Consecutive trans-cis isomerizations slowly change the orientation of the molecules perpendicular to the polarization direction [54]. The change is driven by minimization of the absorption of light by the molecules [52]. Photo-orientation of azobenzenes can be reversed by using circularly polarized light or unpolarized light, which will reestablish a random orientation of molecules within the irradiated sample [27]. The photo-orientation process is presented in Figure 5.

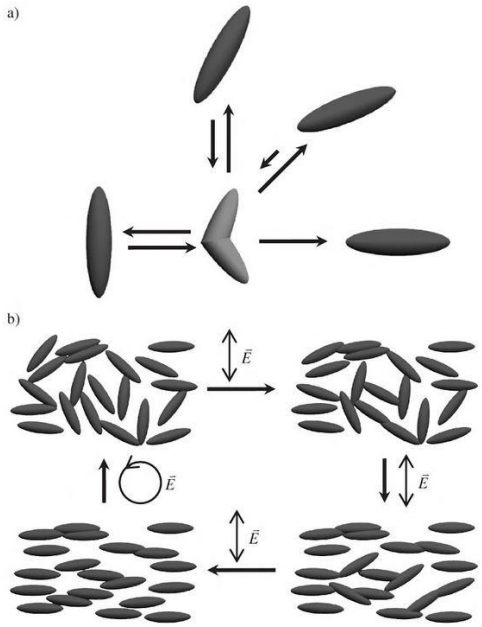

Figure 5. Photo-orientation process of azobenzenes. a) Photo-orientation of a single chromophore driven by the angle of the chromophore relative to the polarized light. b) Gradual photo-orientation of a photoresponsive azobenzene sample [27].

Rotational diffusion rapidly randomizes the orientation of the azobenzene molecules in solutions, but photo-orientation can be observed in solid films, for example in polymer films with azobenzene groups [54]. Koshiba *et al.* [51] discovered that photo-orientation in a polymer thin film containing azobenzene groups also caused partial crystallization of the film. Thermal treatment increased the crystallinity of the film, where the photo-induced crystallites acted as nuclei for further crystallization upon heating.

Amphiphilic azobenzenes can form aggregates, where molecules are gathered together in an ordered fashion. This behavior affects the absorption spectrum. Azobenzene amphiphiles typically form H-type aggregates with parallel orientation of chromophores, which is seen as a decrease in the wavelength of the (π, π^*) band in solutions [55]. Similar aggregation effects are also seen in Langmuir-Blodgett films of azobenzenes [56] and azobenzene molecules incorporated into LDHs [57]. In azobenzene polymers, aggregation takes place along the polymer backbone even in solution [5]. H-type aggregation of azobenzenes is known to hinder or prevent trans-cis photoisomerization, but J-type aggregates do not show a similar effect. Cis-trans

photoisomerization of J-type aggregates is also faster than that of H-type aggregates [58].

Most azobenzene derivatives, like azo compounds in general, do not emit light. The photoisomerization process competes with the radiative relaxation process that causes luminescence. Fluorescence quantum yields of azobenzenes are very small compared to photoisomerization quantum yields. Because of this, fluorescence is only observed for azobenzenes with stabilized isomers [30]. By preventing photoisomerization for example with substitutes coordinating to one of the nitrogen atoms, highly fluorescent azobenzenes can be obtained in solutions [41]. Fluorescence is also seen in self-assembled azobenzene aggregates. Shimomura and Kunitake [58] observed an emission at about 600 nm for the bilayer aggregate of azobenzene amphiphiles.

Photoswitching has certain applications in biological systems. Azobenzene-containing micelles, block copolymers and biomolecules like nucleic acids and peptides as well as cellular control and sensing have been researched [59]. However, UV light can damage living organisms. For this purpose, Beharry *et al.* [60] modified the azobenzene structure commonly used in photoswitching biomolecule applications by introducing methoxy groups in the ortho positions on the phenyl rings. They observed a separation of the (n, π^*) bands of the trans- and cis-isomer, providing a way to switch between the isomers with visible light only, avoiding UV irradiation completely.

Photo-isomerization of azobenzenes has been utilized in preparing photomagnetic switching films. Yamamoto *et al.* [61] prepared Langmuir-Blodgett films from an amphiphilic azobenzene, montmorillonite and Prussian blue. The hybrid films showed reversible change in magnetization of about 11% when irradiated alternately with UV and visible light. Higher density of the azobenzene amphiphiles in the film increased the change in magnetization. This was attributed to the higher molecular organization of the chromophores. Abellán *et al.* [62] prepared a gel containing azobenzene-4,4'-dicarboxylic acid and magnetite nanoparticles. A slight change in

the hysteresis loop for the magnetic material was observed after irradiation with UV light. The reason for this was determined to be the change in distance between the magnetite nanoparticles due to the azobenzene molecules coordinated to them. Abellán *et al.* [63] also prepared thin films of $Co^{2+}Al^{3+}$ -LDH with azobenzene-4,4'-dicarboxylic acid intercalated in the space between the layers and saw a reversible change in magnetization of the CoAl-LDH matrix upon irradiation with UV light. The increase in magnetization was attributed to the decrease in the distance between the layers after irradiation as the azobenzene changes conformation from trans- to cis-isomer. The change could not be reversed by irradiation with visible light, but instead by exposing the films to moisture, which returned the films to their original state through a proton-assisted thermal cis-trans isomerization.

Photo-orientation behavior of azobenzene molecules has been used in polymers combined with liquid crystals to prepare anisotropic films. When azobenzenes go through photo-orientation by irradiation with UV light, they re-orient the other neighboring moieties in the polymer in the same direction, resulting in macroscopic orientation and high optical anisotropy of the sample. Liquid crystal polymers are especially interesting, as they can combine the liquid crystallinity and the photo-orientation behavior of azobenzenes as side groups of the polymer in one molecule [64]. Stumpe *et al.* [65] prepared such films using an azobenzene-containing liquid crystalline polymer. The films showed good cyclability and reversibility upon changing the power and polarization of the laser used for the photo-orientation process. The films were investigated for use in optical storage applications, and the written information was estimated to be stable for several years.

The photo-isomerization process of azobenzenes can also cause a phase transition in liquid crystals. Ikeda and Tsutsumi [66] prepared liquid crystal polymer films containing azobenzene moieties that showed a phase transition from nematic to isotropic upon photoisomerization. When the UV irradiation ended, the thermal back-isomerization reaction returned the liquid crystals back to the nematic phase.

Photoresponsive hybrid materials with photoswitchable optical properties have been prepared. Bućko *et al.* [12] used ellipsometry to measure the refractive index of hybrid material samples containing an azobenzene derivative at different concentrations in a siloxane matrix. The refractive index increased with the concentration of the azobenzene in the sample in the observed range. The changes in refractive index after irradiation were the highest for samples containing 10 and 15 molar percent of the azobenzene, but at higher concentrations the change was much smaller due to decrease of free volume around the azobenzene within the guest-host system caused by aggregation.

Photoswitchable wettability of surfaces containing derivatives of azobenzene has been investigated. Ishihara *et al.* [67] discovered a reversible change in the water contact angle of a droplet upon irradiation with UV and visible light for a polymer film containing azobenzene moieties. They attributed this to the difference in dipole moments between the two isomers. Wang *et al.* [13] noted a comparable reversible change for a LDH film with azo dye molecules intercalated between the layers, with roughly a 11° decrease in the contact angle for the cis-isomer. Bućko *et al.* [12] coated glass surfaces with electro-spun nanofibers of the azobenzene containing hybrid material and saw a similar reversible effect with a 10° decrease for the cis-isomer.

Photoswitchable swelling has been observed for azobenzene-containing amphiphilic polymer membranes. Ishihara *et al.* [68] reported a decrease of the swelling degree in water from 14.0 % to 7.3 % when the membrane was irradiated with UV light. This was attributed to a decrease of free water in the polymer membrane. A reversible change was seen with subsequent cycles of irradiation with UV and visible light. The change in the swelling degree was also dependent on the mole fraction of azobenzene in the polymer. They suggested an application for such membranes in controlled release of water-soluble drugs.

3.2 Stilbene

Stilbene has a structure similar to azobenzene. In stilbene, the two phenyl rings are connected by two carbon atoms with a double bond between them. The photoisomerization reaction and the trans- and cis-forms are also very similar to azobenzene [69]. Trans-stilbene gets its planar shape from stabilizing intramolecular hydrogen interactions, whereas cis-stilbene doesn't have these interactions and has a bent shape instead [70]. Upon isomerization, the dipole moment changes from 0 Debye for the trans-stilbene [71] to 0.3 Debye for the cis-stilbene [72]. The trans-cis isomerization reaction of stilbene is presented in Figure 6.

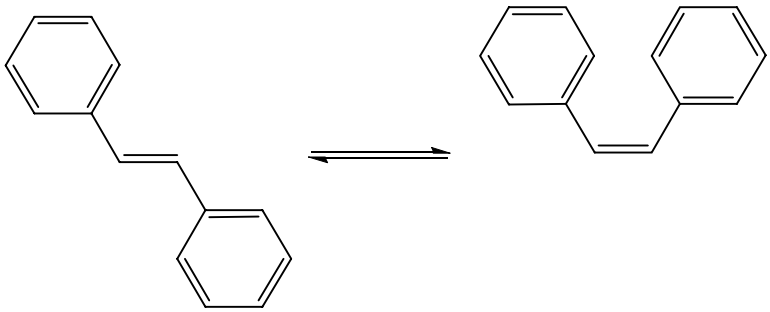

Figure 6. Trans-cis isomerization of stilbene.

Gegiou *et al.* [39] detailed the processes for the photoisomerization of stilbene in 1968. First, the molecule is excited to one of the singlet states. After vibrational relaxation to the first excited singlet state, it can exhibit fluorescent decay, internal conversion to ground state or cross to the triplet system. The higher triplet state relaxes to the first excited triplet state, which in turn relaxes to an intermediate state. From here, it can relax to the ground state of either the cis or the trans isomer. Decaying directly from the first singlet state to the first triplet state or from the first triplet state to the ground state is also possible. The processes are the same for both trans-to-cis and cis-to-trans isomerizations, and they share the intermediate state. The photoisomerization proceeds by a 180° rotation about the double bond between the carbon atoms. In the intermediate state, the molecule has rotated 90° about the double bond, and the phenyl rings are orthogonal to each other [73]. The dipole moment of the intermediate state is 0.6 Debye, which is higher than both the trans-

and the cis-isomers [72]. A diagram of the processes for the trans-cis photoisomerization of stilbene is presented in Figure 7.

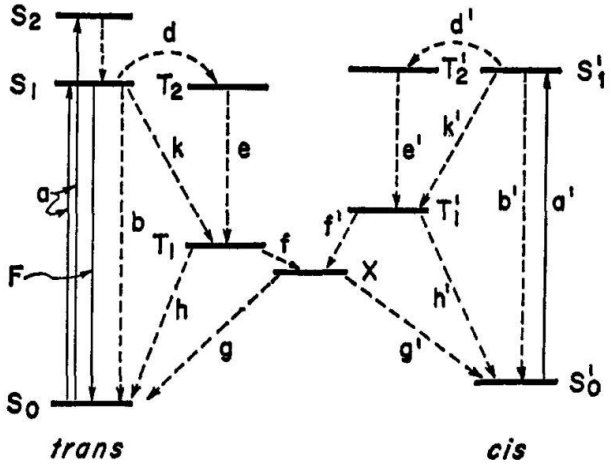

Figure 7. Diagram of the trans-cis isomerization processes of stilbene [39].

Saltiel *et al.* [74] suggested an alternative mechanism for the photoisomerization. Only singlet states are involved in this mechanism. When stilbene is excited to the first singlet state, it can either decay to ground state exhibiting fluorescence or form trans- and cis-isomers through radiationless conversion.

Photodimerization has been observed for stilbenes. Ciamician and Silber [75] first discovered the photodimerization reaction of stilbene after keeping it in benzene solution in sunlight for over two years. Shechter *et al.* [76] later found that the photodimerization reaction yields two different dimers, 1,trans-2,trans-3,cis-4-tetraphenylcyclobutane and 1,trans-2,cis-3,trans-4-tetraphenylcyclobutane. The two dimers are presented in Figure 8.

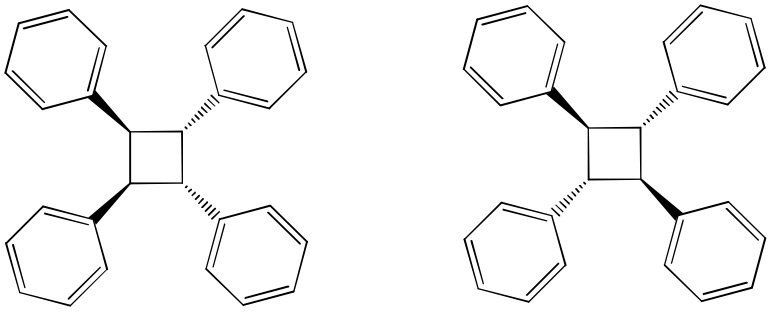

Figure 8. The dimers of stilbene.

Stilbenes can also undergo photocyclization. In the photocyclization reaction, the cis- or trans-isomer forms an excited intermediate state, which is cyclized and later oxidized to form phenanthrene. The excited singlet state is different from the one present in the photoisomerization reaction [77]. The process for the photocyclization reaction of stilbene is presented in Figure 9.

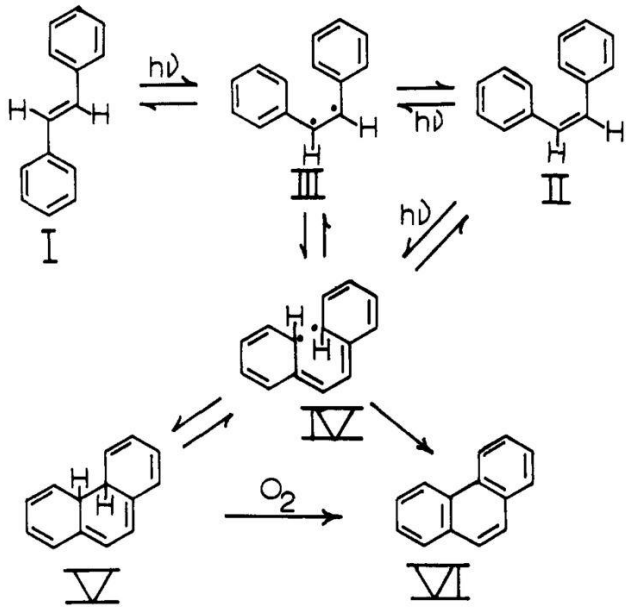

Figure 9. Photocyclization of stilbene [77].

Because stilbenes exhibit photocyclization and photodimerization in addition to photoisomerization depending on conditions and environment, this limits their use in many applications [5]. The melting point of the trans-isomer is 124 °C, whereas the cis-isomer melts already at -5 °C [78], which makes its use in solid thin films difficult, if the molecules are not immobilized within the structure. Their use in hybrid thin

films is often limited to their luminescent emission properties instead of properties rising from the photoisomerization reaction. Stilbene derivatives have been intercalated into LDHs, showing one-photon and two-photon polarized emission [79], as well as incorporated into zirconium-based matrices, showing amplified spontaneous emission, making them suitable for example for dye lasers [80].

Stilbenes have been used in liquid crystal films, where the trans-cis photoisomerization reaction changes the mesophase of the liquid crystal. Haas *et al.* [81] prepared nematic liquid crystals from chlorostilbenes. The trans-cis isomerization caused the transition temperature to drop, changing the molecules from a nematic liquid crystalline state to an isotropic state. This allowed their use in imaging applications, as areas exposed to UV irradiation appear dark and the unexposed areas stay bright. Use of crossed polarizers was required to increase the contrast.

Polymer films have been prepared with stilbenes in the backbone of the polymer. Hahm *et al.* [82] prepared a polyimide with stilbene moieties. Linear polarized UV light can be used to orient the polymer chains either perpendicular or parallel depending on the exposure doses. The stilbene moieties with their long axis parallel to the polarization direction photoisomerize upon irradiation. At doses below 1.4 J/cm^2, fewer moieties isomerize, leading to orientation of chains perpendicular to polarization direction. Maximum alignment in the perpendicular orientation is reached at 0.5 J/cm^2. At doses above 1.4 J/cm^2, chains orient parallel to polarization, reaching maximum alignment at 2.0 J/cm^2. The orientation of the polymer chains is presented in Figure 10. When the polymer film surface was in contact with liquid crystals, it could also align the liquid crystals along the direction the polymer chains were oriented.

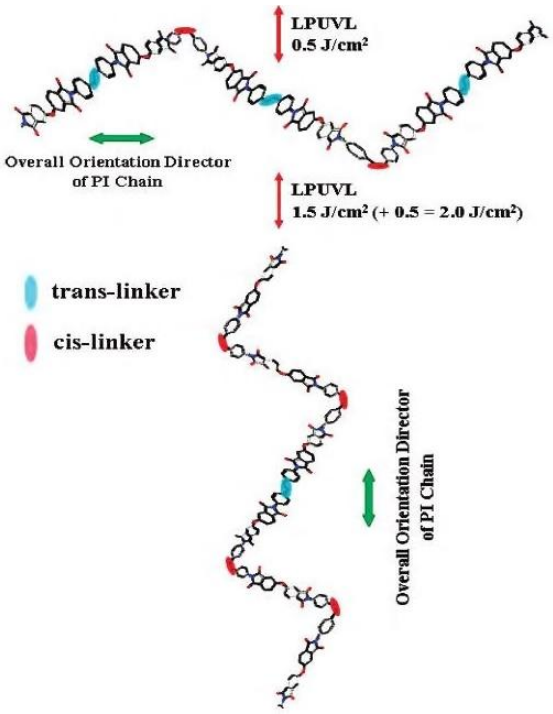

Figure 10. The orientation of the stilbene moieties and stilbene-containing polymer chains with different exposure doses [82].

3.3 Spiropyran

Spiropyrans are photochromic molecules with a benzopyran and a heterocyclic part connected by a tetrahedral carbon atom. The two parts are orthogonal to each other. The benzopyran part is present in all spiropyran derivatives, but the heterocyclic part shows more variation [73]. The photoisomerization reaction of a common spiropyran is presented in Figure 11.

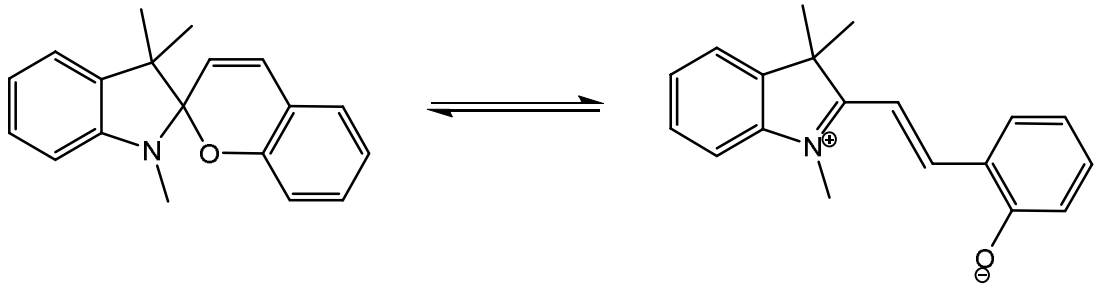

Figure 11. Photoisomerization of 1',3',3'-trimethylspiro-[2H-1-benzopyran-2,2'-indoline] (BIPS).

Fischer and Hirshberg [83] discovered the discovered the photocoloration effect in certain spiropyran derivatives in 1952. Upon irradiation of spiropyran solutions at low temperatures, the colorless spiropyran became strongly colored. They also noted that the colored modification reverted to the colorless form at a rate depending on the temperature. The reversible reaction could be cycled indefinitely.

The absorption spectrum of spiropyrans in solution shows absorption in the UV range between 200 and 400 nm. The band between 320 and 380 nm causes the photoisomerization by cleavage of the bond between the tetrahedral carbon and the oxygen in the benzopyran part. The cleaved form is often called photomerocyanine due to its structural similarity with merocyanine dyes. Photomerocyanine is the colored isomer. Upon irradiation, the system reaches an equilibrium determined by thermal bleaching kinetics and photodegradation, where both forms are present [73].

The photoisomerization reaction of spiropyran induces a change in the dipole moment of the molecule. The ground state of the spiropyran form has a small dipole moment, approximately 5 Debye, whereas the merocyanine form has a larger dipole moment, approximately 20 Debye. The dipole moments for the first excited state differ from these, as the dipole moment for the spiropyran form increases to 20 Debye, but for the merocyanine form, the dipole moment decreases to 12 Debye [84]. These changes can be utilized in photoswitching applications, in a similar manner to azobenzene.

Spiropyrans exhibit luminescence. Spiropyrans containing a nitro group are known to have emission of phosphorescence, intensity of emission depending on the position of the nitro group. Those spiropyrans that do not contain a nitro group like BIPS, only show fluorescence. Some spiropyrans can show both phosphorescence and fluorescence depending on the relative positions of their energy levels. The cis-isomer, photomerocyanine also exhibits intense fluorescence [73]. The absorption and emission spectra of BIPS are presented in Figure 12.

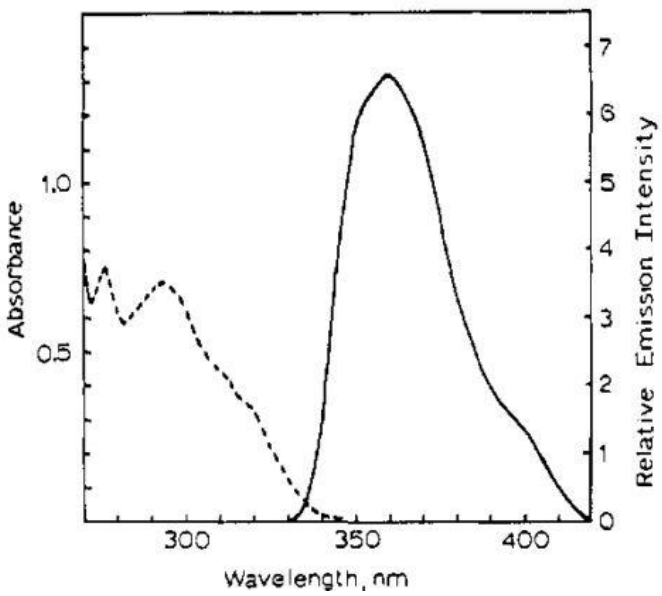

Figure 12. The absorption and emission spectra of BIPS. The dashed line represents the absorption spectrum and the solid line represents the fluorescent emission spectrum [85].

The photoisomerization reaction and the thermal isomerization reaction have been observed to occur in both directions. Irradiating the colored photomerocyanine solutions with visible light gives the original spiropyran isomer. Similarly, heating many spiropyran derivatives will yield the photomerocyanine isomer. Some spiropyrans have colored solutions in the dark, but they can be bleached with UV light [73].

The mechanism of the photochemical reaction of spiropyrans is complex and depends on the substitution and geometry of the spiropyran. The general mechanism has a few phases. When the spiropyran is excited by radiation, it can either relax back to ground state or form a thermally unstable intermediate [85]. In the intermediate, the bond between the tetracyclic carbon atom and the oxygen in the benzopyran has been dissociated, but the two cyclic parts are still orthogonal to each other [73]. The intermediate can then form the original spiropyran or the planar photomerocyanine product [85]. Direct isomerization from the excited state without formation of intermediate is also possible in some cases [73].

The kinetics related to the thermal isomerization reaction of spiropyrans are complex. The thermal reaction can be described as a fast initial process followed by a long, slow process. The substituents on the spiropyran affect the kinetic rates of the thermal isomerization reaction through electronic effects and steric hindrance [73].

The photomerocyanine form has a rather short lifetime due to the thermal back-isomerization reaction, usually in the range of tens of seconds. This limits the use of spiropyran in optical memory and switch applications. However, the environment has a great effect on the lifetime and can therefore be used to tailor the thermal stability of photomerocyanine for different applications. In silica composite films, strong hydrogen bonding can increase the lifetime from tens of seconds to tens of years [86].

Spiropyrans have applications in certain fields related to their photochromic properties, such as photography. The reversibility of the isomerization process brings forth uses in display and optical memory applications [87]. Suzuki *et al.* [8] prepared aggregated spiropyrans with absorption bands at varying wavelengths. By layering films of different aggregates, it was possible to selectively bleach only one of the spiropyran aggregate films in that position using polarized light at different wavelengths. This made the density of the optical memory medium very high [8].

Other applications for spiropyrans utilize the thermal isomerization reaction or chemical properties. Spiropyrans can also be used in biological applications, for example in membranes controlling ion transport [87]. Khairutdinov and Hurst [88] prepared biological membranes with a small amounts of an amphiphilic spiropyran. The addition of spiropyran caused an increase in the rate of leakage for potassium ions through the membrane. When irradiated with UV light, the isomerization reaction caused the rate of leakage to drop to a value comparable to membranes without spiropyran added. Irradiation with visible light increased the rate again, making the process fully reversible. The 4-fold increase in the potassium ion rate of leakage was comparable to those achieved with azobenzenes, but requiring smaller amounts of spiropyran dopant [88].

3.4 Dithienylethene

Dithenylethene has two thiophene rings connected by a bridge of two carbon atoms with a double bond between them. When it is irradiated with UV light, another bond forms between the thiophene rings in an electrocyclization reaction and the double bonds in the thiophenes and bridge migrate. The reaction is reversible upon irradiation with visible light [89]. The photocyclization reaction of a general photochromic dithienylethene derivative is presented in Figure 13.

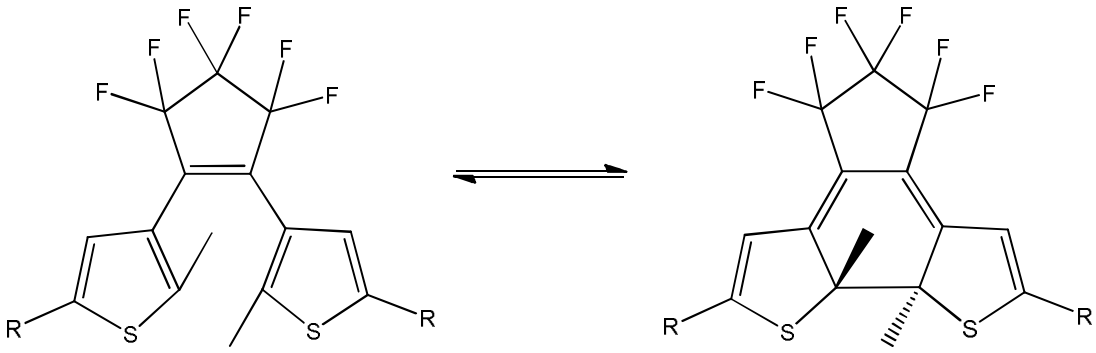

Figure 13. Photocyclization reaction of a dithienylperfluorocyclopentene.

The mechanism of the cyclization reaction is based on the (4n + 2) electrocyclization, similar to the mechanism in the photocyclization reaction of stilbene. It can be classed as a 1,6-electrocyclization [90]. Woodward-Hoffmann rule states that the photocyclization happens in the conrotatory mode, with both of the bond-forming orbitals turning to the same direction [91], resulting in the stereochemistry seen in Figure 13.

Dithienylethene has two conformations, an antiparallel and a parallel form. In solution, they are present in equal amounts. The antiparallel form can undergo cyclization and form the closed-ring isomer. The parallel form cannot isomerize when irradiated, as the conrotatory reaction can only occur through the antiparallel form due to the orientation of the orbitals [92]. The interconversion of the two forms is slow compared to the lifetimes of the photoexcited states of the forms, so they are excited independently and therefore the interconversion does not affect the quantum yield [91]. The two forms are presented in Figure 14.

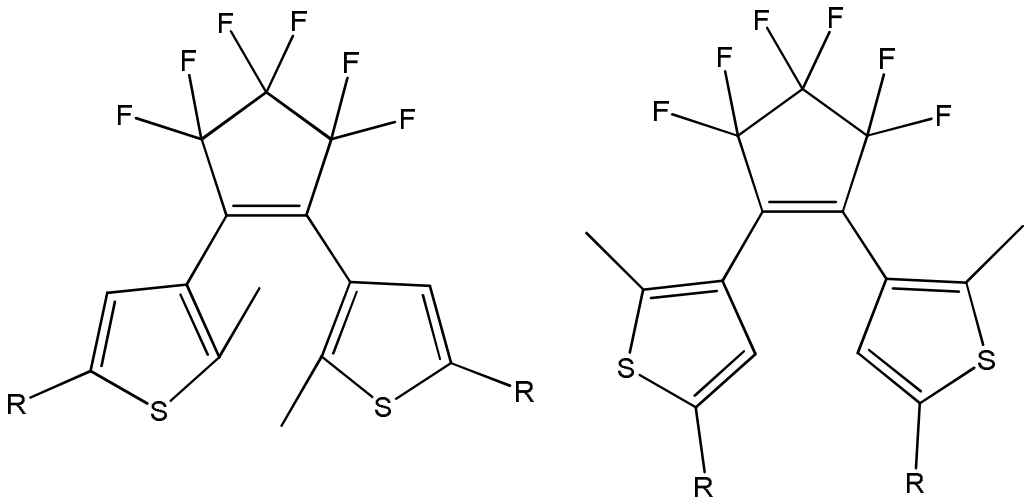

Figure 14. The antiparallel (left) and parallel (right) conformations of a dithienylperfluorocyclopentene.

For dithienylethenes, the quantum yields usually range between 0.4 and 0.6 for the ring closure. For the ring opening reaction when the system is irradiated with UV light, the quantum yields are roughly one order of magnitude smaller, ranging between 0.01 and 0.06. The ring opening reaction is slower when irradiating the system with visible light and the quantum yields are smaller than those from obtained by irradiation with UV light [93].

The quantum yields of the ring opening and ring closing reactions can be affected by complexation or by modifying the dithienylethene molecules. An increase in quantum yield of the ring closure reaction is seen when the dithienylethene is incorporated into cyclodextrin cavities. The dithienylethene molecules favor the antiparallel conformation inside the restricted space of β-cyclodextrin cavities, whereas the cavities of α-cyclodextrin are too small for the dithienylethene molecules and no effect is seen for the quantum yield. γ-cyclodextrin has a similar effect to β-cyclodextrin, but the increase in quantum yield is smaller [94]. The two thiophene rings can be locked in the antiparallel confirmation by connecting the substituents on each thiophene ring with the substituents on the double bond bridge, forming a ring structure. This might however affect the fatigue resistance of the molecule [95]. Connecting dithienylethenes into dimers, trimers and tetramers also improves the photocyclization quantum yields, as the monomers in the inactive

parallel conformation can transfer energy to the antiparallel conformation for photocyclization [96]. By preparing a film from the isolated closed-ring form, the ring-opening reaction yields only the antiparallel form, giving a higher quantum yield for the photocyclization [92]**.** Isomerization of dithienylethenes can be inhibited with substituents on the thiophene rings forming hydrogen bonds, locking the molecules into the parallel form [91].

In the closed-ring isomer of dithienylethene, the delocalization of electrons is increased compared to the open-ring isomer. This causes a notable change in the absorption spectrum. In solution, the absorption maximum observed approximately at 300 nm for the open-ring isomer is shifted to a higher wavelength in the closed-ring spectrum. The spectrum for the closed-ring isomer also has another maximum between 500 and 600 nm [97]. The change in the absorption spectra of the two isomers is reflected in their color. For example, the 2-methyl-5-phenyl- and 2-methoxy-5-phenyl-substituted dithienylperfluorocyclopentenes are colorless in the open-ring form, but exhibit a blue color in the closed-ring form [98]. The absorption spectra of a dithienylethene derivative showing the characteristic maxima are presented in Figure 15.

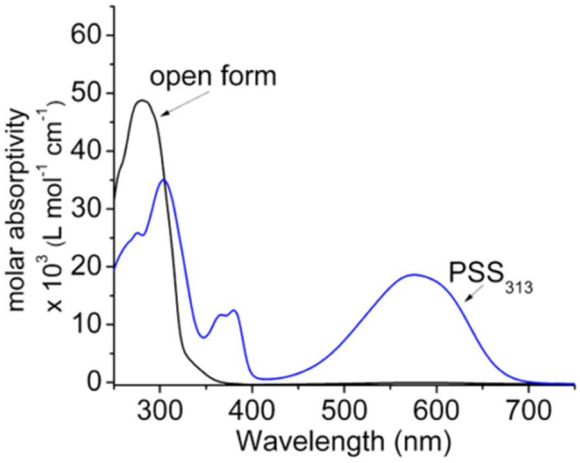

Figure 15. The absorption spectra of a dithienylperfluorocyclopentene derivative in the open-ring form and the photostationary state (PSS) [97].

The dipole moment of dithienylethene is 0 Debye in the open-ring isomer and 1.3 Debye in the closed-ring isomer at zero external field [99]. The change in dipole moment during photoisomerization is quite small compared to other photochromic molecules. The geometry of the molecule also undergoes only a minor change when it transforms from open-ring isomer to closed-ring isomer. Because of this, many of the potential applications for dithienylethene photoswitches are based on the change in the absorption spectrum instead.

Reversible fluorescence intensity changes have upon photoisomerization have been observed for certain dithienylethene derivatives. Tsivgoulis & Lehn [89] excited pyridyl-dithienothiophene-substituted dithienylperfluorocyclopentenes at a wavelength of 459 nm and saw a large change in the fluorescence intensity before and after photoisomerization. The open-ring isomer had a high fluorescence intensity, but only very weak fluorescence was seen for the closed-ring isomer. The fluorescence maxima were approximately at 600 nm, and small changes in the maxima were seen between the derivatives. The fluorescence excitation wavelength used in the experiments had almost no effect on the ring-closing and ring-opening reactions, meaning that fluorescence and photoisomerization could be induced independently with different wavelengths. This can be used in optical recording media, as writing and erasing can be done through interconversion between the two isomers, and the data can be read due to the contrast between fluorescent and non-fluorescent areas.

Dithienylethenes have been used for photoswitchable quenching of fluorescence in hybrid systems. Boyer *et al.* [100] prepared a hybrid system of nanoparticles of Er^{3+}- and Yb^{3+}-doped $NaYF_4$ with dithienylethene-derived molecules on the surface. Upon photoisomerization, the absorption band between 450 and 650 nm for the closed-ring isomer overlaps with the green emission peaks between 510 and 560 nm for the nanoparticles, but only slightly with the red emission peaks between 635 and 680 nm. The intensity of the green emission was 29 % of the original intensity after photoisomerization, while the intensity of the red emission was 75 % of the original intensity, proving the quenching effective. The photoswitchable fluorescence

nanoparticles were suggested for use in fluorescence imaging of biological species in vivo. Similar photoswitchable fluorescence quenching has been observed for hybrid systems of CdSe quantum dots and dithienylethene [101] and a zinc bis(acylamidine) coordination compound containing dithienylethene. The latter was also used to prepare hybrid thin films with poly(methyl methacrylate) by spin-casting, to determine its suitability for optical storage applications, but the quenching was less efficient in the thin films compared to solution [102].

Dithienylethenes generally exhibit high resistance to fatigue upon repeated photoisomerizations. The number of repeatable cycles is determined by measuring the absorption spectra after cycles until the maximum intensity decreases under a certain level compared to the first cycle. Certain derivatives, like those containing benzothiophene moieties, can be cycled over 10 000 times before the intensity decreases to 80 percent due to the side reactions having very low quantum yields [10]. In other derivatives, considerable side reactions occur for example through oxidation of the closed-ring isomer, including some perhydro- and perfluoro-cyclopentene derivatives. A notable side reaction may happen during UV irradiation of the closed-ring isomer, a 1,2-dyotropic rearrangement leading to another ring system through a concerted mechanism or radical intermediates [93]. The structure of the side product is shown in Figure 16.

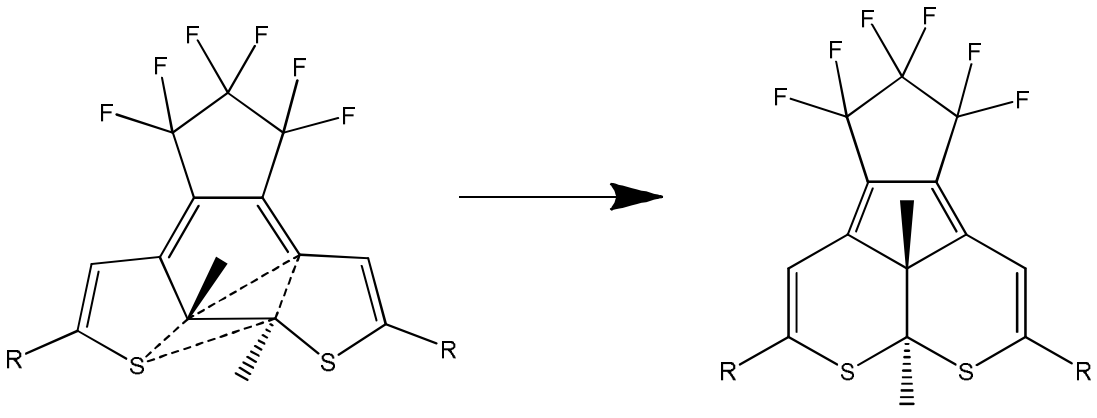

Figure 16. The side reaction of the closed form of a dithienylperfluorocyclopentene upon UV irradiation. The dashed lines represent the forming bonds and breaking bonds.

The fatigue resistivity of dithienylethenes can be improved by incorporating electron-accepting units in the parent structure. Especially CF_3- and SF_5-substituents on phenyl groups attached the thiophenes improve the fatigue resistance of dithienylperhydrocyclopentenes [93]. Adding triplet sensitizer moieties to the dithienylethene parent molecule will also improve the fatigue resistance due to more effective energy transfer preventing side reactions [103].

By using triplet sensitizers such as biacetyl, dithienylethene can be switched between the two forms with visible light. This allows the use of dithienylethenes in biomedical applications, as UV radiation can be harmful to living organisms. UV irradiation also causes side reactions because of its higher energy compared to visible light. When biacetyl molecules are incorporated to the parent molecule through a conjugated covalent linkage, the elongated π-system and push-pull effect from electron-donating thiophenes and electron-withdrawing diketones shift the absorption maximum to higher wavelength. However, this may decrease the efficiency of the ring-opening reaction [103].

For most dithienylethenes, both the open-ring isomer and the closed-ring are thermally stable in room temperature. This is useful in applications like optical recording media, where repeated switching between two stable states is needed. Thermal bistability has been observed in thiophene and benzothiophene derivatives, especially in perfluorocyclopentenes. Electron-withdrawing substituents on the thiophene rings have a negative effect on the thermal stability of the closed-ring isomers, as they weaken the carbon-carbon bond formed during the photoisomerization [9].

Unlike most photochromic molecules, some dithienylethenes show thermally irreversible reactions in the crystalline phase, in which the conformation of the molecules is locked in the reactive antiparallel form, making the photoisomerization reaction highly efficient. 2,4-dimethyl- and 2,5-dimethyl-substituted dithienylperfluorocyclopentenes are thermally bistable up to 100 °C and can be

reversibly photoisomerized for more than 100 cycles without notable side reactions or losing the crystal shape. 2,4,5-trimethylsubstituted derivatives do not show photoisomerization in the crystalline phase [104]. 2-methyl-5-phenyl-substituted dithienylperfluorocyclopentenes and certain derivatives with substituents on the phenyl group also show photoisomerization in the crystalline phase and thermal bistability with a half-life of 1900 years at 150 °C for the closed-ring isomer [105].

The chemical environment of dithienylethenes may affect their thermal stability and photoisomerization. Morimitsu *et al.* [98] prepared polymer films containing 2-methyl-5-phenyl- and 2-methoxy-5-phenyl-substituted dithienylperfluoro-cyclopentenes and noted that while the 2-methyl-5-phenyl-substituted film was thermally bistable in the time frame used and reversibly photoisomerizable, the 2-methoxy-5-phenyl-substituted film did not back-isomerize upon irradiation but was thermally reversible. In solution, the photoisomerization reaction of 2-methoxy-5-phenyl-substituted dithienylethene was reversible.

Dithienylethene can also be isomerized electrochemically. When the open-ringed isomer is oxidized, the ring-closing reaction occurs immediately, forming an intermediate. Reduction of the intermediate leads to formation of the closed-ring isomer. Wesenhagen *et al.* [106] also observed electropolymerization of the dithienylethene derivative due to the oxidation of the methoxystyryl substituents, which form radicals and are further coupled to form polymer films of the closed-ring isomer. The films are reversibly isomerizable electrochemically, but photochemical conversion from the closed-ring isomer to the open-ring isomer may destroy the film.

When dithienylethenes undergo the ring-closing reaction, the conjugation pathway becomes longer, increasing the delocalization of electrons in the molecule and making the closed-ring isomer planar [97]. This increases the polarizability of the molecule and it can be seen as a change in the absorption spectrum. Change in polarizability changes the refractive index of the material containing the photochromic molecules [107].

Hybrid thin films containing dithienylethenes exhibiting a photoswitchable refractive index have been prepared. Biteau *et al.* [6] prepared sol-gel from a silylated dithienylethene copolymerized with methyltriethoxysilane and made hybrid films by spin-coating. When the film was irradiated at a wavelength close to the absorption maximum at 587 nm, the refractive index changed from 1.533 in the open-ring isomer to 1.573 in the closed-ring isomer. They were able to write gratings and waveguides on the films using UV irradiation, suggesting possible uses in photooptical applications. Peretti *et al.* [7] saw similar effects for dithienylethene containing sol-gel films. The photoisomerization was carried out with linearly polarized light, which causes optical anisotropy within the film, as the orientation of the molecules relative to the polarization direction of the light affects the absorption. The refractive index changes depending on whether the light used in the measurement is polarized parallel or perpendicular relative to the light used in the photoisomerization.

Use of dithienylethene derivatives as chiral dopants for achiral liquid crystal hosts to induce photoswitchable reflectivity has been studied. Li *et al.* [108] prepared films of E7 liquid crystal host doped with a binaphthyl-substituted dithienylcyclopentene. They were able to control the change from an achiral nematic mesophase to a chiral nematic mesophase with a helical superstructure reversibly using UV and visible irradiation. Photoswitchable reflectivity was seen for films with higher doping concentration, where the time of irradiation determined the reflected color. The films were red before irradiation, green after 10 seconds of irradiation and blue after 25 seconds of irradiation. The use of dithienylethenes in red-green-blue (RGB) filters in liquid crystal display technology was suggested as a potential application, as dithienylethenes are thermally bistable and resistant to fatigue from repeated isomerizations.

Dithienylethene has been used to gelate water while exhibiting a photochromic response. Van Herpt *et al.* [109] prepared tripeptide gelators incorporating a dithienylethene moiety. Although dithienylethenes are hydrophobic, the derivative containing a glycine-lysine-glycine tripeptide chain formed stable hydrogels in acidic and neutral conditions, while showing a reversible photochromic effect when irradiated with UV and visible light. The mechanical properties of the hydrogels

remained unchanged after irradiation. They determined that the dithienylethene moieties trigger the formation of the gels, forming tube structures made from curled up sheets.

4. Photochromic thin film techniques

Techniques that have been used to prepare photochromic thin films, especially hybrid materials, are limited to just a few common methods, perhaps due to the features of the organic precursors and requirements for the hybrid materials. This chapter outlines the basic concept of four techniques and examples of the materials prepared using them.

4.1 Langmuir-Blodgett

Langmuir-Blodgett is a technique, where the solid substrate is submerged into a liquid. The gas-liquid interface contains monolayers of the wanted thin film, which are deposited on the substrate upon submerging. The monolayers usually consist of amphiphiles, which are compressed with a moveable barrier. This moves the molecules closer together, so that van der Waals interactions become significant enough for the molecules to form a close-packed structure. Multilayers are grown by repeatedly passing the substrate through the interface [110]. The resulting thin films have high degree of order, which helps with the photoisomerization process that needs free volume around the chromophores [5].

Molecules that have extended π-systems, like azobenzenes and other chromophores, tend to form bilayer aggregates that can be used to grow Langmuir-Blodgett thin films [5]. Shimomura *et al.* [55] examined this behavior of azobenzene amphiphiles in aqueous bilayers. They observed two different types of aggregates, H-aggregate with parallel orientation of chromophores, and J-aggregate with a tilted head-to-tail orientation of chromophores. The aggregation behavior is determined by the length of the carbon chain in the tail part of the azobenzene amphiphiles. H-aggregates

show a large blue shift, whereas J-aggregates show a slight red shift in relation to the isolated chromophore [55]. The size of the shift for the aggregate depends on the amount of chromophores in the aggregate as well as their relative distance [5]. The orientation of the chromophores in bilayer aggregates is presented in Figure 17.

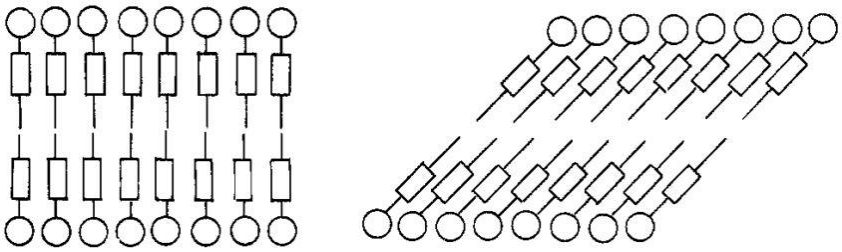

Figure 17. Orientation of the chromophores in bilayer aggregates. a) H-aggregate b) J-aggregate [58].

Rigidity and high order of Langmuir-Blodgett thin films may restrict the photoisomerization reaction, where free volume around the chromophore is needed [5]. Liu *et al.* [111] examined Langmuir-Blodgett films of an azobenzene derivative, and noticed that trans-cis isomerization in the film using UV radiation was initially slow, but after back-isomerization with visible light, subsequent UV and visible light treatments reached photoequilibrium faster. This was attributed to expansion of the film upon the initial photoisomerization cycle and reorganization of the chromophores. However, the degree of isomerization was spectroscopically estimated to be only 30% [111].

Determining the ratio of cis- to trans-isomer present in a Langmuir-Blodgett thin film cannot be reliably done by spectroscopic methods, because the optical properties of the film are not only affected by the photoisomerization reaction, but also by the changes in packing of the chromophores. Methods like cyclic voltammetry give more accurate results due to the difference in the reducing potential between the two isomers [5]. Liu *et al.* [112] measured the degree of isomerization of Langmuir-

Blodgett thin films prepared in the same way as in their previous work [111] by using cyclic voltammetry and determined the actual percentage of cis-isomer present in the photoequilibrium state to be 18.9%, less than the result obtained through the spectroscopic method [112].

Photoisomerization in Langmuir-Blodgett thin films can be improved by introducing other amphiphiles in the film that act as spacer molecules. The azobenzene amphiphiles and spacer molecules can be oppositely charged to improve interactions and disperse azobenzenes to provide more free volume around them. More free volume can also be provided with longer, bulkier substituents on azobenzene amphiphiles [5].

Using azobenzenes, Langmuir-Blodgett has been used to prepare photomagnetic organic-inorganic hybrid thin films with smectite clay as the inorganic material [61], hybrid thin films with several different metal phosphonates as the inorganic material [56] and with zirconium phosphonates using a combination of Langmuir-Blodgett and monolayer self-assembly methods [113].

4.2 Layer-by-layer self-assembly

Self-assembly technique uses chemisorption to form monolayers spontaneously when the substrate comes in contact with the solution. Chemisorption allows the molecules to move close to each other on the surface, using covalent or ionic bonds to bind to the surface. The method can be used to grow monolayers, multilayers or hybrid multilayers, and the deposited films have great conformity [110].

There are several self-assembly methods with slightly different processes. In in-situ self-assembly, inorganic particles are formed in the organic matrix through chemical reactions. In template-induced self-assembly, the template facilitates the self-assembling behavior of the molecules. The template can be a so-called soft template, without a rigid structure like polymers and small organic molecules, or a hard template, with a solid structure like powders and nanoparticles. Evaporation-induced

self-assembly relies on the evaporation of solvent from the template, which forms a hybrid mesophase from the non-volatile compounds [114].

The layer-by-layer assembly methods can also be categorized by the assembly technologies. Immersive assembly requires submersion of the substrate in the solutions containing the desired components with a washing step in between the different solutions. In spin assembly, the solutions are added dropwise on the spinning substrate one at a time, spreading over the substrate as a thin layer. In spray assembly, the components are sprayed on the substrate with washing sprays in between. Electromagnetic assembly requires an applied electric or magnetic field between two electrodes working as substrates in a solution. After the deposition of the first component, the substrate is washed and the electrodes are placed in the second solution with reversed polarities. Fluidic assembly uses fluidic channels to coat the channel walls or the substrate in the fluidic channel. The flow of the solution is usually achieved by using a pump, centrifugal force or capillary forces [115].

In the commonly used layer-by-layer electrostatic assembly, the components used to grow the hybrid thin films have opposite charges. The substrate is subsequently submerged into solutions each containing one of the desired charged components. The charges on the components repel each other, making the process self-limiting [110]. After each submersion, the substrate needs to be washed before submerging it into the solution containing the oppositely charged component [116]. The resulting thin films are uniform and the thickness is easy to control. In addition to electrostatic forces, the layer-by-layer self-assembly techniques can utilize for example hydrogen bonding, covalent bonding and hydrophobic interactions [114].

For azobenzenes, layer-by-layer self-assembly technique has been used in various applications. Layer-by-layer hybrid thin films have been prepared with LDHs as the inorganic matrix [11], with polyanions combined with ionenes containing azobenzene moieties to use in photoswitching and optical storage applications [117], polycations and bolaamphiphiles with azobenzene in the middle of the hydrocarbon chain [118] and polycations and azobenzene-containing polyanions with optical thickness

changing properties. Aggregation behavior of polymers [119] and bolaamphiphiles in self-assembled multilayers has also been observed [118].

The photoisomerization reaction of azobenzenes has also been investigated in self-assembled monolayers. Both the trans-cis isomerization reaction using UV radiation and the cis-trans back-isomerization reaction using blue light occur in self-assembled monolayers. The thermal cis-trans isomerization reaction is slow. Self-assembled monolayers of azobenzenes can also show photo-orientation with linearly polarized UV radiation [120].

4.3 Spin-coating

In spin-coating, the hybrid material is in a solution, which is applied dropwise on the substrate. The substrate is spun, causing the solution to spread evenly over the surface [110]. The centrifugal force causes the spreading and the subsequent flow of excess solution off the edge of the substrate. The thickness of the resulting film can be controlled by the rotation speed and therefore, the centrifugal force [116]. The solvent evaporates, leaving the hybrid material on the surface, often in a crystalline and oriented state. Dip-coating and spray-coating are also used for depositing hybrid thin films. The hybrid materials are often prepared by sol-gel processes before using the aforementioned coating methods to prepare the thin films [110].

Photoresponsive thin films have been prepared with spin-coating using polymers with azobenzene included in the backbone showing photo-orientation and subsequent crystallization [51]. Hybrid thin films have been made by spin-coating with azo dyes and a siloxane matrix working as a guest-host system showing photoreversible changes in refractive index, as well as using the sol-gel material to prepare nanofibers by electrospinning, showing reversible wettability of surfaces [12]. Multi-bilayered films using azobenzene polymer liquid crystals and polyvinyl alcohol with photoswitchable reflectance and structural color properties have been prepared by spin-coating [121]. Thin films containing several layered spiropyrans with

different absorbance spectra for use as multiple recording medium have also been prepared by spin-coating [8].

4.4 Intercalation

In intercalation reactions, molecules or ions are inserted into the structure of a material acting as a host. The host materials are often layered structures, where the intercalating species occupies the spaces between layers. The intercalation does not change the structure of the host material. However, it may change the interlayer spacing, depending on the size of the guest component [122]. Intercalation can be useful in situations when a suitable solution for the organic and inorganic components of the thin film cannot be found to use with other solvent-based techniques like self-assembly. Instead, a solution can be chosen in which the organic precursor is soluble but the inorganic precursor and the hybrid material are not [110].

Intercalation has been used to prepare photoresponsive hybrid thin films from azo dyes intercalated into LDHs, showing reversible wettability of the film [13], azobenzene derivatives intercalated into layered clay minerals as well as hexaniobate, both showing reversible change in the interlayer distance and nanosheet sliding for the hexaniobate, providing possible use in artificial muscles [123].

EXPERIMENTAL PART

5. Goal of experimental part

The purpose of the experiments was to determine if hybrid thin films containing azobenzene could be prepared with the combined ALD/MLD technique. The aim was to prepare films that show reversible photoresponsive properties. Superlattice thin films were of particular interest because of the possibility of changing the properties of the oxide with irradiation. The preparation of the films is described in Chapter 6.

The thickness, crystallinity, composition and photoresponsivity were analyzed using methods outlined in Chapter 7. The analysis results for the thin films are presented in Chapter 8. In Chapter 9, conclusions are made from the obtained results and the analyzed thin films are compared with one another, as well as with similar hybrid systems seen in literature**.** Suggestions for further research possibilities are made in Chapter 11.

6. Preparation of thin film samples

6.1 Choosing the precursors

The precursors for the depositions were chosen based on previous literature and limitations imposed by the ALD/MLD technique. For the organic photoresponsive molecule, azobenzene-4,4’-dicarboxylic acid (ADA) was chosen, as azobenzene has been used in hybrid thin films prepared with other methods. For ALD/MLD, the molecular weight needs to be low so that the molecule can be sublimed in the reactor at a low enough temperature without decomposition. Azobenzene is smaller than many other ring-structured photochromic molecules, which would make it more suitable as a precursor. Carboxylic acid substituents do not affect the rate of thermal

back-isomerization reaction, which simplifies the observation of the photoisomerization reaction by UV-Vis spectrometry.

Trimethylaluminium (TMA) is a widely used ALD precursor, as it is used together with water to prepare aluminium oxide films. This system is considered a model ALD system as the reactions are self-limiting and efficient, showing near-ideal ALD growth [124]. TMA has been used together with different types of organic molecular precursors, including aromatic carboxylic acids [125] to prepare inorganic-organic hybrid thin films. As ADA is similar to the precursors previously used with TMA, they were considered a viable combination for photoresponsive hybrid thin films.

6.2 Preparation of thin films with ALD/MLD

The thin film samples were prepared with the combined atomic/molecular layer deposition technique using F-120, ASM Microchemistry Ltd. as the reactor. The substrates used for the deposition were p-type silicon (Si(100), Okmetic Ltd). For the photoresponsivity measurements, the thin films were deposited on quartz substrates.

Atomic layer deposition (ALD) is a technique for preparing thin films with high uniformity and conformity. It is based on self-limiting surface reactions, providing atomic level control of the thickness of the film by saturating the substrate surface. This is done by pulsing the precursors into the chamber one at a time, separated by sufficient purging after each pulse to ensure that reactions happen only at the surface of the substrate. During one deposition cycle, each precursor is pulsed in the reactor once. The amount of cycles determines the film thickness. In molecular layer deposition (MLD), molecules are deposited on the substrate surface instead of atoms [124].

Hybrid inorganic-organic thin films can be deposited using a combination of atomic and molecular layer deposition. In this context, the term hybrid material refers to a material formed through a reaction between inorganic and organic components. In

such hybrid structures, the direct contact by covalent bonding between the inorganic and organic components can result in interesting combinations of properties. A simple hybrid thin film has alternating layers of the inorganic component and the organic component in 1:1 ratio. In superlattices, thicker inorganic layers usually consisting of oxides are separated by a single organic layer [2]. The ALD/MLD process cycle for a hybrid thin film deposited using TMA and ADA as precursors and an example of an ideal layered superlattice structure are presented in Figure 18.

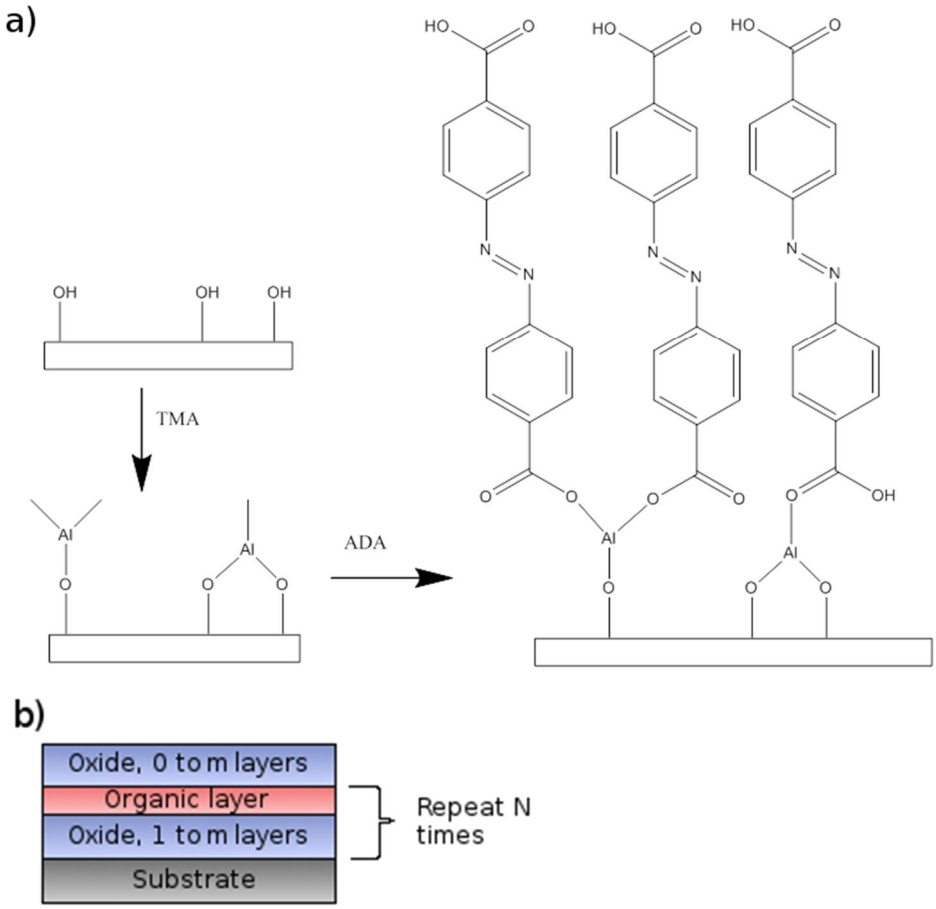

Figure 18. a) The ALD/MLD process cycle for TMA and ADA, b) an ideal superlattice structure.

The precursors used in the depositions were obtained commercially and used as received. TMA with 97 % purity (Sigma Aldrich, CAS: 75-24-1) was kept outside the reactor in a sealed container in room temperature. ADA with 95 % purity (TCI Europe N.V., CAS: 586-91-4) was sublimed in the reactor from an open glass container at the

sublimation temperature of the molecule. The water used to deposit aluminium oxide for the superlattice thin films was distilled water kept in a sealed vessel outside the reactor in room temperature. The carrier gas for the precursors and the purging gas was nitrogen with 99.999 % purity at 300 sccm, prepared from air with Schmidlin UHPN 3000 nitrogen generator.

The deposition parameters for the hybrid thin films were optimized to ensure the saturation of the substrate surfaces and homogeneity of the thin films. Linearity of the increase in film thickness upon increasing the amount of precursor cycles was also examined. The initial parameters used for the optimization are presented in Table 1.

Table 1. Starting parameters for the optimization of the TMA and ADA hybrid thin film process.

	ADA T_{sub} / °C	T_{dep} / °C	Pulse/purge lengths / s	Number of cycles
Hybrid	230	260	1.5/2/8/12	600

The parameters for the oxide layer growth for the superlattice thin films were kept the same for all depositions. The pulse and purge times for the TMA and water process were 1 second pulse of TMA with 3 seconds of purging, and 1 second pulse of water with 4 seconds of purging. The values were deemed suitable for the reactor by growing an oxide film with the corresponding parameters. The temperature for the superlattice depositions was 260 °C, the same temperature that was used for the hybrid thin films. The number of hybrid and oxide cycles used for the superlattice depositions are presented in Table 2.

Table 2. The sequencing of oxide and hybrid cycles in the superlattice thin films.

K/(K+m)	Al_2O_3:ADA ratio	Cycle	N
1:200	199:1	3x[(TMA/H_2O)x149+(ADA)x1]+1x[(TMA/H_2O)x150]	3
1:100	99:1	6x[(TMA/H_2O)x86+(ADA)x1]+1x[(TMA/H_2O)x87]	6
1:75	74:1	8x[(TMA/H_2O)x66+(ADA)x1]+1x[(TMA/H_2O)x67]	8
1:60	59:1	10x[(TMA/H_2O)x54+(ADA)x1]+1x[(TMA/H_2O)x55]	10
1:50	49:1	12x[(TMA/H_2O)x45+(ADA)x1]+1x[(TMA/H_2O)x46]	12
1:40	39:1	15x[(TMA/H_2O)x37+(ADA)x1]+1x[(TMA/H_2O)x38]	15
1:30	29:1	20x[(TMA/H_2O)x28+(ADA)x1]+1x[(TMA/H_2O)x29]	20
1:20	19:1	30x[(TMA/H_2O)x18+(ADA)x1]+1x[(TMA/H_2O)x19]	30
1:15	14:1	40x[(TMA/H_2O)x14+(ADA)x1]+1x[(TMA/H_2O)x15]	40

7. Characterization of thin film samples

7.1 X-ray reflectivity

The thicknesses and densities of the thin film samples were determined with x-ray reflectivity (XRR). The thicknesses were used to calculate the growth per cycle (GPC) values for the optimization of the hybrid thin film deposition. The analysis also gave information about the roughness of the surface of the films. The measurements were done with PANalytical X'Pert PRO diffractometer. The radiation used for the measurements was Cu K_α irradiation with the wavelength 1.5418740 Å. The measuring range for the reflection angle was 0.154-3.194°. The thicknesses were calculated with X'Pert Reflectivity program by using the direct method, determining the critical angle and the distance between the Kiessig fringes from the XRR graph. The calculated thickness values were then divided by the number of cycles used in the deposition to get the GPC values. The intensity and feature decay rate could be used to determine the roughness of the film. An example of an XRR graph with the aforementioned features used in characterization of the thin films marked is presented in Figure 19.

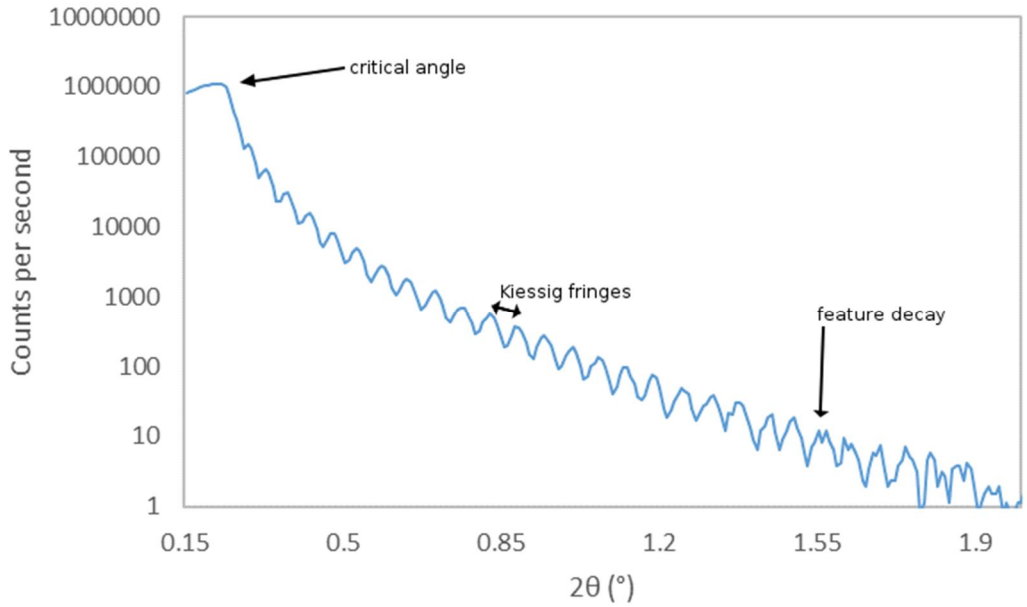

Figure 19. XRR graph for the superlattice thin film with K/(K+m) = 1:15, marked with features used in characterization of the thin films.

The densities of the hybrid thin films can be calculated from the critical angles obtained from the XRR graphs using Equation 1.

$$\rho_m = \frac{\rho_e A}{N_A Z} \quad (1)$$

where ρ_m density of the thin film

ρ_e average electron density

A average molecular weight

N_A Avogadro's constant

Z average atomic number.

The average electron density ρ_e can be calculated from Equation 2.

$$\rho_e = \frac{{\theta_c}^2 \pi}{\lambda^2 r_e} \quad (2)$$

where ρ_e average electron density

θ_c critical angle in radians

λ wavelength of x-rays

r_e classical electron radius.

7.2 Grazing incidence x-ray diffraction

The crystallinity of the films was determined with grazing incidence x-ray diffraction (GIXRD). The measurements were done with PANalytical X'Pert PRO diffractometer, using Cu K_α irradiation with the wavelength 1.5418740 Å. The incidence angle used in the measurements was 0.5° and the measuring range for the 2θ angle was 3.05-69.95°. The peaks were analyzed with X'Pert Data Viewer.

7.3 Fourier transform infrared spectroscopy

The bonding in the thin film samples was determined with Fourier transform infrared spectroscopy (FTIR). The measurements were done with Nicolet Protégé 760 spectrometer. The measurement range was 400-4000 cm^{-1} and the resolution was 2 cm^{-1}. Dry air was used as a purging gas for the spectrometer to get rid of carbon dioxide and water that affect the measurement. Spectra were measured for both the thin film sample and a plain silicon substrate, and the spectrum for the silicon substrate was subtracted from the sample spectrum to obtain the spectrum for the thin film only. The spectra were then used to identify functional groups and covalent bonds in the thin film.

7.4 Ultraviolet-visible light spectroscopy

Ultraviolet-visible light (UV-Vis) spectroscopy was used to identify the presence of the azobenzene moiety in the thin films. The measurements were done with Perkin Elmer Lambda 2 UV-Vis spectrometer. For the measurements, the hybrid and superlattice depositions were repeated on a quartz substrates and the absorbance was measured in the range of 200-1000 nm with a resolution of 1 nm and a scan rate of 240 nm/min. UV-Vis spectra were also measured for a solution of ADA in a quartz cuvette with a 1 cm light path.

Photoresponsivity of the thin film samples and the precursor solution was examined by measuring the UV-Vis absorption spectrum before and after irradiation with an UV lamp. The source was a Labino H135 UV lamp with 365 nm as the irradiation wavelength. The output power of the lamp was 35 Watts and the irradiance was 45 mW/cm^2 at a distance of 38 cm from the lamp. The spectra before and after irradiation were compared to evaluate the photochromic response from the change in the absorption spectra.

7.5 Atomic force microscopy

Atomic force microscopy (AFM) was used to determine possible changes in the roughness on the surface of the film due to photoisomerization. The microscope used in this work was TopoMetrix EXPLORER SPM with ThermoMicroscopes SPMLab software. The scan range was 10 µm with scan rate of 20.03 µm/s. The results were processed and analyzed with Gwyddion.

8. Results of thin film characterization

8.1 Characterization of hybrid thin films

The TMA and ADA process was optimized starting with the parameters shown in Table 1. The order of parameter optimization was sublimation temperature, deposition temperature, ADA pulse length and TMA pulse length. The optimized parameters were used to prove the ALD behavior of the process by showing linear increase in thickness of the film when cycles are increased. The optimization of the parameters are presented in Figures 20-24.

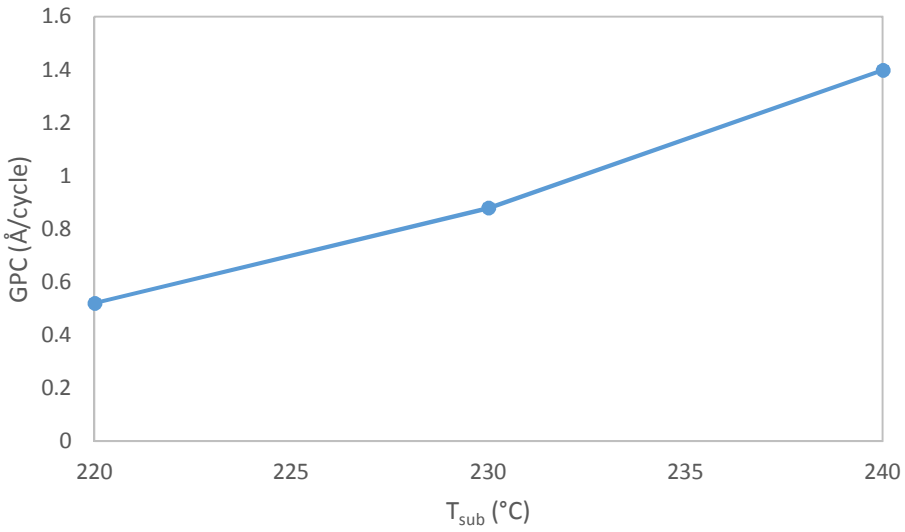

Figure 20. The optimization graph of sublimation temperature for the TMA and ADA process.

The sublimation temperature optimization was done with 200 deposition cycles. The graph shows an increase in the growth rate as the temperature is increased. However, at 240 °C the films become nonhomogeneous and a large gradient appears on the edge of the substrate. 230 °C was chosen as the sublimation temperature to have a good growth rate and film quality. Lower sublimation temperature also gave more control over the deposition temperature.

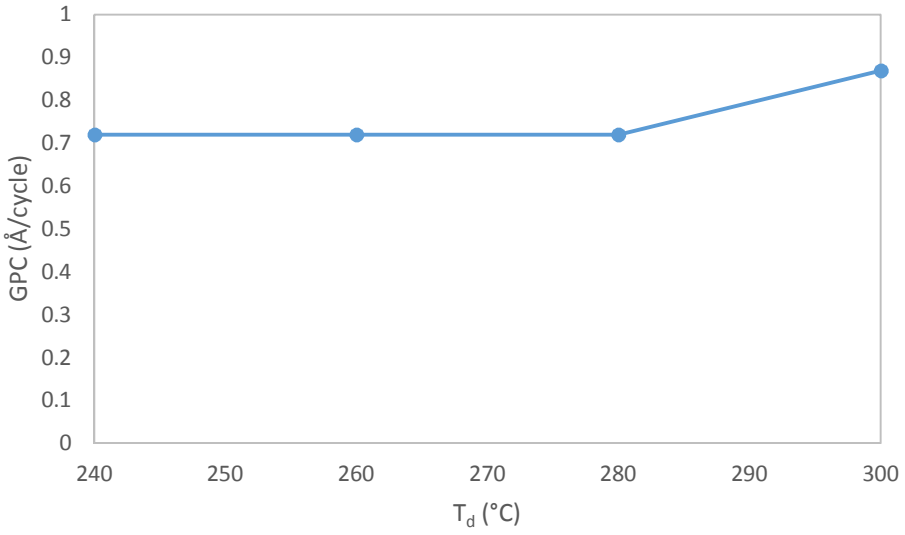

Figure 21. The optimization graph of deposition temperature for the TMA and ADA process.

The amount of cycles was increased from 200 to 600 for the rest of the optimization depositions to make the measurement of film thickness with XRR more accurate. As the thickness of the films was increased, a gradient appeared at the edge of the substrate, similar to the gradient previously seen for the film deposited using 240 °C as the sublimation temperature. The graph shows that deposition temperature does not affect the growth rate between 240 °C and 280 °C. At 300 °C, the thickness of the film increases, the film becomes rougher and the gradient becomes larger. 260 °C was chosen as the deposition temperature for further depositions.

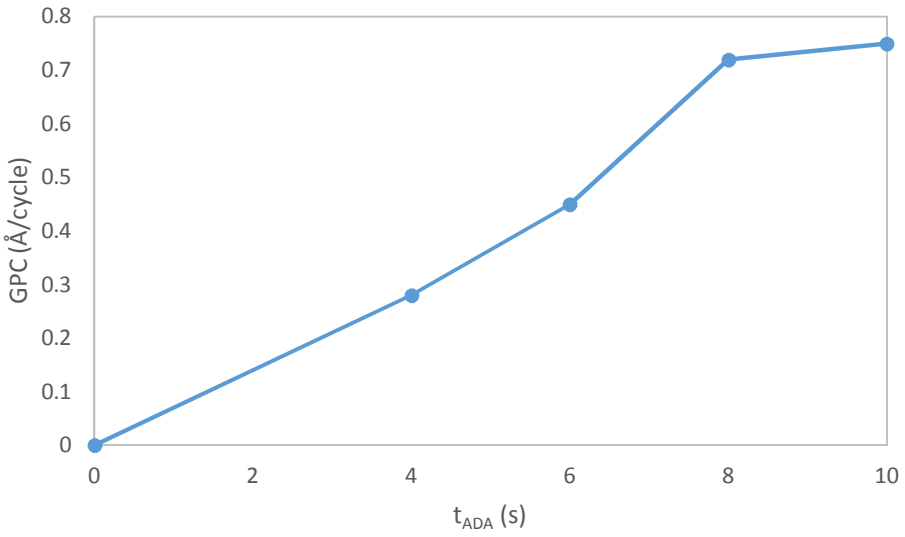

Figure 22. The optimization graph of the pulse time of ADA for the TMA and ADA acid process.

The increase of the pulse time of the precursor increases the growth rate between 4 and 8 seconds. At 8 seconds, saturation is reached and at 10 seconds, the growth rate is approximately the same as for 8 seconds. When pulse time is increased, the gradient on the edge of the substrate grows in size. Even though the thickness of the film does not substantially increase between 8 and 10 seconds, the gradient for the sample with the 10 second pulse time is much larger. 8 seconds was chosen as the pulse time as it was enough for saturation of the substrate surface.

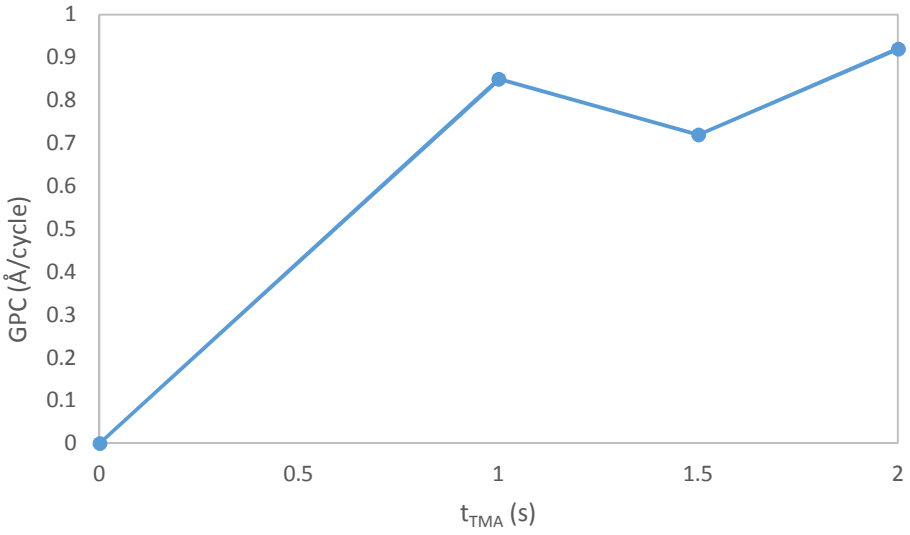

Figure 23. The optimization graph of the pulse time of TMA for the TMA and ADA process.

The graph for the TMA pulse length shows that the surface is already saturated with a pulse length of 1 second. The sample with a pulse length of 1.5 seconds had a slightly lower growth rate but the gradient on the edge of the substrate was considerably smaller than for the other two samples, possibly due to the differences in the shape of the substrates. The other two samples were also rougher, which may have affected the thickness measurement with XRR. For these reasons, 1.5 seconds was chosen as the pulse length for TMA for later depositions.

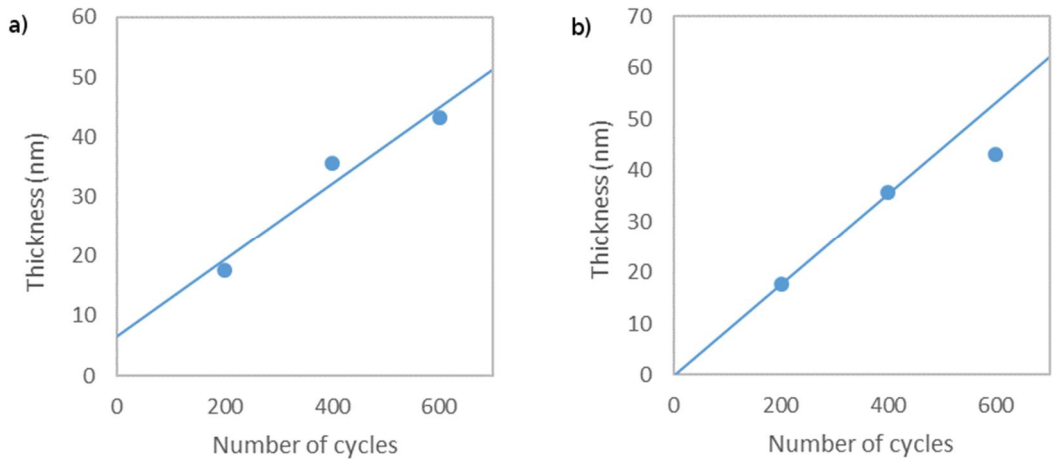

Figure 24. ALD behavior of the TMA and ADA process. a) Linear trendline drawn for all three data points, b) linear trendline drawn through the origin and the data points for the samples with 200 and 400 deposition cycles.

The trend line for all three data points fits the data points reasonably well, showing an increase in film thickness as the amount of cycles is increased. However, the trend line does not intercept at origin and the increase is not linear, as the growth rate of the film at 200 and 400 cycles is the same, but seems to decrease at 600 cycles. This is seen clearly in the trend line drawn through origin and the first two data points. The decrease in growth rate for thicker films may be caused by double surface reactions. As the number of cycles increases, double surface reactions decrease the amount of active surface sites available for the precursors to react with after each deposition cycle, therefore slowing the growth. For films with more than 600 cycles, the films became too rough to measure the thickness with XRR.

The density of the film deposited with the optimized parameters using 600 deposition cycles was calculated with Equations 1 and 2. It was assumed that the thin films consist of the pure hybrid.

$$\mathrm{A(Al-ADA)}$$
$$= \frac{(26.981 + 4 \cdot 15.999 + 10 \cdot 1.008 + 14 \cdot 12{,}011 + 2 \cdot 14.007)\ \mathrm{g/mol}}{31}$$
$$= 5.003\ \mathrm{g/mol}$$

$$Z = \frac{13 + 4 \cdot 8 + 10 \cdot 1 + 14 \cdot 6 + 2 \cdot 7}{31} = 2.871$$

$$\rho_e = \frac{{\theta_c}^2 \pi}{\lambda^2 r_e} = \frac{0.00325^2 \cdot \pi}{(1.54 \cdot 10^{-10}\mathrm{m})^2 \cdot 2.82 \cdot 10^{-15}\mathrm{m}} = 4.950 \cdot 10^{29}\mathrm{m}^{-3}$$

$$\rho_m = \frac{\rho_e A}{N_A Z} = \frac{4.950 \cdot 10^{29}\mathrm{m}^{-3} \cdot 5.003\ \mathrm{g/mol}}{6.022 \cdot 10^{23}\mathrm{mol}^{-1} \cdot 2.871} = 1.432 \cdot 10^6\ \mathrm{g/m^3} = 1.43\ \mathrm{g/cm^3}$$

The calculated density for the optimized thin film was therefore 1.43 g/cm^3. Some variation in the film density was seen during optimization, but this was due to the films being too thin and therefore showing only the critical angle for the silicon substrate. Thicker films all had the same density calculated above.

Attempts were made to improve the quality and homogeneity of the hybrid thin films. Changing the pulse and purge times of TMA showed a slight effect on the thin film quality. With shorter TMA pulse and purge times, the gradient on the film was smaller and the quality was improved. Decreasing the vapor pressure of TMA with the needle valve also improved the film quality slightly. Changing the pulse and purge times of ADA did not affect the film quality in the same way. Shorter pulse and purge times made the film thinner, whereas longer pulse and purge times made the film rougher.

Lowering both the sublimation and deposition temperatures was attempted to make the films more homogenous, but no substantial improvement was observed. Different positions for the substrate and different sample holders were also tried, but the quality of the films did not improve. When the deposition was done using two substrates parallel to direction of the flow, the first sample showed a large gradient, whereas the second sample was almost homogenous.

During the deposition of the superlattices, it was discovered that one of the valves connected to the TMA line was leaking, which affected the quality of the superlattice films. It is therefore possible that the valve had been leaking earlier during the depositions of the hybrid thin films and affected their quality. After the valve was

changed, a hybrid thin film with the optimized parameters was deposited to see the possible effect of the leaking valve. The film had a smaller gradient, but the growth rate was also considerably smaller at 0.36 Å/cycle compared to the 0.72 Å/cycle for the hybrid thin films deposited earlier. It was unclear if the decreased growth rate was caused by changing the valve or if something else changed the flow in the reactor for example during maintenance. The smaller gradient was likely related to the decreased growth rate, as it was seen during optimization that thinner films had smaller gradients.

The crystallinity of the hybrid thin films was determined with GIXRD. GIXRD graph for the hybrid thin film deposited using the optimized parameters is presented in Figure 25.

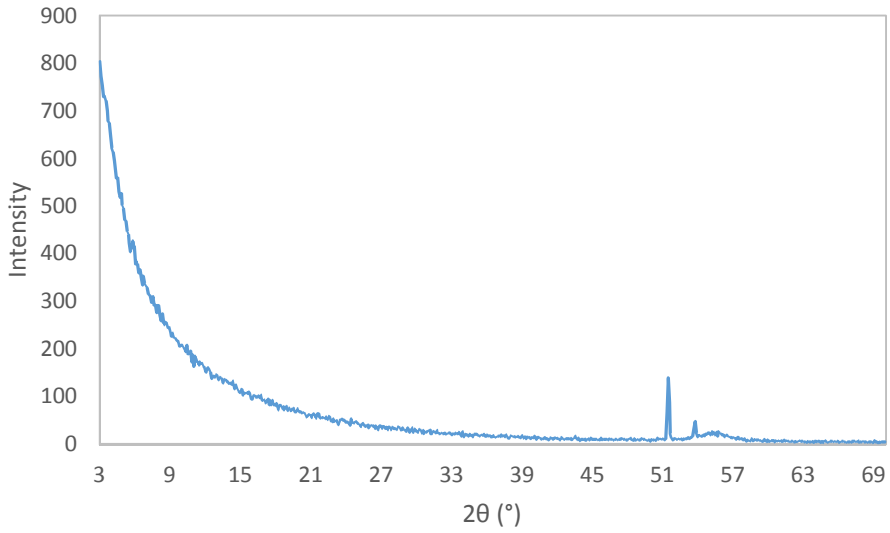

Figure 25. GIXRD for the hybrid film deposited with the optimized TMA and ADA process.

The GIXRD graph shows that the hybrid film is amorphous. Only two peaks are seen in the graph at 51.55° and 53.75°. These can be attributed to the silicon substrate. None of the hybrid films deposited during the optimization showed peaks that could be assigned to the film, which suggests all hybrid films were amorphous.

The bonding in the hybrid films was examined with FTIR. As an example, FTIR spectra of a hybrid film with optimized parameters and the azobenzene precursor are presented in Figure 26.

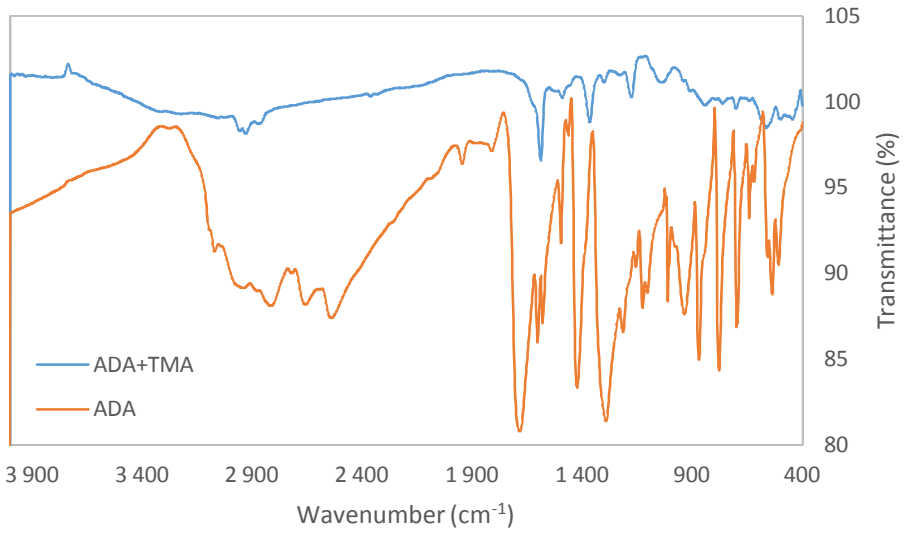

Figure 26. FTIR of the precursor and the hybrid thin film deposited with the optimized TMA and ADA process.

The FTIR spectrum for the hybrid film shows strong peaks at 1032 cm^{-1}, 1176 cm^{-1}, 1365 cm^{-1} and 1587 cm^{-1}. The sharp peak at 1684 cm^{-1} in the spectrum for the precursor is associated with the asymmetric stretching of the carbon-oxygen double bond. Other peaks seen for carboxylic acid groups are a very broad and intense band at 2500-3300 cm^{-1} for the oxygen-hydrogen stretching, 1395-1440 cm^{-1} for the oxygen-hydrogen bending, 1210-1320 cm^{-1} for the carbon-oxygen stretching and 920 cm^{-1} for the out-of-plane bending of the oxygen-hydrogen bond [126]. The peak at 1684 cm^{-1} is not seen in the spectrum for the hybrid film, meaning free, unbound carboxylic acid groups are not present in the hybrid structure. The carboxylate anion shows two bands in FTIR spectra, asymmetric stretching at 1550-1650 cm^{-1} and symmetric stretching near 1400 cm^{-1} [126]. The splitting of these peaks can be used to determine the type of complexation between the carboxylate group and the aluminium atoms. Bidentate complexes show splitting between 50 and 150 cm^{-1}, bridging complexes show splitting between 130 and 200 cm^{-1} and unidentate show splitting at values over 200 cm^{-1} [127]. In the spectrum for the hybrid film, these peaks

are seen at 1365 cm^{-1} and 1587 cm^{-1}. Therefore, it is reasonable to assume that the azobenzene precursor has reacted with and bound to TMA in the hybrid films. The separation of the peaks is 222 cm^{-1}, which suggests the formation of a unidentate complex between aluminium and carboxylate groups as the dominating binding geometry. The different coordination types between aluminium atoms and carboxylate groups are presented in Figure 27. The peaks between 2800 and 3000 cm^{-1} are related to the stretching vibrations of carbon-hydrogen bonds. The peak at 1225 cm^{-1} is related to the carbon-nitrogen asymmetric stretch. Smaller peaks seen at 1490 cm^{-1}, 1300 cm^{-1}, 1174 cm^{-1}, 1032 cm^{-1} and 841 cm^{-1} are all related to carbon-carbon stretching and carbon-hydrogen bending vibrations in the benzene ring [128].

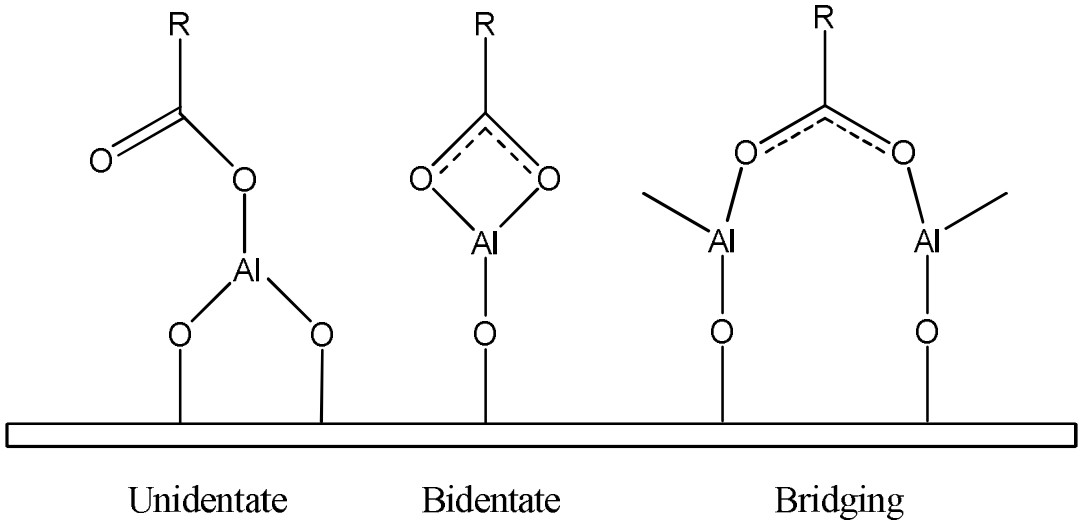

Figure 27. The types of complexes between aluminium and carboxylate group [125].

8.2 Characterization of superlattice thin films

The thicknesses of the superlattice films were measured with XRR to monitor the effect of superlattice period thickness to the growth rate of the films. XRR was also used to examine the superlattice structure. The growth rate as a function of the ratio of organic layers to total number of layers is presented in Figure 28. The XRR graphs are presented in Figure 29.

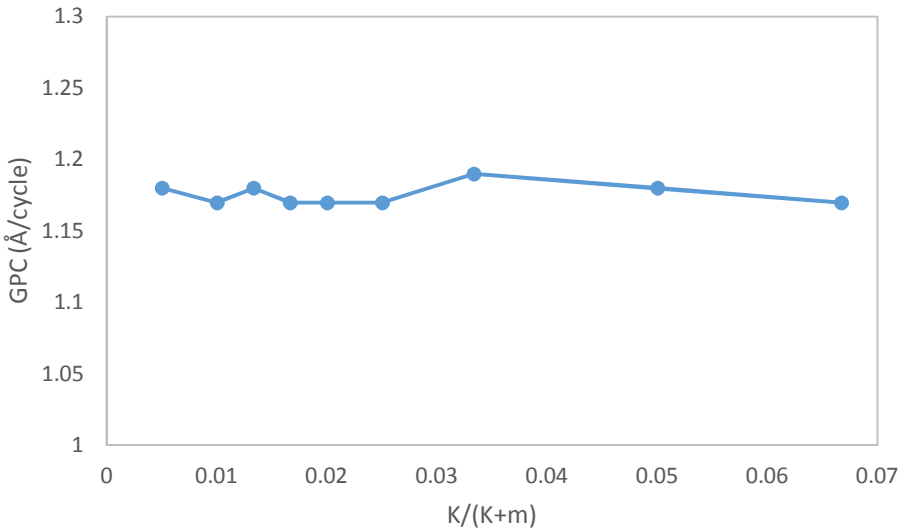

Figure 28. The growth rates of the superlattice thin films as a function of the ratio of organic layers to total number of layers.

The ratio of organic layers to total number of layers does not affect the growth rate in the observed range. For all superlattice thin films, the growth rate was between 1.17 and 1.19 Å/cycle. This may be because the growth rates for the TMA and ADA process and the TMA and water process are close to one another. The growth rate for oxide thin films deposited in this work was 1.20 Å/cycle. All the deposited superlattice films were homogenous with no visible gradients on the sample surface.

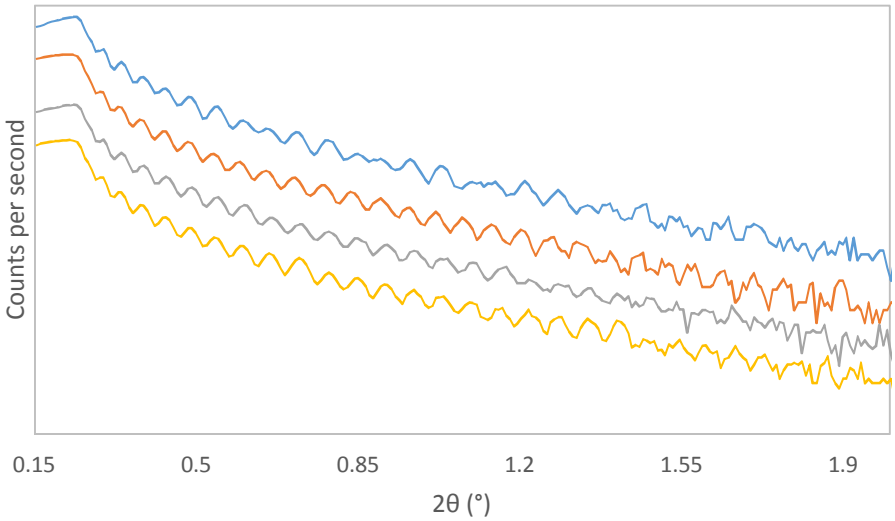

Figure 29. XRR graphs for the superlattice thin films with K/(K+m) = 1:200, 1:100, 1:75 and 1:60.

The XRR graphs do not show the peak structure often seen for superlattices. This may be because the growth rates of the inorganic and organic layers are close to one another and the layers cannot be distinguished from one another using XRR. The sample with K/(K+m) = 1:200 and N = 3 seems to show a pattern that is similar to those seen in superlattice films. However, the peaks do not follow the N-2 rule seen for superlattices, where the peaks with higher intensities are separated by N-2 peaks. Instead, the graph shows 2 peaks with higher intensities followed by 2 peaks with lower intensities. The rest of the graphs seem to have some peaks with slightly higher intensities, but no superlattice structure can be determined, as the distinction is not clear enough.

GIXRD was used for examining the crystallinity of the superlattice thin films. As an example, GIXRD graph for the superlattice with the highest ratio of organic layers to total number of layers is presented in Figure 30.

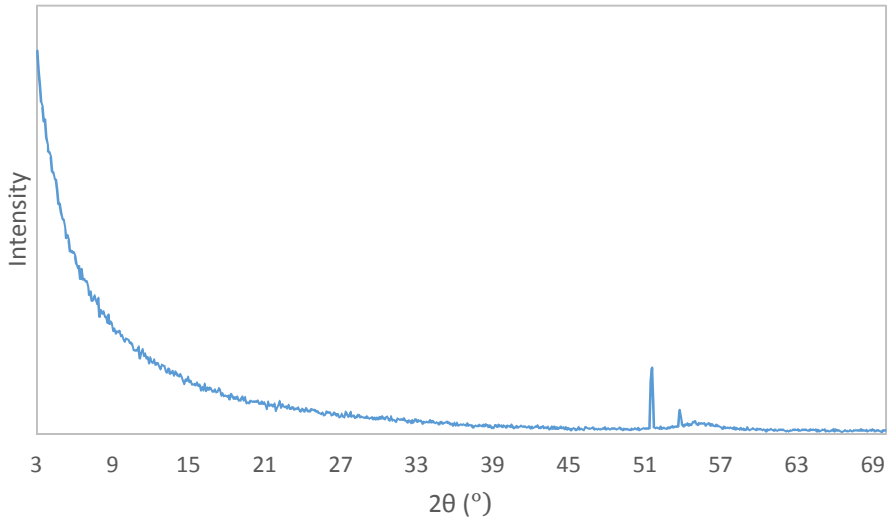

Figure 30. GIXRD for the superlattice thin film with K/(K+m) = 1:15.

All superlattice films are amorphous, since no peaks attributable to the thin film can be seen in the GIXRD spectra. The peaks at 51.55° and 53.75° are related to the silicon substrate. Aluminium oxide deposited with ALD is always amorphous in the temperature range used in these depositions. Crystalline phases have been deposited at higher temperatures with other precursors [129].

FTIR was used for determining the structure of the superlattice films, specifically the bonds between the atoms in the superlattice. The FTIR spectrum for the superlattice with the largest amount of organic, with the ratio K/(K+m) = 1:15 is presented in Figure 31. The FTIR spectra for all superlattice samples are presented in Figure 32.

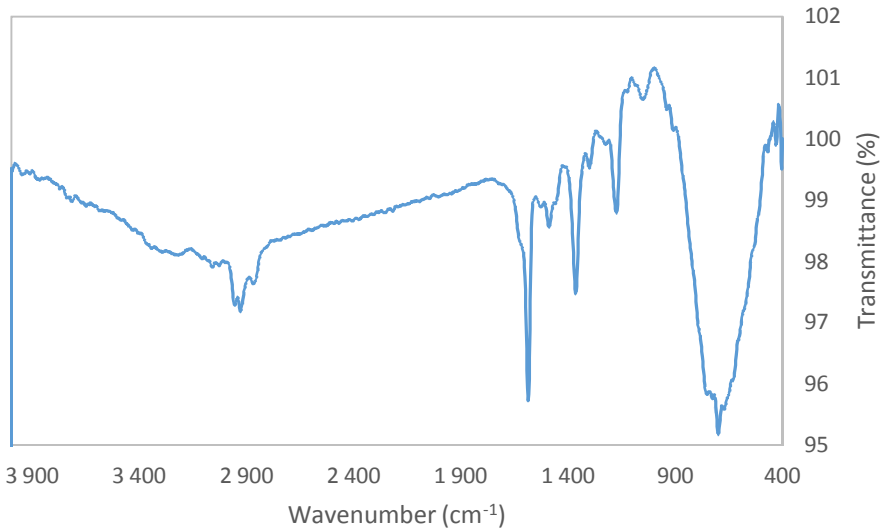

Figure 31. FTIR spectrum for the superlattice thin film with the ratio K/(K+m) = 1:15.

The FTIR spectrum for the superlattice film shows the same strong peaks at 1176 cm^{-1}, 1365 cm^{-1} and 1587 cm^{-1} seen in the hybrid film spectrum. The sharp peak at 1684 cm^{-1} is not seen in the spectrum, suggesting that all carboxylic acid groups in the superlattice film are bound to aluminium, correlating to the carboxylate peaks at 1365 cm^{-1} and 1587 cm^{-1} like in the hybrid films. Other smaller peaks, such as those related to the carbon-carbon and carbon-hydrogen vibrations in the benzene ring are at same positions as seen in the hybrid film spectrum in Figure 26. The broad, strong absorption band centered near 700 cm^{-1} comes from the aluminium oxide. The disordered, amorphous film has a large number of oscillators with slightly varying aluminium-oxygen stretching vibrations, resulting in the broadening of the peak [130].

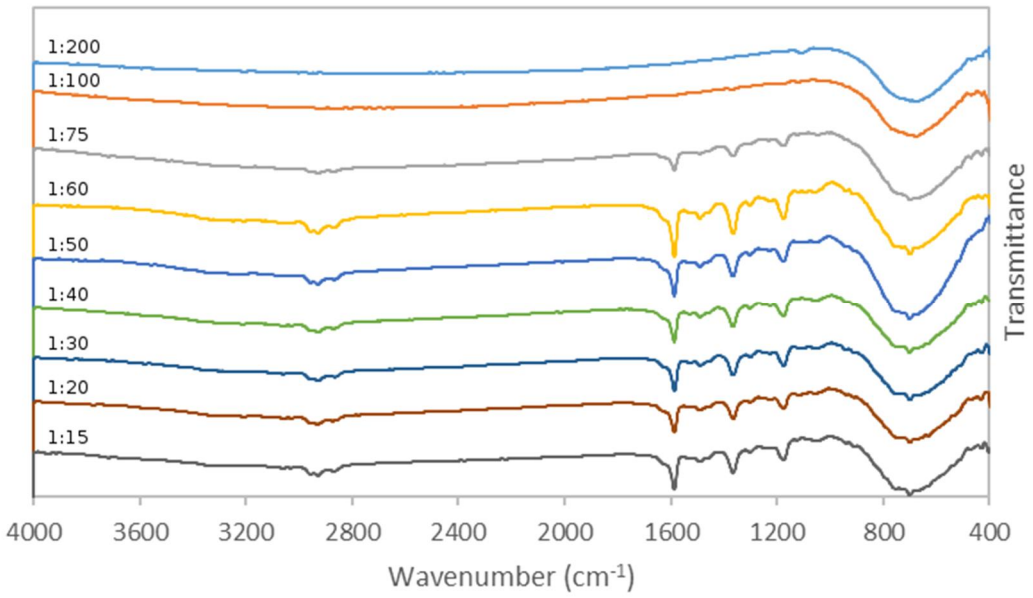

Figure 32. FTIR graphs for the superlattice thin films.

The superlattice thin film with K/(K+m) = 1:200 does not appear to show peaks that could be attributed to the azobenzene precursor. Only the large peak attributed to aluminium oxide can be seen at 400-1000 cm^{-1}. In the spectrum for the K/(K+m) = 1:100 sample, the three major peaks can be seen with very small intensities. As the amount of organic material in the film increases, the peaks become more distinguishable. All major peaks are at the same positions, suggesting no differences in bonding of the organic layer in the superlattice films.

8.3 Photoresponsivity of the thin films

A 10^{-5} M solution of ADA was prepared to measure the absorption spectrum of the precursor using water as the solvent. The solution was made basic by adding 2 M sodium hydroxide to help dissolve the azobenzene precursor. The absorption spectrum was measured before irradiation and after 15, 30, 45 and 60 minutes of irradiation with a UV-Vis spectrometer. After this, the sample was irradiated with visible light for 30 minutes and 45 minutes to examine the reversibility of the photoisomerization reaction. To investigate the thermal back-isomerization of the precursor solution, the sample irradiated with UV light was kept in the dark. The

absorption spectrum was measured again after 5000 minutes. The spectra for the UV irradiation, visible light irradiation and thermal relaxation of ADA are presented in Figure 33.

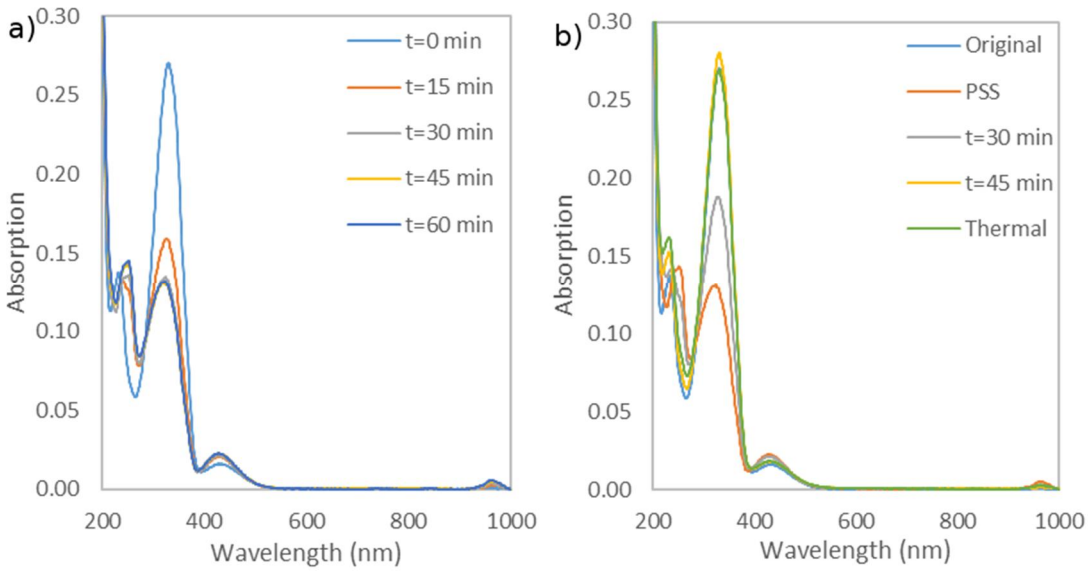

Figure 33. a) The absorption spectra of ADA in aqueous solution before and after 15, 30, 45 and 60 minutes of irradiation, b) the absorption spectra of ADA in aqueous solution before UV irradiation, in the PSS, after 30 and 45 minutes of irradiation with visible light and after 5000 minutes of thermal relaxation.

The spectrum before irradiation shows peaks at 232 nm and 330 nm corresponding to the (π, π*) transition and a peak at 436 nm corresponding to the (n, π*) transition. After 15 minutes of irradiation, the peak at 232 nm disappears. The peak at 330 nm decreases in intensity and the peak at 436 nm increases in intensity until PSS is reached at 45 minutes. A new peak appears at 252 nm after 15 minutes of irradiation, corresponding to the (n, π*) transition. The intensity of this peak increases until PSS is reached. A very small peak also appears at 964 nm, increasing in intensity until PSS is reached. This peak may result from a two-photon excitation process related to the (n, π*) transition. After 60 minutes of irradiation, intensities of all the peaks remained the same as they were after 45 minutes, indicating that PSS had been reached. As the decreasing peaks for the (π, π*) transition are related to the trans-isomer and the increasing peaks for the (n, π*) transition are related to the cis-isomer, this proves

that photoisomerization is taking place and the trans-isomer is being converted to the cis-isomer.

After reaching PSS under UV irradiation, exposure to subsequent visible light irradiation gradually returns the absorption spectra back to the intensities seen before UV irradiation. The reversibility is seen in all peaks at the observed range. At shorter wavelengths, especially for the peak at 232 nm, the intensities are not the exact same before UV irradiation and after visible light irradiation, but this is likely to be related to a measurement error and not a change in the sample.

For the sample kept in dark for 5000 minutes after irradiation, the peak at 330 nm is equal in intensity to the peak seen in the sample before irradiation. This proves that the precursor undergoes reversible thermal back-isomerization in solution, and the cis-isomer is thermally unstable. The other peaks return to their intensities before irradiation as well, although some variation is seen. The peak at 232 nm is higher in intensity after the thermal back-isomerization, but this may again be due to the inaccuracy of the spectrometer at lower wavelengths.

The absorption spectrum of the hybrid thin film deposited on quartz was measured before irradiation to verify the presence of the azobenzene moiety in the film and to compare the absorption of the film to the absorption of the precursor solution. The growth rate of the hybrid film on quartz was 1.80 Å/cycle, which is much higher than the growth rate on silicon, 0.72 Å/cycle. However, this is likely due to the gradient in the hybrid process covering the measured area in XRR. Because of smaller size of the quartz substrate compared to the silicon substrates used in the depositions, the gradient covers more of the substrate surface affecting the determination of the film thickness. The hybrid thin film was irradiated with a UV lamp to induce photoisomerization. The effect of the irradiation was examined by measuring the absorption spectra every 45 minutes with a UV-Vis spectrometer. After UV irradiation, the hybrid thin film was kept in the dark for 2500 minutes to examine the thermal back-reaction and the absorption spectrum was measured. The UV irradiated sample was also irradiated with visible light for 45 minutes and the absorption

spectrum was measured again. The absorption spectra of the hybrid thin film before and after UV irradiation and the spectrum for the precursor solution are presented in Figure 34, as well as the spectra after thermal relaxation and after visible light irradiation.

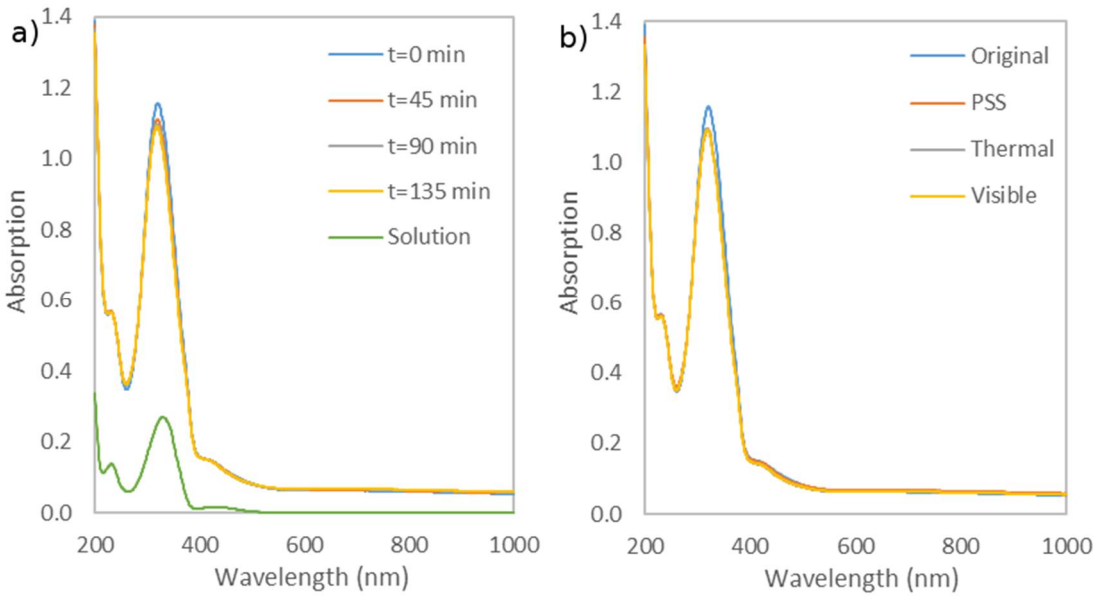

Figure 34. a) The absorption spectra of ADA in aqueous solution and the hybrid film deposited with the optimized TMA and ADA process before and after 45, 90 and 135 minutes of UV irradiation, b) the absorption spectra of the hybrid thin film before irradiation, in the PSS, after 2500 minutes in the dark and after 45 minutes of visible light irradiation.

The hybrid thin film shows the peak for the (π, π*) transition at 321 nm with high intensity. The peak has been shifted to a shorter wavelength when compared to the peak in solution at 330 nm, likely due to interaction between azobenzene and aluminium. The peak at 231 nm has also been slightly shifted to a shorter wavelength from 233 nm in solution. A distinct peak for the (n, π*) transition at 436 nm in solution is not seen in the hybrid thin film. The absorption seems to decrease overall with longer wavelengths, but between 415 and 418 nm the absorption stays almost constant. It is possible that this is related to the (n, π*) transition, but has been shifted to shorter wavelengths like the other peaks.

Irradiating the hybrid thin film induced partial photoisomerization. After 45 minutes of UV irradiation, the intensity of the peak at 321 nm decreased slightly, and the other peaks showed no change in intensity. Further irradiation decreased the intensity only marginally, and the intensity of the peak at 321 was the same after 90 minutes and 135 minutes. This suggests PSS was reached at 90 minutes.

After the film was kept in the dark for 2500 minutes, the intensity of the peak at 321 nm did not increase. Furthermore, no increase was seen after irradiation for 45 minutes with visible light. The UV-induced isomerization in the hybrid thin film does not seem to be reversible, as the original intensity was not reached with visible light irradiation or by thermal back-reaction.

The absorption spectra of the superlattice thin films were measured before irradiation. Superlattices with K/(K+m) = 1:2, 1:6, 1:15, 1:30 and 1:60, as well as an aluminium oxide film for comparison were deposited on quartz for the measurements. The growth rates for the superlattices grown on quartz were between 1.26 and 1.28 Å/cycle, slightly smaller than the growth rate of the oxide on quartz at 1.30 Å/cycle, but higher than the superlattice thin films deposited on silicon substrates. The thickness of the superlattice with K/(K+m) = 1:2 could not be measured. This is likely due to the roughness of the film caused by the gradient present in the hybrid process, similar to the increased thickness caused by the gradient seen on the hybrid thin film on quartz. To examine the photoresponsivity, the superlattice thin films were irradiated for 45 minutes, after which the absorption spectrum was measured again. The absorption spectra for the superlattice thin films before and after UV irradiation are presented in Figures 35-36.

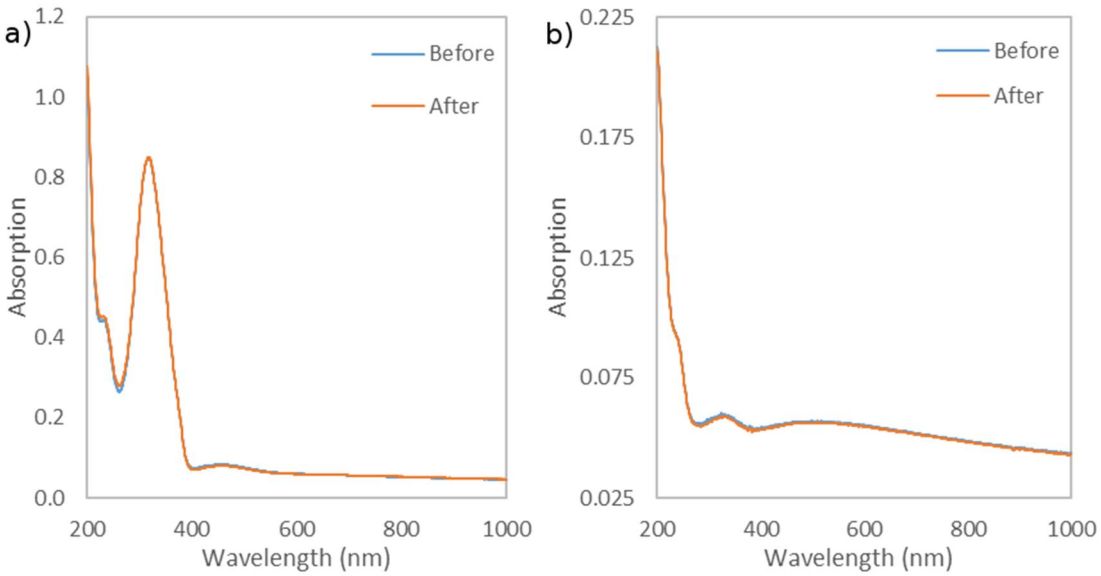

Figure 35. a) The UV-Vis absorption spectra of the K/(K+m) = 1:2 superlattice thin film before and after irradiation, b) The UV-Vis absorption spectra of the K/(K+m) = 1:6 superlattice thin film before and after irradiation.

The superlattice thin film with K/(K+m) = 1:2 shows the (π, π*) transition peaks at 317 nm and 230 nm clearly. Another peak can be seen at 454 nm, which may be related to the (n, π*) transition, but as it is at a higher wavelength than the peak seen for the solution, it is also possible that the peak is related to the aluminium oxide or caused by the spectrometer. Irradiating the thin film for 45 minutes had no effect on the absorption spectrum apart from minor differences below 300 nm, possibly due to inaccuracy of the spectrometer.

The K/(K+m) = 1:6 superlattice thin film shows the (π, π*) transition peak at 324 nm with very weak intensity. The peak or shoulder seen at 234 nm may be related to the second (π, π*) transition peak. No peak is seen in the absorption spectrum that can be attributed to the (n, π*) transition. This is due to the decreased amount of azobenzene present in the film, lowering the intensity of all peaks related to azobenzene. As the (n, π*) transition peak was already very low in intensity in solution, in thin films it disappears completely when the amount of azobenzene decreases. After 45 minutes of irradiation, no notable differences were seen in the absorption spectrum.

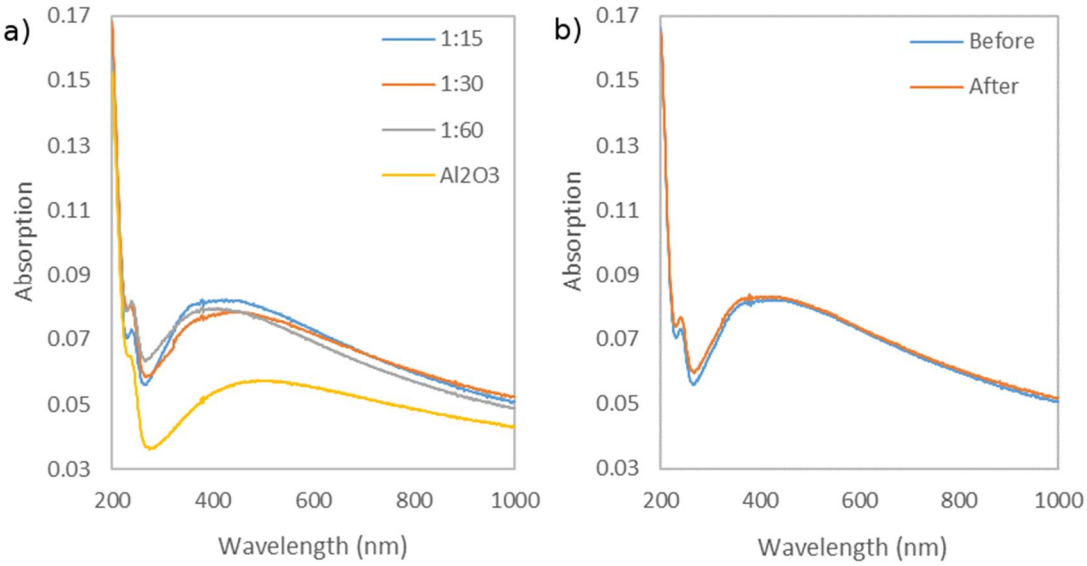

Figure 36. a) The UV-Vis absorption spectra of the K/(K+m) = 1:15, 1:30 and 1:60 superlattice and aluminium oxide thin films before irradiation, b) The UV-Vis absorption spectra of the K/(K+m) = 1:15 after 45 minutes of UV irradiation.

The superlattice thin films have a slightly higher absorbance than the aluminium oxide thin film. In the superlattice spectra, no clear absorption peak can be seen that could be attributed to the azobenzene precursor. In the spectra for K/(K+m) = 1:30, a slight increase in the absorbance at 320 nm can be seen. This would roughly correspond to the (π, π*) transition of azobenzene, but as the other superlattice spectra do not show a similar increase, the increase may also have been caused by an error during measurement. The absorption peak at 240 nm could be related to the weaker (π, π*) transition seen at 232 nm for the azobenzene precursor, but the aluminium oxide thin film also shows a small peak or shoulder at this wavelength, thus making it unlikely to be related to azobenzene. Aluminium oxide thin films with comparable thicknesses grown on quartz substrates do not show a peak at this wavelength [131], making the peak at this wavelength more likely to be caused by the spectrometer.

The absorption spectra before and after irradiation look mostly the same for the superlattice thin film with K/(K+m) = 1:15. The absorption intensities are slightly

higher after irradiation of the sample throughout the entire range. As the intensity of the major absorption peak at 316 nm should decrease in intensity when the sample is irradiated, it is unlikely that the changes in the spectra are caused by photoisomerization. The superlattices with K/(K+m) = 1:30 and 1:60 similarly showed a slight overall increase in absorption with no peaks that can be attributed to azobenzene. The changes in intensity are more likely related to the spectrometer itself or the position of the sample in the spectrometer.

To see if photoisomerization could be improved by having the azobenzene moiety only on the surface of the film to increase the free volume around it, a film was deposited with approximately 40 nm of aluminium oxide followed by an hour-long pulse of ADA to ensure full saturation of the surface. The absorption spectra of the film before and after irradiation are presented in Figure 37.

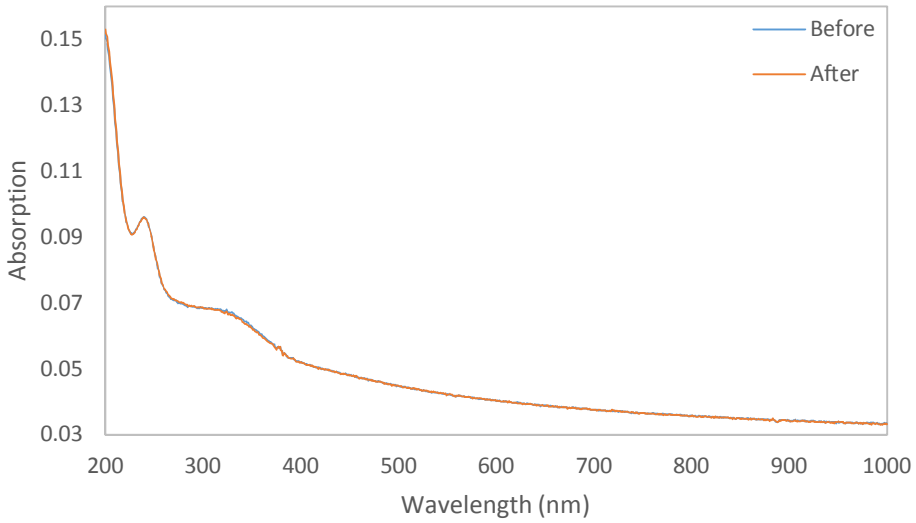

Figure 37. The absorption spectra of aluminium oxide thin film with a surface saturated with ADA before and after UV irradiation.

The film shows a peak centered approximately at 330 nm, which corresponds to the (π, π^*) transition of azobenzene. The other peaks for azobenzene transitions cannot be seen in the spectra. The peak at 244 nm is likely either caused by the spectrometer or related to the aluminium oxide, as the peak was seen in all of the superlattices as well as the aluminium oxide film. After 45 minutes of irradiation, the absorption

spectrum looks almost identical to the spectrum before irradiation. The peak at 330 nm seems to decrease in intensity after irradiation, but as the intensity of the peak is low even before irradiation, the change is negligible and therefore it is difficult to determine if this is due to photoisomerization occurring on the surface or inconsistency of the spectrometer.

The aluminium oxide thin film with the surface saturated with ADA was analyzed with AFM before irradiation and after 45 minutes of UV irradiation to see if photoisomerization changes the roughness of the surface. The AFM measurements are presented in Figure 38.

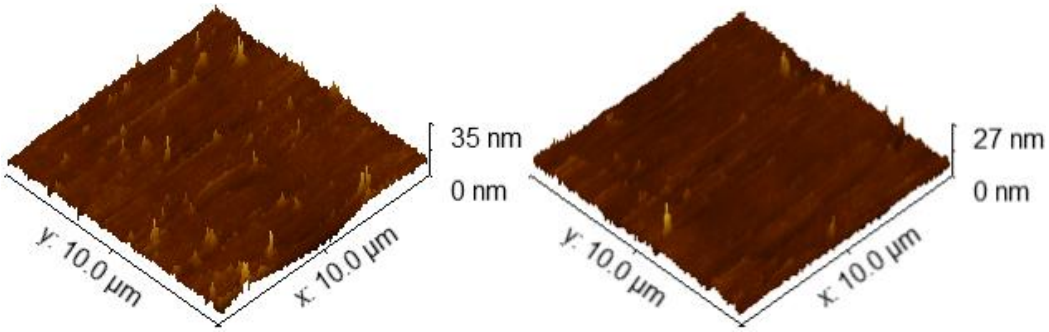

Figure 38. AFM measurements for the aluminium oxide thin film with a surface saturated with ADA before irradiation (left) and after 45 minutes of UV irradiation (right).

Comparing the images taken before and after irradiation, the roughness of the surface seems to have decreased slightly. The peaks seen on the surface are smaller and less peaks are seen overall after irradiation. The root mean squared roughness calculated for the sample is 1.19 nm before irradiation and 0.95 nm after irradiation. This could be a result of the molecules changing from the stick-like trans-isomer pointing away from the surface to the more compact, bent cis-isomer, reducing the roughness of the surface. Because the calculated roughness can change to some degree depending on the measured position on the surface, it cannot be conclusively determined that the change seen here is due to photoisomerization, but it is possible that at least some of the azobenzene molecules on the surface change conformation after irradiation.

9. Comparison of results and conclusions

Hybrid thin films were successfully deposited using the ALD process for the TMA and ADA precursors. FTIR and UV-Vis measurements prove that the azobenzene precursor is present in the thin films as FTIR shows the expected bonding and UV-Vis confirms that the azo group absorbs light at expected wavelengths. Based on these results, it can be concluded that the composition of the thin films is that of the desired material and that the developed process works.

The optimization of the TMA and ADA process showed a stable growth rate of 0.72 Å/cycle, but was unable to yield fully homogenous films. Previous ALD processes of TMA with aromatic carboxylic acids had growth rates between 2.5 and 13.5 Å/cycle [125]. The smaller growth rate measured here cannot be explained with the size of the precursor, as ADA is a larger molecule than the previously used aromatic carboxylic acid precursors. The low growth rate could be explained by the prevalence of double surface reactions or tilting of the organic molecules in the process. The non-linearity in the ALD behavior graph also seemed to suggest that double surface reactions do occur in the process. Both carboxylic acid groups of the molecule can react with the surface during the precursor pulse, making the azobenzene molecule lie parallel to the surface. The organic precursor may also tilt from the ideal perpendicular direction relative to the surface and cause steric hindrance. This limits active surface sites as well as decreases the thickness of the organic layer, lowering the growth rate [132]. ADA has shown significant tilting on gold surfaces when used as a linker molecule for copper in MOFs grown with layer-by-layer method. Similar tilting was not seen on gold substrates coated with self-assembled monolayers terminated with carboxylic acid groups, on which the azobenzene derivative showed a preference of an upright position [47]. This means the substrate and the inorganic precursor in the ALD deposition may have an influence on the orientation of ADA. The double surface reaction and tilting models for ADA are presented in Figure 39.

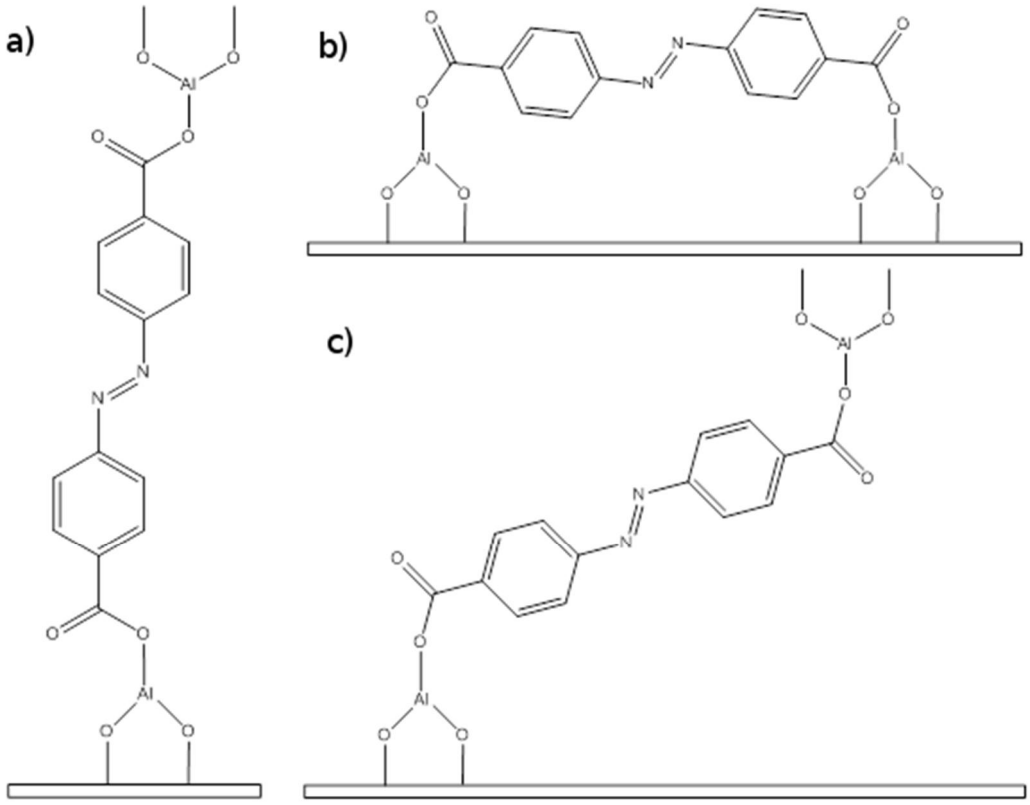

Figure 39. a) Ideal surface reaction, b) double surface reaction and c) tilting of ADA.

FTIR spectra for the hybrid thin films show that no free carboxylic acid groups are present in the films, and that they are instead all bound to aluminium atoms. The optimization graph for ADA pulse time also shows saturation at 8 seconds. This further suggests that the low growth rate may be caused by double surface reactions or tilting instead of incomplete surface saturation.

Growth rate for the superlattices was 1.17 - 1.19 Å/cycle on silicon and 1.26 - 1.28 Å/cycle on quartz. Similar change in growth rate was seen for aluminium oxide films with 1.20 Å/cycle on silicon and 1.30 Å/cycle on quartz. The larger growth rate on quartz is likely related to a slight substrate-dependency for the growth of the oxide and does not suggest a change in bonding or structure of the hybrid layers, as the difference between superlattice and oxide growth rates is similar on both silicon and quartz substrates. Differences in the growth rate of aluminium oxide on (100) and (111) silicon substrates have been reported earlier [133]. The difference in crystal structure of the substrates could also explain the different growth rates seen here.

A small gradient was seen at the edge of the substrate in all deposited films. This suggests that a chemical vapor deposition (CVD) process is involved in the deposition, where the precursor materials are reacting in the reactor chamber instead of the surface of the sample. Purging the chamber with nitrogen gas between the precursor pulses prevents this in ALD processes. TMA in particular is known to be a highly reactive molecule, so it could easily react with other molecules within the reactor chamber. XRR measurements showed that the films had high surface roughness, making the measurement of thickness for films with over 600 deposition cycles impossible. This further suggests that a CVD process might be involved in the deposition.

When two substrates parallel to the flow direction were used, the gradient on the first substrate was very large. The gradient on the second substrate was smaller than in depositions where only one substrate was used, although the position of the substrate inside the reaction chamber was the same. Despite the smaller gradient, the growth rate of the film was almost the same as for the film deposited with the optimized process with one substrate. This suggests the substrate surfaces are saturated normally, but during the precursor pulses, the carrier gas also contains small amounts of the other precursor. The precursors react, causing a gradient on the first surface they come in contact with. As longer purge times did not make the films more homogenous, it is possible one or both of the precursors are constantly leaking into the reaction chamber. One of the valves on the TMA line was found to be leaking during the superlattice depositions and possibly even during the hybrid thin film deposition, but fixing or changing the valve did not make the hybrid thin films fully homogenous. It is also possible the gradient is related to factors regarding the flow inside the reactor.

The gradient seen on the samples could also be related to decomposition of the organic precursor. ADA should not decompose at the set deposition temperature, but the actual deposition temperature may differ from the measured value because of the position of sample relative to the thermocouple measuring the temperature inside the reactor. When deposition temperature was increased to 300 °C, the

gradient was larger and the film was very rough, indicating that temperature affects the homogeneity of the film. Weisler and Helmkamp [134] determined the melting point of ADA to be 330 °C, but noted that decomposition takes place at this temperature. Therefore, partial decomposition causing the gradient in the hybrid films cannot conclusively be ruled out.

For the superlattice thin films with K/(K+m) = 1:15, 1:30 and 1:60, the azobenzene moiety was seen in FTIR spectra but not in UV-Vis spectra. The azobenzene moiety could be seen in the UV-Vis absorption spectra of superlattice thin films with K/(K+m) = 1:2 and 1:6, although the peak at 321 nm was very low in intensity in the latter. This suggests that the amount of azobenzene in the other superlattice thin films was too small to be seen in the UV-Vis spectra, because the aluminium oxide layers also absorb in the same range.

Only the hybrid thin film showed a response to being irradiated. The only change in the absorption spectrum seen for the hybrid film after irradiation was a small decrease in the peak at 321 nm. UV irradiation did not cause any differences in the absorption spectra of the superlattice thin films. However, in solution the precursor showed reversible photoisomerization. The lack of photoisomerization in the thin films could be due to the double surface reactions restricting the change of conformation from trans-isomer to cis-isomer. Because both carboxylic acid groups are bound to the same surface, the distance between the two groups is fixed as the rigid structure prevents the aluminium atoms from moving. No isomerization can therefore occur for the azobenzenes bound to the same surface on both ends of the molecule. The small changes in intensity can therefore only be related to azobenzene moieties bound to surfaces of two different layers. Lack of free volume around the azobenzene in the thin films deposited with ALD may also contribute to poor photoresponsivity, as the non-ideal growth makes the structure less ordered instead of forming consecutive layers.

The aluminium oxide film with the surface saturated with the azobenzene precursor showed some absorption at a wavelength corresponding to the (π, π^*) transition of

azobenzene. As the surface is the only layer containing azobenzene, the amount of azobenzene in the thin film is very small. Superlattices in which the ratio of azobenzene layers was K/(K+m) = 1:15 or less showed no peaks corresponding to azobenzene, although the amount of azobenzene should be higher in the superlattices than in the film with the saturated surface. It is therefore possible that the thicker aluminium oxide layers absorb the UV irradiation better than the small amount of azobenzene present in the film, but on the surface azobenzene can absorb irradiation without interference from aluminium oxide. The film with the saturated surface may also contain excess of azobenzene, as the precursor could have been absorbed within the aluminium oxide layers during the hour-long pulse, explaining the higher absorption intensities. The superlattice thin films were twice as thick at 600 deposition cycles compared to the film with the saturated surface at 300 deposition cycles. The thickness of aluminium oxide film on quartz affects its absorption spectrum [131], which may in part explain the differences.

Photoisomerization seen in the hybrid thin film is very limited compared to other photoresponsive systems with azobenzene. Polymer films in general show a strong photochromic response, as seen with films prepared from polyanions and polycations with layer-by-layer method [119] and films prepared from bolaamphiphiles with azobenzene moieties and polyelectrolytes with layer-by-layer method [118]. Good results have also been seen for LDH hybrid films, either with azobenzene polymers introduced between the nanosheets with layer-by-layer self-assembly [11] or azobenzene derivatives intercalated between the nanosheets [13]. Other systems showing good photochromic responses are Langmuir-Blodgett hybrid films with clay minerals and azobenzene [61], spin-coated films of hybrid materials with azobenzene in silane matrix [12] and metal phosphonate multilayer films with azobenzene by combined Langmuir-Blodgett and self-assembly method [113]. Common for these systems are free volume around the azobenzene moieties and a well-ordered, layered structure, both of which promote photoresponsivity. Systems like MOFs containing azobenzene in pores [135], [136] and metal phosphonate films prepared only by using Langmuir-Blodgett method, in which azobenzene molecules are organized into bilayers [56] show much weaker photochromic responses. In both

cases, the free volume around azobenzene is limited, which restricts photoisomerization. For metal phosphonates, the layered structure gained from using the combined Langmuir-Blodgett and layer-by-layer method greatly enhanced the photochromic response compared to the less-organized films prepared by simple Langmuir-Blodgett method. Similar factors related to lack of free volume and poorly defined layers in the structure could be behind the poor photochromic response seen for thin films in this work.

The photoisomerization seen in the hybrid film was not reversible, as the absorption spectrum showed no changes after visible light irradiation or thermal relaxation. In other hybrid systems with azobenzene, the photoisomerization can show only partial reversibility. This non-ideal behavior can be a result of a photobleaching effect or steric hindrance [136]. Confinement of azobenzene molecules and lack of free volume caused by double surface reactions are also likely reasons for irreversibility of the photoisomerization reaction in the hybrid thin films in this work.

This work proves that photochromic molecules such as azobenzene can be used in ALD/MLD processes to prepare hybrid thin films. ALD/MLD as a technique for preparing photoresponsive thin films seems promising, but more research has to be done to find a combination of organic and inorganic precursors that show better growth behavior and photochromic response than those observed in this work. Only then can the effect of the photochromic response on the properties of the inorganic component be studied effectively. The uniformity, high conformity and accurate control of thickness and composition of thin films prepared with ALD/MLD makes it a viable alternative to methods currently used to prepare photoresponsive thin films, which should encourage further research in the field.

10. Summary

Photochromic molecules change their absorption spectrum when they are irradiated. The difference is caused by a change in the structure of the molecule. The structure

change can be for example trans-cis isomerization or ring-opening or ring-closing reaction. The thermally stable form usually absorbs in the UV range and converts to a colored form, which in most cases can return either thermally or with irradiation to its original form. Such photochromic molecules have been used in different kinds of applications. Some applications are related to the differences in the absorption spectra of the two forms, such as photochromic sunglasses, whereas others utilize the change in chemical and physical properties of the molecules, as is the case with optical switches.

Well-known examples of photochromic molecules are azobenzenes, stilbenes, spiropyrans and dithienylethenes. The former two undergo trans-cis isomerization when irradiated with UV light, spiropyran undergoes a ring-opening reaction and dithienylethene undergoes a ring-closing reaction. These molecules have been used together with inorganic precursors in hybrid materials with photoresponsive properties. Thin films of the hybrid materials are commonly prepared with Langmuir-Blodgett method, layer-by-layer self-assembly, spin-coating or intercalation. Preparing similar films with ALD/MLD would provide several advantages to previously used methods, such as good control of film thickness, as well as uniformity and conformity of the thin films. The layered, rigid structure provided by ALD/MLD should also improve the photochromic response.

In this work, hybrid thin films were deposited with ALD/MLD using a photoresponsive organic molecule. The precursors for the thin films were TMA and ADA. The resulting hybrid films were amorphous and nearly homogenous, with a slight gradient seen on the leading edge of the substrate. Superlattice thin films were also deposited, using TMA and water for the aluminium oxide layers and the aforementioned process for the hybrid layers. UV-Vis spectroscopy showed absorption bands corresponding to azobenzene only in the hybrid thin film and superlattice thin films with very thin aluminium oxide layers. As the thickness of the oxide layers increased in the superlattice thin films, the absorption bands disappeared, although the azobenzene moiety could still be seen in FTIR. Photoresponsivity of the thin films was poor, as the hybrid thin film showed only a slight irreversible change in absorption after

irradiation. No changes were seen in the absorption spectra of the superlattice thin films upon irradiation. Further research is necessary to find a better combination of inorganic and organic components for use in ALD/MLD to prepare photoresponsive thin films.

11. Suggestions for further research

The low growth rates of the hybrid were likely caused by double surface reactions and tilting of the organic precursor. This could possibly be solved with heterobifunctional precursors, where the functional groups on the benzene rings are different from one another. One of the groups could be more reactive toward the inorganic precursor bound on the sample surface and saturate the surface more efficiently, decreasing the amount of double surface reactions [137]. Finding a suitable heterobifunctional azobenzene precursor may be difficult. Reactive functional groups of organic precursors in hybrid thin film depositions with ALD have previously been limited to alcohols, acids and amines [132]. Hydroxy-substituted azobenzenes and pseudo-stilbene-type azobenzene derivatives with both electron-donating and electron-withdrawing groups have fast thermal back-isomerization reactions [21]. Observing the photoresponsivity of such derivatives could be difficult using equipment and set-ups used in this work. However, the incorporation of hydroxy-substituted azobenzenes into a rigid matrix with covalent bonds could slow down the thermal reaction by eliminating the hydrogen bond formation that weakens the nitrogen-nitrogen double bond.

One possible candidate for a heterobifunctional azobenzene precursor would be 4-amino-4'-hydroxyazobenzene. Both the amine and the hydroxy group are electron-donating groups, making them aminoazobenzene-type derivatives. The push-pull effect causing fast thermal back-isomerization seen in pseudo-stilbene-type azobenzenes is avoided, as the cis-isomers are usually stable for minutes. Amines and alcohols have both been used as organic ALD precursors [132]. Aminophenols have been shown to inhibit double surface reactions, resulting in higher growth rates

[137]. The (n, π*) and (π, π*) states in aminoazobenzenes are close in energy, which may hinder the photoisomerization process. However, a rigid layered matrix provided by the ALD process should improve the photoresponsivity and thermal stability of aminoazobenzenes.

As the hybrid thin films deposited in this work were not fully homogenous, more factors could be considered in attempt to decrease the size of the gradient. One approach could be to study the flow inside the reactor. For example, the flow inside the reactor could be changed by using different parts and configurations to see if they have any effect on homogeneity, the effect of the position of the substrate on the gradient size could be examined, or the deposition could be attempted with a different reactor. More accurate optimization of the hybrid process could also be performed, to determine the saturation points more accurately and to examine the temperature stability on a wider range.

As decomposition of the organic precursor could not be ruled out as the cause of the gradient seen on the samples, further analysis should be made to verify the azobenzene structure stays intact in the deposition temperatures. Thermogravimetric analysis (TGA) would show if the weight of the precursor changes upon heating it to temperatures measured in the reactor during deposition, indicating decomposition. TGA could also be used to determine the sublimation temperature of the azobenzene precursor.

Hybrid thin film depositions with other inorganic precursors should be attempted to find a suitable match for ADA. This could improve the homogeneity of the thin films as well as result in a higher growth rate. The oxides prepared from different precursors in superlattice thin films would also have different properties, such as optical properties or magnetization, which could potentially be affected by irradiation to some degree.

Other organic precursors could also be used in photoresponsive thin films. Of the photochromic molecules discussed in the literature part, stilbene seems like a

suitable candidate for use in ALD/MLD. As it is analogous to azobenzene, their molecular weights are close, which suggests their sublimation temperatures should also be close to one another. Side reactions for stilbene, such as photodimerization and photocyclization, as well as the low melting point of the cis-isomer should not affect the performance of hybrid thin films prepared with ALD/MLD, as the molecules would be covalently bound to the matrix and therefore immobilized, which prevents the side reactions and phase change from occurring during UV irradiation. The other two photochromic molecules discussed in this work, spiropyran and dithienylethene, are much larger. They may not be suitable for ALD/MLD, as it is likely that they would decompose before reaching their sublimation temperature.

As the thickness of the oxide layers in the superlattice thin films increased, the transitions related to azobenzene disappeared from the absorption spectrum. It could be useful to determine the minimum ratio of organic layers to total number of layers still showing the transitions in the absorption spectrum. Using other inorganic precursors for different oxides, the minimum ratios could be compared to see if the oxide has an effect on the ratio due to its absorption. As the overall thickness of aluminium oxide in the superlattice films also seemed to affect the absorption spectrum, it should also be considered when comparing oxides. This may impose limits on the thickness of the film in possible applications, if the aim is to use azobenzene for the photoswitching of properties of oxides. The film has to be thin enough not to hinder absorption of UV irradiation by azobenzene.

References

[1] Bouas-Laurent, H., and Dürr, H., Organic photochromism (IUPAC Technical Report), *Pure Appl. Chem.* **73** (2001) 639–665.

[2] Tynell, T., Yamauchi, H., and Karppinen, M., Hybrid inorganic–organic superlattice structures with atomic layer deposition/molecular layer deposition, *J. Vac. Sci. Technol. A Vacuum, Surfaces, Film.* **32** (2014) 1–5.

[3] Rau, H., Photoisomerization of azobenzenes, in *Photoreact. Org. Thin Film.*, eds. Sekkat, Z., and Knoll, W., 1st ed., Academic Press, 2002, 3–39.

[4] Hartley, G. S., The cis-Form of Azobenzene and the Velocity of the Thermal cis-trans-Conversion of Azobenzene and Some Derivatives, *J. Chem. Soc.* (1938) 633–642.

[5] Menzel, H., Photoisomerization in Langmuir-Blodgett-Kuhn Structures, in *Photoreact. Org. Thin Film.*, eds. Sekkat, Z., and Knoll, W., 1st ed., Academic Press, 2002, 179–212.

[6] Biteau, J., Chaput, F., Lahlil, K., Boilot, J.-P., Tsivgoulis, G. M., Lehn, J.-M., et al., Large and Stable Refractive Index Change in Photochromic Hybrid Materials, *Chem. Mater.* **10** (1998) 1945–1950.

[7] Peretti, J., Biteau, J., Boilot, J.-P., Chaput, F., Safarov, V. I., Lehn, J.-M., et al., Remanent photoinduced birefringence in thin photochromic sol-gel films., *Appl. Phys. Lett.* **74** (1999) 1657–1659.

[8] Suzuki, M.-A., Hashida, T., Hibino, J., and Kishimoto, Y., Multiple Optical Memory using Photochromic Spiropyran Aggregates, *Mol. Cryst. Liq. Cryst. Sci. Technol. Sect. A. Mol. Cryst. Liq. Cryst.* **246** (1994) 389–396.

[9] Irie, M., Diarylethenes for Memories and Switches, *Chem. Rev.* **100** (2000) 1685–1716.

[10] Irie, M., Photochromic diarylethenes for photonic devices, *Pure Appl. Chem.* **68** (1996) 1367–1371.

[11] Han, J., Yan, D., Shi, W., Ma, J., Yan, H., Wei, M., et al., Layer-by-layer ultrathin films of azobenzene-containing polymer/layered double hydroxides with reversible photoresponsive behavior, *J. Phys. Chem. B* **114** (2010) 5678–

5685.

[12] Bućko, A., Zielińska, S., Ortyl, E., Larkowska, M., and Barille, R., Synthesis of organic-inorganic hybrid azobenzene materials for the preparation of nanofibers by electrospinning, *Opt. Mater. (Amst).* **38** (2014) 179–187.

[13] Wang, X., Lu, J., Wei, M., and Duan, X., Photoresponsive thin films containing an azobenzene derivative intercalated with a layered double hydroxide, *Chinese Sci. Bull.* **55** (2010) 3894–3900.

[14] Dürr, H., General Introduction, in *Photochromism Mol. Syst.*, eds. Dürr, H., and Bouas-Laurent, H., 1st ed., Elsevier, Amsterdam, 2003, 1–13.

[15] Crano, J. C., and Guglielmetti, R. J., Introduction, in *Org. Photochromic Thermochromic Compd. Vol. 1 Main Photochromic Fam.*, eds. Crano, J. C., and Guglielmetti, R. J., 1st ed., Springer Science+Business Media, New York, 2002, 1–8.

[16] Gauglitz, G., Photophysical, Photochemical and Photokinetic Properties of Photochromic Systems, in *Photochromism Mol. Syst.*, eds. Dürr, H., and Bouas-Laurent, H., 2nd ed., Elsevier, Amsterdam, 2003, 15–60.

[17] Dürr, H., and Bouas-Laurent, H., *Photochromism: Molecules and systems*, 2nd ed., Elsevier, Amsterdam, 2003.

[18] Stranius, K., and Börjesson, K., Determining the Photoisomerization Quantum Yield of Photoswitchable Molecules in Solution and in the Solid State, *Sci. Rep.* **7** (2017) 1–9.

[19] Fischer, E., The Calculation of Photostationary States in Systems A - B When Only A Is Known, *J. Phys. Chem.* **71** (1967) 3704–3706.

[20] Porter, G., Flash photolysis and spectroscopy: A new method for the study of free radical reactions, *Proc. R. Soc. A* **200** (1950) 284–300.

[21] García-Amorós, J., and Velasco, D., Recent advances towards azobenzene-based lightdriven real-time information-transmitting materials, *Beilstein J. Org. Chem.* **8** (2012) 1003–1017.

[22] Fujino, T., Arzhantsev, S. Y., and Tahara, T., Femtosecond Time-Resolved Fluorescence Study of Photoisomerization of trans -Azobenzene, *J. Phys. Chem. A* **105** (2001) 8123–8129.

[23] Mills, P., and Raymont, J., Ultraviolet (UV) Measurement for Formulators:

Part I., *Paint Coatings Ind.* **25** (2009) 18–25.

[24] Koleske, J. V., Curing Equipment, in *Radiat. Curing Coatings (MNL 45)*, ed. Koleske, J., 1st ed., ASTM International, West Conshohocken, 2002, 15–30.

[25] Linden, K. G., and Mamane, H., Ultraviolet Disinfection Process Concepts and Equipment Systems, in *Ultrav. Disinfect. Wastewater - Low-Dose Appl. Guid. Second. Tert. Discharges*, WEF, Alexandria, 2015, 18–40.

[26] Gaska, R., and Zhang, J., Deep-UV LEDs: physics, performance, and applications, **6037** (2005) 603706.

[27] Yager, K. G., and Barrett, C. J., Azobenzene Polymers as Photomechanical and Multifunctional Smart Materials, in *Intell. Mater.*, eds. Shahinpoor, M., and Schneider, H.-J., Royal Society of Chemistry, Cambridge, 2007, 424–446.

[28] Hartley, G. S., The Cis-form of Azobenzene, *Nature* **140** (1937) 281–281.

[29] Melorose, J., Perroy, R., and Careas, S., *UV ATLAS of Organic Compounds*, 1st ed., Springer Science+Business Media, New York, 1967.

[30] Rau, H., Spectroscopic Properties of Organic Azo Compounds, *Angew. Chem Int. Ed.* **12** (1973) 224–235.

[31] Rau, H., Azo Compounds, in *Photochromism Mol. Syst.*, eds. Dürr, H., and Bouas-Laurent, H., 1st ed., Elsevier, Amsterdam, 2003, 165–188.

[32] Bandara, H. M. D., Friss, T. R., Enriquez, M. M., Isley, W., Incarvito, C., Frank, H. A., et al., Proof for the concerted inversion mechanism in the trans-cis Isomerization of azobenzene using hydrogen bonding to induce isomer locking, *J. Org. Chem.* **75** (2010) 4817–4827.

[33] Curtin, D. Y., Grubbs, E. J., and McCarty, C. G., Uncatalyzed syn-anti Isomerization of Imines, Oxime Ethers, and Haloimines, *J. Am. Chem. Soc.* **88** (1966) 2775–2786.

[34] Rau, H., and Lüddecke, E., On the rotation-inversion controversy on photoisomerization of azobenzenes. Experimental proof of inversion, *J. Am. Chem. Soc.* **104** (1982) 1616–1620.

[35] Diau, E. W. G., A New Trans-to-Cis Photoisomerization Mechanism of Azobenzene on the S 1(n,π*) Surface, *J. Phys. Chem. A* **108** (2004) 950–956.

[36] Crecca, C. R., and Roitberg, A. E., Theoretical study of the isomerization mechanism of azobenzene and disubstituted azobenzene derivatives, *J. Phys.*

Chem. A **110** (2006) 8188–8203.

[37] Pancur, T., Renth, F., Temps, F., Harbaum, B., Krüger, A., Herges, R., et al., Femtosecond fluorescence up-conversion spectroscopy of a rotation-restricted azobenzene after excitation to the S1 state., *Phys. Chem. Chem. Phys.* **7** (2005) 1985–1989.

[38] Asano, T., Okada, T., Shinkai, S., Shigematsu, K., Kusano, Y., and Manabe, O., Temperature and Pressure Dependences of Thermal Cis-to-Trans Isomerization of Azobenzenes Which Evidence an Inversion Mechanism, *J. Am. Chem. Soc.* **103** (1981) 5161–5165.

[39] Gegiou, D., Muszjat, K. A., and Fischer, E., Temperature Dependence of Photoisomerization. V. The Effect of Substituents on the Photoisomerization of Stilbenes and Azobenzenes, *J Am Chem Soc* **90** (1968) 3907–3918.

[40] Dokić, J., Gothe, M., Wirth, J., Peters, M. V, Schwarz, J., Hecht, S., et al., Quantum chemical investigation of thermal cis-to-trans isomerization of azobenzene derivatives: substituent effects, solvent effects, and comparison to experimental data., *J. Phys. Chem. A* **113** (2009) 6763–6773.

[41] Yoshino, J., Kano, N., and Kawashima, T., Synthesis of the most intensely fluorescent azobenzene by utilizing the B – N interaction, *Chem. Commun.* (2007) 559–561.

[42] Bandara, H. M. D., Cawley, S., Gascón, J. A., and Burdette, S. C., Short-circuiting azobenzene photoisomerization with electron-donating substituents and reactivating the photochemistry with chemical modification, *European J. Org. Chem.* (2011) 2916–2919.

[43] Bunce, N., Ferguson, G., Forber, C. L., and Stachnyk, G. J., Sterically hindered azobenzenes: isolation of cis isomers and kinetics of thermal cis-trans isomerization, *J. Org. Chem.* **52** (1987) 394–398.

[44] Han, M., and Honda, T., Correlation between the molecular structure and trans ↔ cis isomerization characteristics of azobenzenes, *Sci. China Chem.* **54** (2011) 1955–1961.

[45] Serra, F., and Terentjev, E. M., Effects of solvent viscosity and polarity on the isomerization of azobenzene, *Macromolecules* **41** (2008) 981–986.

[46] Yu, X., Wang, Z., Buchholz, M., Füllgrabe, N., Grosjean, S., Bebensee, F., et al.,

Cis-To-Trans Isomerization of Azobenzene Investigated By Using Thin Films of Metal-Organic Frameworks., *Phys. Chem. Chem. Phys.* **17** (2015) 22721–22725.

[47] Zhuang, J. L., Lommel, K., Ceglarek, D., Andrusenko, I., Kolb, U., Maracke, S., et al., Synthesis of a new copper-azobenzene dicarboxylate framework in the form of hierarchical bulk solids and thin films without and with patterning, *Chem. Mater.* **23** (2011) 5366–5374.

[48] Ramakrishnan, V., Yamamoto, D., Sasamoto, S., Shimada, T., Nabetani, Y., Tachibana, H., et al., Remarkable enhancement of the photoreactivity of a polyfluoroalkyl azobenzene derivative in an organic-inorganic nano-layered microenvironment., *Phys. Chem. Chem. Phys.* **16** (2014) 23663–23670.

[49] Bronner, C., Schulze, M., Hagen, S., and Tegeder, P., The influence of the electronic structure of adsorbate-substrate complexes on photoisomerization ability, *New J. Phys.* **14** (2012) 1–16.

[50] Tseng, C. W., Huang, D. C., and Tao, Y. T., Azobenzene-functionalized gold nanoparticles as hybrid double-floating-gate in pentacene thin-film transistors/memories with enhanced response, retention, and memory windows, *ACS Appl. Mater. Interfaces* **5** (2013) 9528–9536.

[51] Koshiba, Y., Yamamoto, M., Kinashi, K., Misaki, M., Ishida, K., Oguchi, Y., et al., Photo-induced alignment behavior of azobenzene compound in thin film, *Thin Solid Films* **518** (2009) 805–809.

[52] Kempe, C., Rutloh, M., and Stumpe, J., Photo-orientation of azobenzene side chain polymers parallel or perpendicular to the polarization of red HeNe light, *J. Phys. Condens. Matter* **15** (2003) S813–S823.

[53] Bergmann, E., Engel, L., and Sándor, S., Beiträge zur Kenntnis der doppelten Bindung , II.: Über die räumliche Konfiguration der aromatischen Azokörper., *Chem. Ber.* **63** (1930) 2572–2575.

[54] Sekkat, Z., Photo-orientation by Photoisomerization, in *Photoreact. Org. Thin Film.*, eds. Sekkat, Z., and Knoll, W., 1st ed., Academic Press, 2002, 63–97.

[55] Shimomura, M., Ando, R., and Kunitake, T., Orientation and Spectral Characteristics of the Azobenzene Chromophore in the Ammonium Bilayer Assembly, *Berichte Der Bunsengesellschaft/Physical Chem. Chem. Phys.* **87**

(1983) 1134–1143.

[56] Petruska, M. A., and Talham, D. R., Organic/Inorganic Langmuir−Blodgett Films Based on Metal Phosphonates. 3. An Azobenzene-Derivatized Phosphonic Acid Forms Continuous Lattice Layers with Divalent, Trivalent, and Tetravalent Metal Ions 1, *Chem. Mater.* **10** (1998) 3672–3682.

[57] Rad, F. A., Rezvani, Z., and Khodam, F., Molecular design confirmation for proposition of improved photophysical properties in a dye-intercalated layered double hydroxides, *RSC Adv.* **6** (2016) 11193–11203.

[58] Shimomura, M., and Kunitake, T., Fluorescence and Photoisomerization of Azobenzene-Containing Bilayer Membranes, *J. Am. Chem. Soc.* **109** (1987) 5175–5183.

[59] Goulet-Hanssens, A., and Barrett, C. J., Photo-control of biological systems with azobenzene polymers, *J. Polym. Sci. Part A Polym. Chem.* **51** (2013) 3058–3070.

[60] Beharry, A. A., Sadovski, O., and Woolley, G. A., Azobenzene photoswitching without ultraviolet light, *J. Am. Chem. Soc.* **133** (2011) 19684–19687.

[61] Yamamoto, T., Umemura, Y., Sato, O., and Einaga, Y., Photomagnetic Langmuir-Blodgett films consisting of azobenzene and Prussian Blue: Correlation between the film structure and the photomagnetic efficiency, *Sci. Technol. Adv. Mater.* **7** (2006) 134–138.

[62] Abellán, G., García, H., Gómez-García, C. J., and Ribera, A., Photochemical behavior in azobenzene having acidic groups. Preparation of magnetic photoresponsive gels, *J. Photochem. Photobiol. A Chem.* **217** (2011) 157–163.

[63] Abellán, G., Coronado, E., Martí-Gastaldo, C., Ribera, A., Jordá, J. L., and García, H., Photo-switching in a hybrid material made of magnetic layered double hydroxides intercalated with azobenzene molecules, *Adv. Mater.* **26** (2014) 4156–4162.

[64] Kozlovsky, M. V., Blinov, L. M., and Haase, W., Chiral Polymers With Photoaffected Phase Behavior For Optical Data Storage, in *Photoreact. Org. Thin Film.*, eds. Sekkat, Z., and Knoll, W., 1st ed., Academic Press, 2002, 145–172.

[65] Stumpe, J., Läsker, L., Fischer, T., Rutloh, M., Kostromin, S., and Ruhmann, R.,

Photo-orientation in amorphous and aligned films of photochromic liquid crystalline polymers, *Thin Solid Films* **284–285** (1996) 252–256.

[66] Ikeda, T., and Tsutsumi, O., Optical switching and image storage by means of azobenzene liquid-crystal films., *Science* **268** (1995) 1873–5.

[67] Ishihara, K., Hamada, N., Kato, S., and Shinohara, I., Photo-induced change in surface free energy of azoaromatic polymers, *J. Polym. Sci. Polym. Chem. Ed.* **21** (1983) 1551–1555.

[68] Ishihara, K., Hamada, N., Kato, S., and Shinohara, I., Photoinduced swelling control of amphiphilic azoaromatic polymer membrane, *J. Polym. Sci. Polym. Chem. Ed.* **22** (1984) 121–128.

[69] Saltiel, J., and Sun, Y.-P., Cis-Trans Isomerization of C=C Double Bonds, in *Photochromism Mol. Syst.*, eds. Dürr, H., and Bouas-Laurent, H., 1st ed., Elsevier, Amsterdam, 2003, 68–114.

[70] Kawaguchi, Y., The new photoisomerization mechanism of stilbene, *J. Chem. Phys.* **100** (1994) 8856–8868.

[71] Dolgova, O. V., Sokolova, I. V., and Vasilyeva, N. Y., Quantum chemical calculations by INDO/S method of stilbene photoisomers, *Revs. Mod. Phys* **71** (1998) 1267–1274.

[72] McGill, R. A., Rice, J. K., Baronavski, A. P., Owrutsky, J. C., Lowrey, A. H., Stavrev, K. ., et al., Using Theoretical Descriptors to Model Solvent Effects in the Isomerization of cis-Stilbene, *Int. J. Quantum Chem.* **60** (1996) 383.

[73] Guglielmetti, R., 4n+2 Systems: Spiropyrans, in *Photochromism Mol. Syst.*, eds. Dürr, H., and Bouas-Laurent, H., 1st ed., Elsevier, Amsterdam, 2003, 314–466.

[74] Saltiel, J., Megarity, E. D., and Kneipp, K. G., The Mechanism of Direct cis-trans Photoisomerization of the Stilbenes, *J. Am. Chem. Soc.* **259** (1966) 2336–2338.

[75] Ciamician, G., and Silber, P., Chemische Lichtwirkungen. V. Mittheilung, *Eur. J. Inorg. Chem.* **32** (1902) 4128–4131.

[76] Shechter, H., Link, W., and Tiers, G., Halogenation, dehydrohalogenation and dehalogenation of stilbene photo-dimers (1, 2, 3, 4-tetraphenylcyclobutanes), *J. Am. Chem. Soc.* **4128** (1963) 1601–1605.

[77] Moore, W. M., Morgan, D. D., and Stermitz, F. R., The Photochemical Conversion of Stilbene to Phenanthrene. The Nature of the Intermediate, *J. Am. Chem. Soc.* **85** (1963) 829–830.

[78] Gangolli, S., stilbene, in *Dict. Subst. Their Eff.*, ed. Gangolli, S., 3rd ed., The Royal Society of Chemistry, Cambridge, 2005, S115.

[79] Yan, D., Lu, J., Wei, M., Evans, D. G., and Duan, X., Anionic stilbene intercalated layered double hydroxide with two-photon excited polarized photoemission, *Chem. Eng. J.* **225** (2013) 216–222.

[80] Saraidarov, T., Reisfeld, R., Kazes, M., and Banin, U., Blue laser dye spectroscopic properties in solgel inorganic-organic hybrid films., *Opt. Lett.* **31** (2006) 356–358.

[81] Haas, W. E., Nelson, K. F., Adams, J. E., and Dir, G. A., U.V. Imaging with Nematic Chlorostilbenes, *J. Electrochem. Soc.* **121** (1974) 1667–1669.

[82] Hahm, S. G., Lee, S. W., Lee, T. J., Cho, S. A., Chae, B., Jung, Y. M., et al., UV-driven switching of chain orientation and liquid crystal alignment in nanoscale thin films of a novel polyimide bearing stilbene moieties in the backbone, *J. Phys. Chem. B* **112** (2008) 4900–4912.

[83] Fischer, E., and Hirshberg, Y., Formation of Coloured Forms of Spirans by Low-temperature Irradiation., *J. Chem. Soc.* (1952) 4522–4524.

[84] Bletz, M., Pfeifer-Fukumura, U., Kolb, U., and Baumann, W., Ground-and first-excited-singlet-state electric dipole moments of some photochromic spirobenzopyrans in their spiropyran and merocyanine form, *J. Phys. Chem. A* **106** (2002) 2232–2236.

[85] Tyer, N. W., and Becker, R. S., Photochromic spiropyrans. II. Emission spectra, intramolecular energy transfer, and photochemistry, *J. Am. Chem. Soc.* **92** (1970) 1295–1302.

[86] Kinashi, K., Harada, Y., and Ueda, Y., Thermal stability of merocyanine form in spiropyran/silica composite film, *Thin Solid Films* **516** (2008) 2532–2536.

[87] Guglielmetti, R., Spiropyrans and Related Compounds, in *Photochromism Mol. Syst.*, eds. Dürr, H., and Bouas-Laurent, H., 1st ed., Elsevier, Amsterdam, 2003, 855–878.

[88] Khairutdinov, R. F., and Hurst, J. K., Photocontrol of ion permeation through

bilayer membranes using an amphiphilic spiropyran, *Langmuir* **17** (2001) 6881–6886.

[89] Tsivgoulis, G. M., and Lehn, J. M., Photoswitched and functionalized oligothiophenes: Synthesis and photochemical and electrochemical properties, *Chem. - A Eur. J.* **2** (1996) 1399–1406.

[90] Dürr, H., 4n+2 Systems Based on 1,5-Electrocyclization, in *Photochromism Mol. Syst.*, eds. Dürr, H., and Bouas-Laurent, H., 1st ed., Elsevier, Amsterdam, 2003, 210–265.

[91] Irie, M., Miyatake, O., Uchida, K., and Eriguchi, T., Photochromic Diarylethenes with Intralocking Arms, *J. Am. Chem. Soc.* **116** (1994) 9894–9900.

[92] Kawai, T., Fukuda, N., Groschl, D., Kobatake, S., and Irie, M., Refractive index change of dithienylethene in bulk amorphous solid phase, *Japanese J. Appl. Phys. Part 2-Letters* **38** (1999) L1194–L1196.

[93] Herder, M., Schmidt, B. M., Grubert, L., Pätzel, M., Schwarz, J., and Hecht, S., Improving the fatigue resistance of diarylethene switches, *J. Am. Chem. Soc.* **137** (2015) 2738–2747.

[94] Takeshita, M., Kato, N., Kawauchi, S., Imase, T., Watanabe, J., and Irie, M., Photochromism of dithienylethenes included in cyclodextrins, *J. Org. Chem.* **63** (1998) 9306–9313.

[95] Dinescu, L., and Wang, Z. Y., Synthesis and photochromic properties of helically locked 1,2-dithienylethenes, *Chem. Commun.* **24** (1999) 2497–2498.

[96] Kaieda, T., Kobatake, S., Miyasaka, H., Murakami, M., Iwai, N., Nagata, Y., et al., Efficient Photocyclization of Dithienylethene Dimer , Trimer , and Tetramer : Quantum Yield and Reaction Dynamics, *J. Am. Chem. Soc.* **124** (2015) 2015–2024.

[97] Kudernac, T., Kobayashi, T., Uyama, A., Uchida, K., Nakamura, S., and Feringa, B. L., Tuning the temperature dependence for switching in dithienylethene photochromic switches, *J. Phys. Chem. A* **117** (2013) 8222–8229.

[98] Morimitsu, K., Shibata, K., Kobatake, S., and Irie, M., Dithienylethenes with a novel photochromic performance, *J. Org. Chem.* **67** (2002) 4574–4578.

[99] Zahedi, E., Mozaffari, M., Karimi, F.-S., and Nouri, A., Density functional

theory study of electric field effects on the isomerization of a photochromic molecular switch based on 1,2-dithienylethene, *Can. J. Chem. Can. Chim.* **92** (2014) 317–323.

[100] Boyer, J. C., Carling, C. J., Chua, S. Y., Wilson, D., Johnsen, B., Baillie, D., et al., Photomodulation of fluorescent upconverting nanoparticle markers in live organisms by using molecular switches, *Chem. - A Eur. J.* **18** (2012) 3122–3126.

[101] Dworak, L., Reuss, A. J., Zastrow, M., Rück-Braun, K., and Wachtveitl, J., Discrimination between FRET and non-FRET quenching in a photochromic CdSe quantum dot/dithienylethene dye system., *Nanoscale* **6** (2014) 14200–14203.

[102] Zhao, H., Al-Atar, U., Pace, T. C. S., Bohne, C., and Branda, N. R., High-contrast fluorescence switching using a photoresponsive dithienylethene coordination compound, *J. Photochem. Photobiol. A Chem.* **200** (2008) 74–82.

[103] Fredrich, S., Göstl, R., Herder, M., Grubert, L., and Hecht, S., Switching diarylethenes reliably in both directions with visible light, *Angew. Chemie - Int. Ed.* **55** (2016) 1208–1212.

[104] Irie, M., Lifka, T., and Uchida, K., Photochromism of single crystalline diarylethenes, *Mol. Cryst. Liq. Cryst. Sci. Technol. Sect. A. Mol. Cryst. Liq. Cryst.* **297** (1997) 81–84.

[105] Irie, M., Lifka, T., Kobatake, S., and Kato, N., Photochromism of 1,2-Bis(2-methyl-5-phenyl-3-thienyl)perfluorocyclopentene in a Single-Crystalline Phase, *J. Am. Chem. Soc.* **122** (2000) 4871–4876.

[106] Wesenhagen, P., Areephong, J., Landaluce, T. F., Heureux, N., Katsonis, N., Hjelm, J., et al., Photochromism and electrochemistry of a dithienylcyclopentene electroactive polymer, *Langmuir* **24** (2008) 6334–6342.

[107] Chaput, F., Biteau, J., Lahlil, K., Boilot, J. P., Darracq, B., Levy, Y., et al., Photochromic sol-gel films containing dithienylethene and azobenzene derivatives: From the design of optical components to the optical data storage, *Mol. Cryst. Liq. Cryst.* **344** (2000) 77–82.

[108] Li, Y., Urbas, A., and Li, Q., Reversible light-directed red, green, and blue reflection with thermal stability enabled by a self-organized helical

superstructure, *J. Am. Chem. Soc.* **134** (2012) 9573–9576.

[109] Van Herpt, J. T., Stuart, M. C. A., Browne, W. R., and Feringa, B. L., A dithienylethene-based rewritable hydrogelator, *Chem. - A Eur. J.* **20** (2014) 3077–3083.

[110] Mitzi, D. B., Thin-film deposition of organic-inorganic hybrid materials, *Chem. Mater.* **13** (2001) 3283–3298.

[111] Liu, Z. F., Loo, B. H., Baba, R., and Fujishima, A., Excellent Reversible Photochromic Behavior of 4-Octyl-4'-(5-carboxyl-pentamethyleneoxy)-azobenzene in Organized Monolayer Assemblies, *Chem. Lett.* **19** (1990) 1023–1026.

[112] Liu, Z.-F., Hashimoto, K., and Fujishima, A., A Novel Electrochemical Quantification Method for Trans/Cis Interconversion of Azo Compounds in a Solid Monolayer Film, *Chem. Lett.* **19** (1990) 2177–2180.

[113] Wu, A., and Talham, D. R., Photoisomerization of azobenzene chromophores in organic/inorganic zirconium phosphonate thin films prepared using a combined Langmuir-Blodgett and self-assembled monolayer deposition, *Langmuir* **16** (2000) 7449–7456.

[114] Cong, H. P., and Yu, S. H., Self-assembly of functionalized inorganic-organic hybrids, *Curr. Opin. Colloid Interface Sci.* **14** (2009) 71–80.

[115] Richardson, J. J., Björnmalm, M., and Caruso, F., Technology-driven layer-by-layer assembly of nanofilms, *Science (80-.).* **348** (2015) aaa2491-aaa2491.

[116] Mozafari, M., Ramedani, A., Zhang, Y. N., and Mills, D. K., Thin films for tissue engineering applications, in *Thin Film Coatings Biomater. Biomed. Appl.*, ed. Griesser, H. J., 1st ed., Elsevier, Cambridge, 2016, 167–189.

[117] Toutianoush, A., and Tieke, B., Photoinduced switching in self-assembled multilayers of azobenzene-containing ionene polycations and anionic polyelectrolytes, *Macromol. Rapid Commun.* **19** (1998) 591–595.

[118] Saremi, F., and Tieke, B., Photoinduced switching in self-assembled multilayers of an azobenzene bolaamphiphile and polyelectrolytes, *Adv. Mater.* **10** (1999) 388–391.

[119] Dante, S., Advincula, R., Frank, C. W., and Stroeve, P., Photoisomerization of Polyionic Layer-by-Layer Films Containing Azobenzene, *Langmuir* **15** (1999)

193–201.

[120] Sekkat, Z., and Knoll, W., Photoisomerization and Photo-Orientation of Azo Dye in Films of Polymer: Molecular Interaction, Free Volume, and Polymer Structural Effects, in *Photoreact. Org. Thin Film.*, eds. Sekkat, Z., and Knoll, W., 1st ed., Academic Press, 2002, 107–141.

[121] Kurihara, S., Moritsugu, M., Kuwahara, Y., and Ogata, T., Photochemical on-off switching of structural color of a multi-bilayered film consisting of azobenzene-polymer liquid crystal and polyvinylalcohol, *Proc. SPIE* **8114** (2011) 81140J.

[122] Inagaki, M., and Kang, F., Fundamental Science of Carbon Materials, in *Mater. Sci. Eng. Carbon Fundam.*, eds. Inagaki, M., and Kang, F., 2nd ed., Elsevier, Amsterdam, 2014, 175–191.

[123] Nabetani, Y., Takamura, H., Hayasaka, Y., Sasamoto, S., Tanamura, Y., Shimada, T., et al., An artificial muscle model unit based on inorganic nanosheet sliding by photochemical reaction., *Nanoscale* **5** (2013) 3182–93.

[124] George, S. M., Atomic layer deposition: An overview, *Chem. Rev.* **110** (2010) 111–131.

[125] Klepper, K. B., Nilsen, O., and Fjellvåg, H., Deposition of thin films of organic-inorganic hybrid materials based on aromatic carboxylic acids by atomic layer deposition, *Dalt. Trans.* **39** (2010) 11628–11635.

[126] Silverstein, R. M., Webster, F. X., and Kiemle, D. J., Infrared Spectroscopy, in *Spectrom. Identif. Org. Compd.*, 7th ed., John Wiley & Sons, Inc., Hoboken, 2005, 95–96.

[127] Verpoort, F., Haemers, T., Roose, P., and Maes, J. P., Characterization of a surface coating formed from carboxylic acid-based coolants, *Appl. Spectrosc.* **53** (1999) 1528–1534.

[128] Tecklenburg, M. M. J., Kosnak, D. J., Bhatnagar, A., and Mohanty, D. K., Vibrational characterization of azobenzenes, azoxybenzenes and azoaromatic and azoxyaromatic polyethers, *J. Raman Spectrosc.* **28** (1997) 755–763.

[129] Miikkulainen, V., Leskelä, M., Ritala, M., and Puurunen, R. L., Crystallinity of inorganic films grown by atomic layer deposition: Overview and general trends, *J. Appl. Phys.* **113** (2013) 1–101.

[130] Brüesch, P., Kötz, R., Neff, H., and Pietronero, L., Vibrational properties of Al2O3 films on gold, aluminum, and silicon, *Phys. Rev. B* **29** (1984) 4691–4696.

[131] Avci, N., Musschoot, J., Smet, P. F., Korthout, K., Avci, A., Detavernier, C., et al., Microencapsulation of Moisture-Sensitive CaS:Eu2+ Particles with Aluminum Oxide, *J. Electrochem. Soc.* **156** (2009) J333–J337.

[132] Sundberg, P., and Karppinen, M., Organic and inorganic-organic thin film structures by molecular layer deposition: A review, *Beilstein J. Nanotechnol.* **5** (2014) 1104–1136.

[133] Wang, J., Baroughi, M. F., Bills, B., Galipeau, D., Samadzadeh, R., and Sivoththaman, S., Substrate dependence of surface passivation using atomic layer deposited dielectrics, *2009 34th IEEE Photovolt. Spec. Conf.* (2009) 001988–001991.

[134] Weisler, L., and Helmkamp, R. W., The Action of Some Benzyl Halides on Salts of Phenylnitromethane and Phenylnitro-acetonitrile, *J. Am. Chem. Soc.* **67** (1945) 1167–1171.

[135] Fu, W.-Q., Liu, M., Gu, Z.-G., Chen, S.-M., and Zhang, J., Liquid Phase Epitaxial Growth and Optical Properties of Photochromic Guest-Encapsulated MOF Thin Film, *Cryst. Growth Des.* **16** (2016) 5487–5492.

[136] Modrow, A., Zargarani, D., Herges, R., and Stock, N., Introducing a photo-switchable azo-functionality inside Cr-MIL-101-NH2 by covalent post-synthetic modification, *Dalt. Trans.* **41** (2012) 8690–8696.

[137] Sundberg, P., and Karppinen, M., Organic-inorganic thin films from TiCl4 and 4-aminophenol precursors: A model case of ALD/MLD hybrid-material growth?, *Eur. J. Inorg. Chem.* (2014) 968–974.